

The Resistance Committee

Final Report and Recommendations to the 23rd ITTC

1. INTRODUCTION

Dr. Hoyte C. Raven
Maritime Research Institute Netherlands,
NETHERLANDS

1.1. Membership

Chairman:

Prof. Fred Stern
Iowa Institute of Hydraulic Research,
UNITED STATES OF AMERICA

Secretary:

Dr. Emilio F. Campana
Istituto Nazionale per Studi ed Esperienze
di Architettura Navale, ITALY

Members:

Dr. Eng. Tomasz Bugalski
Ship Design and Research Centre,
POLAND

Prof. De-Bo Huang
Harbin Engineering University, CHINA

Dr. Yoshiaki Kodama
National Maritime Research Institute,
JAPAN

Dr. Yuzo Kusaka
Akishima Laboratories (Mitsui Zosen)
Inc., JAPAN

Prof. Seung-He Lee
Inha University, Republic of KOREA

Prof. Luis Perez-Rojas
Escuela Técnica Superior de Ingenieros
Navales, SPAIN

1.2. Meetings

The committee met 5 times:
15-17 March 2000, Tokyo, Japan
11-13 September 2000, Wageningen,
Netherlands
12-14 March 2001, Madrid, Spain
8-10 October 2001, Gdansk, Poland
18-19 March 2002, Inchon, Korea

1.3. Tasks and Report Structure

Below we list the tasks given to the 23rd Resistance Committee (RC), and indicate how these have been carried out.

- Review the state-of-the-art, comment on the potential impact of new developments on the ITTC, and identify the need for research and development for resistance and flow. Monitor and follow the development of new experimental techniques and extrapolation methods.
- Develop guidelines for model tests and extrapolation methods to predict far field waves and wash.
- Prepare an up-to-date bibliography of relevant technical papers and reports.

State-of-the-art reviews are given regarding New Developments in Modeling of Relevance to Resistance (Section 2), Trends in Experimental Fluid Dynamics (EFD) (Section 3), Trends in Computational Fluid Dynamics (CFD) (Section 4), and Far-Field Waves and Wash (Section 5).

The reviews focus on the last three years, except for topics not covered in recent RC reports, which cover a longer time period.

The RC was unable to develop guidelines for model tests and extrapolation methods to predict far field waves and wash.

- Develop procedures for model tests to measure sinkage and trim, wave profiles and elevations and nominal wake, for both deep and shallow water.

In order to improve and facilitate EFD uncertainty analysis for typical towing tank tests, spreadsheets for calculating the bias and precision limits and total uncertainty using single or multiple test methods, have been prepared as QM procedures. The QM procedure 4.9-03-02-03 “Uncertainty Analysis Spreadsheet for Resistance Measurements” provides the procedure for the resistance test. The QM procedure 4.9-03-02-04 “Uncertainty analysis Spreadsheets for Speed Measurements” is the analysis of speed errors. The speed is considered an independent procedure because of its importance in several tests. The sinkage and trim analysis is presented as QM procedure 4.9-03-02-05 “Uncertainty Analysis Spreadsheets for Sinkage and Trim Measurements”. The QM procedure 4.9-03-02-06, “Uncertainty Analysis Spreadsheets for Wave Profile Measurements”, is dedicated to the analysis of the wave profile on the model hull. The wave elevations analysis can be done using the same spreadsheet as for the wave profile case.

- Continue work on CFD uncertainty assessment methodology and examples, including further developments for error

sources and solution techniques. Compare and evaluate the results of the application of codes of ITTC member institutes to selected examples, specifically those of the Gothenburg 2000 Workshop on CFD in Ship Hydrodynamics.

Revision 01 QM Procedure 4.9-04-01-01 “Uncertainty Analysis in CFD, Verification and Validation Methodology and Procedures” was updated for clarity of presentation and expanded discussion of verification procedures and implementation based on three years experience, as discussed in Section 7. In particular, verification procedures are expanded to include user options of either correction factors or factor of safety approaches for estimating numerical errors and uncertainties and discussion is provided on fundamental and practical issues to aid in implementation of verification procedures. Validation procedures were not changed.

- Review research and development and provide recommendations for extrapolation methods and turbulence treatment in EFD and in CFD.

RC reviewed two- and three-dimensional extrapolation methods as well as recent work on friction lines. Uncertainty analysis for full-scale resistance (including a sample calculation) and full-scale power prediction was conducted for the 1978 ITTC Performance Prediction Method (ITTC QM Procedure 4.9-03-03-01.2). The extrapolation equations are treated as data-reduction equations and propagation of error analysis was conducted following standard EFD uncertainty analysis procedures with appropriate estimates for resulting uncertainties to estimate the uncertainty in predicting full-scale performance.

- Identify the requirements for new procedures, benchmark data, validation, uncertainty analyses and stimulate the necessary research for their preparation.

- Procedures must be in the format defined in the Manual of ITTC Recommended Procedures and they should be included in the Committee report as separate appendices. Symbols and terminology should agree with those used in the 1999 version of the ITTC SaT List; if necessary, new symbols should be proposed.

Procedures were identified and prepared and submitted according to the Manual of ITTC Recommended Procedures.

2. NEW DEVELOPMENTS IN MODELLING OF RELEVANCE TO RESISTANCE

New developments in modelling of relevance to resistance, mainly in the past three years since the last 22nd ITTC Conference, have been summarized in this section. The relevant topics in the fields of hull form design, propulsion, waves and free surface effects, viscous flow, turbulence, and drag reduction & bubbly flow are reviewed below.

2.1. Hull Form Design

Hull form optimization. Hamalainen and Heerd (1998) designed a fast mono hull 1400-passenger RO-RO ferry with service speed of about 30 knots. The hull shape was optimised using CFD and validated by model experiments, especially on the stern configuration at the Froude number (Fr) of 0.35 and higher. Full scale measurements were also carried out to investigate properties such as powering, cavitation patterns, and vibration levels.

Tanaka et al. (1999) have developed a hull form of “wave-locking catamaran”, a new type of catamaran aiming at locking the wave-making phenomena between the demi-hulls. It has been also demonstrated by model experiments that the locked waves can be reduced

with a wing or pod in which the propulsion unit is housed.

Scragg et al. (1998) developed a hull form of a SWATH-type catamaran called *SEA SHADOW*. The LOA of the hull was 50 m and was optimized to minimize its resistance at the speed of 13 knots. The wave patterns both in model and full scale were measured to validate the design.

Kang et al. (2001) optimised the shape and location of the side hulls of a 2500 ton class trimaran. Wave resistance calculation was performed to find the best location of side hulls at two different Fr and the results were confirmed by towing tank tests.

Sailing vessel design. Milgram (1998) reviewed the implementations of fluid dynamics in modern sailing vessel design. The review includes experiments, theories, computational methods and especially the existing methods used in VPP (velocity prediction program) for modelling air and water forces acting on the vessel. The evaluation of designs and design ideas, the decomposition of the force components, towing tank testing, individual resistance components, and the computation of lift and induced drag of sails were also discussed.

2.2. Propulsion

Propeller-hull interaction. The detailed information on the wake of a propeller working behind a solid body is indispensable for understanding propeller-hull interactions and for developing turbulence models suitable for such flows. Sirviente & Patel (2000a, b) measured mean velocity, turbulence, and pressure fields in the wake of an axisymmetric body propelled by a jet with or without swirl or by a rotating propeller. They found that the wake evolves in three distinct stages: a zone close to the jet exit where the jet periphery mixes with the wall region of the body boundary layer, an intermediate region where the mixing between the

boundary layer and the jet spreads up to the axis, and the region where the two flows lose their identities to become a single shear layer of negligible turbulence production.

CFD methods also have been used to predict flow fields around ships with propeller. Bugalski (1997) reported a RANS method for prediction of self-propulsion parameters of a Wigley hull. Relevant contributions to this subject have also been provided by papers presented at the Gothenburg 2000 Workshop (Larsson et al., 2002), as discussed in Section 4.2. Maksoud et al. (2000, 2002) calculated unsteady turbulent flow fields around the KCS (KRISO Container Ship) model with and without propeller. Chou et al. (2000) and Tahara et al. (2000) also reported the numerical results for the KCS with and without propeller.

The above CFD methods indicate that unsteady simulation of a self-propulsion test will become feasible in the near future with fast growing computing power and with continuous efforts to improve mathematical and physical models involved in the propeller-hull interaction problem.

Rudder-propeller interaction. The influence of the propeller slipstream on the rudder resistance can be more important than the thrust increase due to the presence of a rudder, which decelerates the propeller upstream flow. Simple theoretical models based on linear theory or on experimental results are not sufficient for correct prediction of parameters for rudder hydrodynamics. Laurens & Grosjean (2002) used a Boundary Element Method (BEM) code to simulate unsteady flow fields around a propeller and a rudder. The code adopted the body thickness representation to enable accurate surface pressure distributions both on rudder and blades. El Moctar (1999) and Simonsen (2000) performed full Reynolds-averaged Navier-Stokes (RANS) simulations on the rudder-propeller interaction problem. The RANS approach still requires considerable computer re-

sources and would render the system too complex for practical applications.

Yoon et al. (1999) performed self-propulsion tests for KCS and a 98K crude oil tanker with different propeller and rudder positions. They found that the relative position of the propeller and rudder were influential on self-propulsion factors.

Rowing. Rowing, in addition to being a popular water sport, is an efficient way to propel a boat with human power. Doi et al. (1999) simulated the boat motion, the angular motion of the oar, and the motion of the rower. They also carried out full-scale measurements. They concluded that a boat runs faster as the outboard length of an oar becomes longer, as the blade area of an oar becomes larger, as the stroke length becomes larger, and as the timing of blade immersion, “catch”, becomes earlier.

2.3. Waves and Free-Surface Effects

Breaking waves. Wave breaking processes have been the subjects of extensive experimental and numerical investigations in the last few years. A detailed review, mainly on spilling breaking condition, is provided in Duncan (2001).

Brocchini & Peregrine (2001a, 2001b) addressed breaking waves with intention of developing a comprehensive theory, which can describe the dynamic of the turbulence for this type of flow. Hong & Walker (2000) presented a formulation for the Reynolds-averaged flow near a free surface, using a newly developed governing equation to address the evolution of a surface current in high Froude number jet flow.

Tulin (1996) presented a numerical investigation on the effects of surface tension on the jet development. In the study, carried out with the aid of a potential flow solver, waves of different length are followed along their evolution toward the breaking. As the wavelength is decreased, surface tension forces are relatively increased and modifications occur to the jet: initially its tip is rounded and finally

initially its tip is rounded and finally the jet is suppressed and replaced by bulge on the crest of the wake. Due to the adopted model, the flow was simulated only before the jet impact.

The growing of the bulge was also shown by some calculations of Longuet-Higgins (1997). Based on potential flow assumptions (with and without surface tension) he also showed the appearance of a train of *parasitic* capillary waves upstream of the leading edge of the bulge (referred here as the toe).

Surface-tension effects on the bulge capillary system have also been addressed numerically by Cenicerros & Hou (1999), where results for a wide range of surface tension coefficients are reported. Furthermore, by modifying a BEM for water waves to include weak viscous effects, they show the ability of viscosity in suppressing these capillary waves.

These parasitic capillaries waves were indicated as a possible source of vorticity shedding initially by Longuet-Higgins (1992). Numerical computations of Mui & Dommermuth (1995) and experimental measurements by Lin & Rockwell (1995) confirmed Longuet-Higgins' calculations. In a later paper, Longuet-Higgins (1994) suggested that the vorticity shed by these capillaries (named Type I) may also explain the unexpected appearance of longer capillary waves above the toe (named Type II), propagating downstream, experimentally observed by Duncan et al. (1994). In his theory, Longuet-Higgins assumed that these Type II ripples might be primarily caused by shear flow instabilities induced by the vorticity generated by the Type I capillaries. In two later papers Duncan et al. (1999) and Qiao & Duncan (2001), by performing an experimental study on gentle spilling breakers generated by the wave focusing technique, observed that when the bulge becomes fairly steep the toe begins to move, sliding down on the forward face of the wave. He also argued that the Type II capillaries were likely induced by an instability of the shear layer generated between the downslope flow of the bulge and the underlying upslope incoming flow. Lin & Perlin (2001) performed

an experimental investigation of near-surface flow beneath gravity-capillary waves. If the steepness exceeds a threshold value, parasitic capillary ripples are generated. Velocity and vorticity fields are obtained from the experiment, and compared with Longuet-Higgins's theoretical model, and with numerical simulations by Mui & Dommermuth (1995). PIV measurements of instantaneous velocity field under a breaking wave are also reported in Chang & Liu (1998). Fluid particle accelerations and vorticity distributions derived from the velocity measurements are also provided in it.

Beside the experimental activities, several computational methods have been applied to the study of two-dimensional wave breaking flows. Iafrafi et al. (2000) and Chen et al. (1999) numerically simulated the wave breaking flow by using a two-fluid Navier-Stokes modelling suitably coupled with interface capturing techniques. Surface tension effects are included but physical properties are not always the same as those in the experiments. Also, since the calculation is two-dimensional, turbulence effects might not be reliable. In spite of these limitations, the free surface evolution appears to be in agreement to the experimental observation (Bonmarin, 1989).

Bow and stern flow. The need of reducing the hydrodynamic noise and the air-entrainment at the sonar dome, responsible for the remote sensing of ships, has motivated an intense numerical and experimental activity on the flow around the bow of a flared ship and on the bubble dynamics behind the stern.

Dong et al. (1997) and, more recently, Roth et al. (1999) performed detailed PIV measurements intending to resolve the flow structure within ship bow waves. By taking measurements on planes orthogonal to the wave crest, it is shown that vorticity is formed near the toe, and further downstream, this shear layer lengthens and encompasses the entire forward face. Vorticity of the opposite sign has been observed, but its origin is not clearly identified.

Tulin & Landrini (2000) numerically studied the bow flow through a 2D+t approach by using a smoothed particle hydrodynamics (SPH) technique to handle the complex free surface flow. The method is based on the solution of Euler's equation, so that vorticity effects are included while viscosity is neglected. Some relevant aspects of the vorticity production due to the jet impact are qualitatively recovered. It is seen that a very important role in the development of the vorticity field is played by the beam growth of the ship section when moving toward midship. In particular, the beam growth in the 2D plane behaves like a wave maker whose motion generates an intense breaker. The jet impact gives rise to the formation of counter-rotating vortex structures and good qualitative agreement with experimental observation was obtained.

Simulations of the viscous flow about the bow have been carried out by Sussman and Dommermuth (2000) through a Level-set approach to capture the interface location. Although promising, the results are not yet reliable due to the poor grid resolution employed. However, this kind of approach can well represent the effects of vorticity dynamics onto the free surface flow.

Concerning the bubbly flow past the ship stern, Smirnov et al. (2001) developed a random flow generation technique to describe the dynamics of bubbles in the turbulent flow behind a ship. This approach uses the RANS solution at the stern plane to start the large-eddy simulation (LES) calculation in the wake and an appropriate model is introduced to describe the dynamics of bubbles in the turbulent flow.

LES and DNS and free-surface turbulence. Considerable computational works have been done in the last few years to characterize hydrodynamics near a free surface. In Zhang et al. (1999), direct numerical simulations (DNS) of Navier-Stokes equations with linearized viscous free-surface boundary conditions are used to infer information on the three-dimensional

vortex dynamics and viscous effects when an oblique vortex ring impinges on a free surface flow. The distinction of an outer "blockage" layer and an inner "surface" layer near the free-surface region is introduced. The vortex connection time dependence on the main non-dimensional parameters is also investigated.

An attempt to computationally clarify the turbulence/free-surface interactions can be found in Nagaosa (1999). The main goal of the paper is to study the dynamics of the tube-like coherent structures and turbulent scalar transfer associated with the vortex/surface interactions. A free-slip wall condition as an approximation to the free-surface evolution has been employed.

The "free-surface boundary layer" has been computationally and analytically studied in a recent work by Shen et al. (2000). The DNS data are used to confirm the predicted theoretical behaviour and the scaling properties of such a boundary layer. A new "function model" for LES of turbulent flows near a free surface is also introduced. Shen & Yue (2001) also investigated via LES the interaction of a turbulent shear flow and a free surface flow at low Fr .

Moving contact lines. The hydrodynamics of moving contact lines, *i.e.* lines of intersection between a solid body and a free surface, has drawn the attention of CFD researchers engaged in free-surface computations, because of the apparent contradiction between the solid wall boundary condition and the moving free surface. Stoev et al. (1999) investigated the effects of inertia on the hydrodynamics in the microscopic vicinity of moving contact lines. Experiments have been carried out at low capillary number ($Ca < 0.1$) and in the range of negligible (10^{-4}) to moderate (≈ 1) Reynolds number (Re) based on capillary length. It is found that, on a microscopic scale, inertia decreases the dynamic curvature of the free surface near the contact line and, on a macroscopic scale, it lowers the apparent contact angle.

2.4. Viscous Flow

Stern longitudinal vortices. A pair of longitudinal vortices formed near the bilge at the stern of a full hull form has strong influence on the flow behaviour such as the deformation of the wake pattern at the propeller plane into the “hook” shape. They also consume energy and induce drag.

Okamoto & Matsuda (1999) devised a method to utilize the hydrodynamic energy of the vortices by installing a fin on the hull side upstream of the propeller. They combined the method with another energy-saving device attached on the rudder bulb downstream of the propeller, and tested the idea by carrying out towing tank experiments on three different model ships.

Fish motion. Fish are good swimmers and the motion of a fish can be viewed as a novel form of marine propulsion and manoeuvring. Triantafyllou et al. (2000) reviewed recent experimental and theoretical studies to identify the principal mechanism for producing propulsive and transient forces in oscillating flexible bodies and fins of both live and robot fish in water, through the formation and control of large-scale vortices.

The boundary layer developing on fish is a target for drag reduction studies. Anderson et al. (1999) measured, using PIV, the velocity profile in the boundary layer developing on live and robot fish. They observed that the measured velocity profiles had unique features such as a high-speed event close to the wall, and were significantly different from the laminar profile on a flat plate.

2.5. Turbulence

LES and DNS. The development of LES and DNS is rapidly growing in hydrodynamic research. While DNS is able to resolve the essential turbulence scales without any approximation, it has to be limited to low Re . With the LES approach, only the large scales (grid-scale)

are resolved explicitly, while the motions from subgrid-scale (SGS) have to be modelled.

Using a DNS approach, Na & Moin (1998) have provided statistical information on the kinetics, and structural features of a spatially evolving separated turbulent boundary layer over a flat plate. Such a detailed investigation provides also a comprehensive database for improving turbulent models. Coleman et al. (2000) carried out DNS of time-developing strained-channel flow as idealization of pressure-driven three-dimensional turbulent boundary layer. In broad terms, the study helps in clarifying several unanswered questions related to the effects of mean three dimensionalities with and without the mean deceleration of an adverse pressure gradient. As before, an understanding of these mechanisms might provide help in facing several modelling issues.

An overview of LES, the present status of development of this technique, and some of the challenges that lay ahead can be found in a recent review paper by Meneveau & Katz (2000).

Turbulence property at high Reynolds numbers. One of the important characteristics of the flow around ships is that it is a high Re flow. Computation of such flows using RANS equations necessitates the use of turbulence models but all turbulence models existing at present are based on experimental data at relatively low Re and therefore their validity at high Re is open to question. In order to clarify turbulence properties at the high Re range, De Graaff & Eaton (2000) put an entire circulating wind tunnel in a pressurized chamber and measured turbulence of a flat plate boundary layer in the Re range of $R_\theta = 1.43 \times 10^3$ to 3.1×10^4 , approximately corresponding to $Re_x = 5.6 \times 10^5$ to 2.6×10^7 , with a high-resolution LDV. The wall-normal Reynolds stress and Reynolds shear stress collapsed fairly well onto self-similar solutions in classic inner scaling, but the streamwise Reynolds stress seemed to suggest that its proper scaling is $u_\tau^2 (2/C_f)^{1/2}$ where u_τ is the friction velocity.

Osterlund & Johansson (1999), in a wind tunnel, also measured flat plate boundary layers in the Re range of $R_\theta = 2500$ to 27000 using hot film and hot wire techniques.

Full-scale boundary layers. In the sonar dome of a 151 m-long ship, Sato et al. (1998) installed an LDV system housed in a 48 mm diameter circular cylinder, and measured velocity profiles across the boundary layer up to 384 mm from the surface, and at speeds up to 18 knots. The measured velocity profiles agreed well with $1/7$ power law.

2.6. Drag Reduction & Bubbly Flow

Drag reduction methods. The development of drag reduction technology is important from the point of view of energy conservation of ships as well as transport systems of all kinds. Major components of the drag exhibited on ships moving near the free surface are wave drag, viscous pressure drag and friction drag, among others. Drag can be reduced by diminishing boundary layer thickness, controlling flow separation or by modifying the shape and considerable progress has already been achieved in this area. However, the reduction of friction drag is far from a practical realization in spite of the recent extensive experimental and computational studies on the details of the turbulent structure near the surface.

The intention of the present section is not to discuss drag reduction methods in whole since many of those are already well understood but rather to concentrate only on the friction drag reduction technologies. The International Symposium on Seawater Drag Reduction (Newport, 1998) and the 1st and 2nd Symposium on Smart Control of Turbulence (Tokyo, 1999 and 2001) are major sources of recent research activities in the field.

The major contributors to the friction drag are fluid viscosity, Reynolds stresses, coherent structures and pressure fluctuations. Careful examination on each of these components will

be necessary if significant drag reduction is to be achieved (Hoyt, 1998).

Since the shear stresses of both the laminar and turbulent flow depend on the viscosity the very first idea to reduce the friction drag would be reducing fluid viscosity. The flow viscosity may be reduced by heating the water or by introducing a fluid with lower viscosity around the body surface. The effect of reducing the molecular viscosity on the drag at typical full-scale Reynolds numbers is rather small. With the same reasoning, delay of transition or laminar flow control (LFC) will not be effective for ships.

The most popular turbulent drag reduction methods at present can be categorized as active control methods utilizing wall motions, spanwise fluid motions or electromagnetic force; passive methods using Riblets, LEBU's and compliant coatings; and additive methods injecting polymer, surfactant, air or microbubbles and more details of the methods will be discussed below.

Near-wall turbulence. With rapid development of experimental and computational methods, much of details on the near wall turbulence have been revealed. Meng (1998) summarized the latest findings on the geometrical patterns and the dynamics and cause-effect relationships of near-wall microturbulent events. Horseshoe or hairpin-shaped vortices are the most frequently recurrent patterns in the boundary layer and low speed streaks also are the result of the vortex motion (Zhou et al., 1997). The spacings $\lambda^+ = \lambda u_\tau / \nu$ between both the hairpin vortices and the streaks are around 100 for Newtonian flow with the kinematic viscosity. The streaks terminate by lifting away from the wall (ejection), oscillating, then bursting and followed by sweeps of new, higher-speed fluid entering the region. The bursting is believed to be a major source of Reynolds stress which dominates the viscous stress and has the maximum values at $y^+ = y u_\tau / \nu$ of about 30. With proper control of the above so-called

‘ejection-burst-sweep’ process, the friction drag can be reduced efficiently.

Injection of additives. Injection of additives such as the polymer, surfactant or fiber suspensions, and possibly microbubbles (Merkle et al., 1990), into the boundary layer can dramatically reduce the Reynolds stress almost to insignificance and the friction drag as much as 60% by decorrelating the axial and transverse fluctuating velocity components. The drag reduction is not as great as the decrease in the Reynolds stress due to the existence of coherent structures. In the polymer solutions λ^+ becomes substantially larger and the burst rate, a major source of the Reynolds stresses, is also reduced more than 50%. But it is not clear yet whether the polymers affect the hairpin vortices or not (Hoyt, 1998). Surfactants of rod-shaped structures are also effective for the drag reduction of turbulent flow and claimed to be more effective than the polymer additives since defragmented structures in the strong shear flow tend to rebound as soon as the shear weakens. Many researches for the application to the practical engineering problems including pipelines and heating and cooling systems are also reported recently (Gasljevic, 1998).

Injection of polymers or surfactants may be too expensive and not environmentally friendly; efficient methods for retrieval of additives downstream may be necessary if used for drag reduction of real ships.

Passive devices. It has been known that compliant coatings can delay transition of boundary layers to turbulence by suppressing the growth of Tollmien-Schlichting waves (Davies et al., 1997). The same group investigated the effect of compliant rotating disk and shows that compliant wall has a stabilizing effect on the Type I inviscid instability while the Type II viscous instability, caused by the Coriolis acceleration, is stabilized only when the compliance of the wall coating is increased (Cooper et al., 1997). Recently, it is found that compliant coatings also reduce skin friction drag and pressure fluctuations up to 7% and 19%, respectively (Kulik et al., 1996, Choi et

al., 1997). The results also indicate reductions in turbulent intensity of up to 5% across almost the entire boundary layer and upward shift of the logarithmic velocity profile, indicating thickening of viscous sublayer. See also Gad-el Hak (1998).

Riblets are small V-shaped grooves extending in the axial flow direction. The riblets appear to suppress the lateral motion and spreading of the low-speed streak. Drag reductions of about 8% seem obtainable if the groove size is adequately tailored to the flow. It is also reported that the transition of an excited laminar boundary layer is significantly delayed by the riblet surface (Choi, 1999).

A considerable improvement in drag reduction is obtained in recent years by optimising the shape of riblet systematically and as much as 10% of drag reductions are achieved in an oil channel (Bechert, 1997). Riblets have been employed in several Olympic events, America’s cup races and are offered to the US military airplanes and Airbus A340 to save weight of paint as well as to provide drag reduction (Bushnell, 1998). It is pointed out, however, that the heights of riblets for full-scale ships are too small to be applied practically (Kodama et al., 1999).

Large-eddy break-up devices have been used to control large-scale coherent structures for the purpose of drag reduction. LEBU’s have been successful in reducing the skin friction just behind the devices and skin friction can be reduced as much as 40% but unfortunately create a drag themselves which cancels out most of the gains thus obtained. The passive devices involve small length scales and may be vulnerable to fouling.

Active controls. With knowledge of the near-wall turbulence that it has rather orderly coherent structure and cause-effect relationships, it has become possible to devise methods to disrupt the turbulence production chain of ejection-burst-sweep (Meng, 1998). In the early stage of the application, results of DNS and LES indicated that considerable reduction in

friction drag is possible with such methods but experimental evidence has only come out quite recently. Choi et al. (1998) reported that 45% reduction in friction drag is achieved within five boundary layer thickness by suppressing near-wall burst activity. Breuer et al. (1998) successfully used a feed-forward algorithm to moderate the turbulence intensity in the near-wall region of a fully turbulent boundary layer. Over 30% reduction in turbulent intensity is achieved with three sensors and three micro-jet actuators downstream, apart 40 times of the viscous length scales each other in the span wise direction.

Studies using a micro-electromechanical system (MEMS), an integrated array of micro-sensor and micro-actuator, are increasingly popular in these days (Yoshida et al., 1998, Segawa et al., 2001). Possibility of controlling wall turbulent boundary layer by applying unsteady Lorentz force perpendicular to the wall is studied recently but no apparent drag reductions are evidenced by experiments yet (Bandyopadhyay et al., 1998, Eidelman et al., 1998, Thibault et al., 1998).

At the present stage, the methods for active control of turbulent boundary layer seem to be too expensive and technically premature for practical use and further development in technologies for, for example, micro-fabrication of MEMS will be necessary.

Laminar-flow control. As discussed earlier, LFC will not be effective for drag reduction of a ship since the shear stresses of both the laminar and turbulent flow depend on the fluid viscosity which is relatively insignificant comparing to the other components of the drag as the Re is increased to the values of typical ships.

In aircraft industries, however, LFC has been extensively studied to reduce skin friction of wings, tails, and engine nacelles. Because of the similarities in the geometry and the Re range, the knowledge may be also useful for designs of marine hydrofoils and propellers. LFC is usually implemented by air suction through slots or minute holes. Joslin (1998)

reviewed LFC in the period from 1930s through 1990s as well as the recent status. He showed that the significant technological advancement is HLFC, a combination of natural laminar flow and LFC to reduce suction requirements and system complexity. He also discussed flow physics of boundary layer, manufacturing tolerance, insect-contamination avoidance, and experimental studies on slot-, porous-, and perforated-suction studies in flight and at wind tunnel.

Bubbly flows and drag reduction. Bubbly flows are mixture regions of low gas contents where individual bubbles of irregular shapes, clusters of bubbles and gas packets are surrounded by a continuous liquid medium (Chanson, 1996). Bubbly flows play significant roles in various engineering problems involving liquid and gas.

Bubbly flows are easily formed beneath the air-water free surface in high velocity flows by mixing or wave breaking. Bubbly flows are important in ship signature problems since it can modulate acoustic fields by scattering and attenuation. The bubbles formed beneath breaking waves or within ship wakes can provide optical scattering and back scattering. Furthermore, bubbly flows can reduce turbulence intensity and so the ship drag.

The effectiveness of the bubbles on the drag reduction depends on sizes, positions (Kato et al., 1999) and contents of the bubbles. It has been reported that micro-bubbles whose diameters are order of few μm 's can be generated by electrolyses or through porous plates and injected into the turbulent boundary layer to reduce the drag up to 80% as reviewed in Merkle & Deutsch (1990) in detail. However, these accomplishments do not guarantee reduction of ship drag with micro-bubbles since almost all of those are achieved in the laboratories for simple geometries. And the scale and three-dimensional effects should be understood before being practically applicable. However, the most serious flaw obstructing the utilization of the micro-bubbles is that the energy necessary

for micro-bubble injection usually exceeds the gains from drag reduction and an efficient method for bubble injection should be found before practical implementation become possible.

Computational investigation of bubbly flows also has been done to understand the underlying mechanisms. Bubbly flows are modelled as a transport of a single and multiple bubbles (Smirnov et al., 2001) or as two-phase flows (Kato et al., 1998) in which local properties such as density, viscosity and mixing length are modified according to the void fraction. The results indicate that the scale effects and bubble interactions in the turbulent boundary layer should be more closely studied before a full-scale application is possible. Recently, new numerical tools using the Lattice Boltzmann model have been introduced and show good possibility of simulating two-phase flow efficiently (Rothmann & Zaleski, 1997).

Instead of injecting micro-bubbles into boundary layers, a thin layer of air may be formed over the wall to lubricate and reduce skin friction. Indeed, such an air lubrication method has been practiced extensively for a long time, in Russia, and considerable reductions in ship resistance have been reported. The air layer or the air cavity has to be maintained as thin and stable as possible to avoid increase in form drag and to obtain net energy gains. And not only the air supplying devices but also the hull geometries, motions and attitudes also have to be carefully controlled. Employing water repellent paints (Fukuda et al., 2000) and bottom steps are also a part of measures to stabilize the air cavity. Recently, the technologies are applied to high-speed ships, including a semi-planning passenger ship and high-speed Catamarans to show considerable increases in ship speeds (Jang et al., 1999, 2001, Latorre, 1997).

At the present stage, it seems that use of air is the only method appropriate for ship application since the air is inexpensive and not harmful to the environment. However, the scale and three-dimensional effects, efficient ways of

stabilizing the air cavity and injecting and maintaining micro-bubbles inside the turbulent boundary layer have to be found before rigorous applications are possible.

Drag increase by bio-films. Understanding and prevention of drag increase due to marine fouling is as important as drag reduction. Schultz & Swain (1999) compared turbulent boundary layers on natural marine bio-films and a smooth plate. The average increases in C_f for slime films with mean thickness of 160 μm and 350 μm were 33% and 68%, respectively. The average increase in C_f for a surface dominated by filamentous green algae with a mean thickness of 310 μm was 190%. Waving algae filaments seemed to draw a greater amount of momentum from the mean flow than do slime films alone.

2.7. Conclusions

Numerous studies have been conducted concerning turbulent flow, waves and free surface effects, propeller-hull interaction, and drag reduction and bubbly flow offering considerable insight and in some cases useful models for improving physical understanding of ship resistance; however, more effort is needed in transitioning these developments for implementation in current ship hydrodynamics CFD codes and practical applications. More work is needed on full-scale physical understanding and modelling.

3. TRENDS IN EXPERIMENTAL FLUID DYNAMICS

3.1. Introduction

This section summarizes trends in EFD, i.e. developments in experimental techniques used in towing tanks, circulating water channels, and wind tunnels, mainly in the past three years since the last 22nd ITTC Conference. In the next subsection, new developments in meas-

urement techniques are reviewed for measuring velocity and vorticity, flow visualization, pressure, skin friction, free-surface waves, bubbly and cavitating flow, body motion, forces and moments, and uncertainty analysis. In the third subsection, new developments in experimental facilities, model manufacture, and measurement systems are reviewed, based on the results of the questionnaire. Finally, in the fourth subsection, conclusions are given.

3.2. New Developments in Measurement Techniques

Velocity and vorticity.

PIV/PTV/tracers: PIV/PTV techniques, being based on flow visualization using tracers, TV cameras, and image processing, can measure velocity at multi-points simultaneously. Intensive research continues, and not only two-component but also three-component measurement is becoming a standard procedure. Interested readers should read the proceedings of an annual conference devoted to PIV.

Application of PIV/PTV to ship-related flows increases. Gui et al. (2001a) developed a towed PIV system for a towing tank. The light from a 20 mJ YAG laser is guided through a strut to a submerged torpedo, from which the light sheet is emitted. Tracer images are recorded by a digital camera housed in another submerged torpedo. Using the system they measured the mean three-component velocity and Reynolds stresses in the nominal wake of a 3 m-long DTMB 5512 ship model. The mean velocities agreed well with 5-hole pitot probe data, except that V and W components near the ship hull showed disagreement up to 20%. Nishio et al. (1997) developed a simple PIV method that measures three mean velocity components using a single light sheet and a TV camera and the statistical analysis of temporal and spatial gradients. They applied it to measure ship wake in a circulating water channel. A PIV technique was used in a cavitation tunnel

to measure the evolution of the wake of a marine propeller including tip vortex and hub vortex in a uniform flow, showing tip vortex instability leading to breakdown (Cotroni et al., 1999). Kim et al. (2001) applied the wavelet transform method to analyse PIV images using a correlation method, and reduced CPU time to 1/3 for a single application.

Recent developments in both EFD and CFD have increased the demand for instantaneous full-field 3D flow velocity measurements resolved in space and time. Pu & Meng (2000) developed an off-axis holographic PIV (HPIV), in which 90 deg scattering, dual reference beam recording, and *in situ* reconstruction are used. Using the system, they measured hairpin vortices in the wake of a surface mounted tab, and obtained 80000 3D velocity vectors in the measurement volume. Prasad (2000) reviewed the trends in stereoscopic PIV techniques for in-plane measurement at instantaneous time, so-called (3,2,0) methods, and discussed stereoscopic configurations, error analysis, and reconstruction methods, in which he showed relative merits of calibration-based reconstruction in comparison to geometric reconstruction.

Anderson et al. (1999) measured the flow near the wall, less than 1 mm, over free-swimming live or robot fish using PTV. The result suggested that the most part of the boundary layer was laminar. The near-boundary flow around a yaw-free swimming robot fish (MIT *Robo Tuna*) was measured in a circulating water channel (Techet et al., 1999).

Pereira et al. (1999) developed a new technique called defocusing DPIV, which uses defocused multiple images of a bubble formed through three separate apertures at the lens and measures bubble size and 3D bubble location simultaneously.

LDV (LDA): For propeller flows, detailed information on propeller wake evolution is needed for turbulence modelling and validation of CFD. Stella et al. (2000) measured the wake

of a propeller operating in uniform flow using two-component LDV with phase sampling, and elucidated the flow structure including the formation of viscous blade wake, the roll-up of trailing vortex sheets, the slipstream contraction, and the turbulent diffusion.

Turbulence characteristics in boundary layers at very high Re are important for ship flows. But their measurement is difficult because the viscous scale becomes very small at such high Re and therefore high resolution is needed. In order to measure turbulence characteristics in such flow in a pressurized wind tunnel, De Graaff & Eaton (2001) developed a high-resolution two-component LDA with the measurement volume size of $35\ \mu\text{m}$ in diameter and $60\ \mu\text{m}$ in length. The system used three laser light beams, i.e. one 7 MHz frequency-shifted beam for the streamwise velocity component, one 5 MHz frequency-shifted beam for the wall-normal velocity component, and one common reference beam, thus avoiding the need for coincidence windows, which are necessary in conventional two-colour systems.

There were only a few full-scale flow velocity measurements in the past few years, in spite of their importance. Sato et al. (1998) measured the boundary layer on a sonar dome in the bow of a 150 m-long ship using LDV, which was installed in a thin circular cylinder with a focusing lens at the outer end, so that, by sliding the cylinder through a plug, the measurement location moved from zero to 384 mm from the surface. The measured result agreed well with $1/7$ power law. Becker et al. (1999) developed an LDA system for measuring velocity and turbulence on an airplane wing in the flight for testing laminar wings. In order to detect light signals from aerosols of size less than $1\ \mu\text{m}$, which are dominant in the in-flight condition, they used Nd-YAG laser as light source, near-forwardscatter mode, and BSA for signal processing, thus increasing the light signal power by two or three orders of magnitude compared with the previous design. The system was in-

stalled on the wing of a powered sailplane, and velocity and turbulence were measured.

Hot wire: The developments for multiple hot wires with more than three sensors continue. Holzäpfel et al. (1999) developed a quintuple hot wire system where all five wire elements extended radially from the center at equal angles, and measured velocity and Reynolds stress components of a swirling flow in a model combustion chamber. Zhu & Antonia (1999) made a new device that measures all three components of vorticity vector simultaneously by four sets of X-wire probes arranged to form a square whose separation distances between the centers are 2.5 mm. They measured wake of a circular cylinder and turbulent channel flow, and, after correction for the sensor separation, obtained good agreement with other measurement and DNS computation.

Pressure probe: Tsukada et al. (1997) applied a conventional five-hole pressure probe of modified NPL type to measure wake distribution of a ship advancing in regular head waves or a ship in forced pitch motion. The ship was a training ship with $C_b = 0.519$. They first confirmed time response and then measured the wake. They observed increase of wake parameter $1-w$ in both “in wave” and “forced pitch” conditions.

Efforts on seven-hole probe systems continue in aerodynamics. Rediniotis & Vijayagopal (1999) developed a series of five-hole and seven-hole miniature pressure probes whose tip diameter was 0.9 mm. They also developed a backpropagation-based neural network calibration algorithm. They applied the system to a uniform flow in a wind tunnel, and obtained accuracies of 0.28 deg in the flow angles and 0.35% in the velocity magnitude. Wenger & Devenport (1999) developed a seven-hole pressure probe system to measure three mean velocity components. The probe consists of a cylinder of 2 mm diameter, having a conical tip with one hole in the center and six holes on the cone side of 30 degrees semi-

vertex angle. They devised a two-step calibration scheme that involves interpolation of error look-up table. They measured pipe and wind tunnel flows, and found Re dependence.

Ultrasonic waves: Desabrais & Johari (2000) measured circulation around a tip vortex directly in a wind tunnel, by using the Doppler effect of ultrasonic waves along a rectangular path with four sides surrounding the tip vortex.

Flow visualization. Tufts and oil film are conventional techniques for surface flow visualization. Ostafichuk et al. (2000) used the two techniques to visualize the flow around a semi-submersible vehicle model in a wind tunnel. First, they used yarn tufts attached to the main body to measure local flow angle at positions of three control planes. Second, they used oil film to measure separation region on each control plane. They observed root separation. They also used soap bubbles filled with helium gas for neutral buoyancy. The diameter of the bubbles was 1.5 mm. The bubbles showed streamlines and visualized the tip vortex from the bow plane.

The visualization of the flow away from a body surface is carried out using tracer techniques. Many of the PIV techniques already described in this subsection can be regarded as such tracer techniques. In addition, Hoyt & Sellin (1998) made a new tracer formulated from a surfactant-polymer-emulsion mixture, and injected it from a small tube into the turbulent boundary layer near a solid wall at a speed equal to the local flow speed, so that the injected tracer maintained its cylindrical shape long enough to visualize hair-pin vortices.

Pressure. Surface pressure fluctuations of high frequency play a dominant role in wall turbulent flows and flow noise. Lee & Sung (1999) developed an array of pressure sensors made of 28 μm thick PVDF film with 4×10 circular sensors of 3 mm diameter and 6 mm spacing. They applied it to wall turbulence and obtained good agreement with existing studies.

Pressure-sensitive paint (PSP) emits luminescence whose intensity is inversely proportional to absolute pressure due to “oxygen quenching”, and therefore can measure surface pressure by measuring the ratio of the intensity of the luminescence in “wind-on” and “wind-off” conditions. Using PSP, one can measure continuous surface pressure distribution, in contrast to pressure tap methods. Bell et al. (2001) reviewed the status of the PSP technique including several compensation techniques such as illumination compensation, to which the use of binary pressure paint, i.e., the additional use of pressure-insensitive reference luminophore, has been found to be the most effective. They also discussed the measurement uncertainty. PSP is usually applied to high-speed flows, but Merienne & Bouvier (1999) applied it to air speed as low as 24 m/s in a wind tunnel.

Skin friction. Methods for measuring skin friction, or wall shear stress, can be categorized into two, i.e., indirect and direct methods. Indirect methods include Preston tubes and hot-film gauges, where measured quantities such as total pressure and surface heat flux are related to skin friction. Direct methods commonly use a floating element technique, where no assumptions have to be made to relate the skin friction to the measured quantities. For review, see Hanratty & Campbell (1996).

Pan et al. (1999) and Hyman et al. (1999) developed microfabricated skin friction sensors with on-chip signal amplification electronics using MEMS technique. The sensor had a floating element, which was of the size of the order of 0.1 mm, operated in active modes such that the element did not move, and acted with resonant frequencies over 10 kHz, which should be particularly useful in measuring turbulence. Direct methods can be applied to multiphase flows. Kodama et al. (2000) used commercial skin friction sensors of the floating element type, with a 10 mm diameter sensing disk and capacity of 2 gf full scale, to measure time-mean skin friction in bubbly turbulent boundary layer.

Liquid surface tracing is an intermediate between direct and indirect methods. The method has an advantage of global measurement over pointwise measurement by skin friction sensors mentioned above. Using nematic liquid crystal, Buttsworth et al. (2000) measured the skin friction distribution in the turbulent boundary layer triggered by a cylindrical bump. The method utilizes the twist of the liquid crystal due to skin friction, which is detected by measuring the intensity of the light that comes through the liquid crystal and two polarizers.

The surface hot film method is an indirect method. Sturzebecher et al. (2001) developed a “surface hot wire”, which is a flush-mounted thermal resistive wire with a tiny slot underneath to avoid conductive heat transfer to the surface and thus to obtain better signal-to-noise ratio and frequency response. Cut-off frequencies between 20 and 30 kHz were obtained at an overheat ratio of 1.7. A 20-sensor array was employed in flight experiments on the wing of a glider, and the Tollmien-Schlichting waves were measured in the velocity range of 23÷26 m/s.

Free-surface waves. Roesgen et al. (1998) developed a new optical technique for free-surface wave distribution measurement. The method uses microlens array and detects free-surface slope at typically 4000 points based on the spot displacement at the focal plane, and waveheight is then estimated. Nishio et al. (1998) used a laser light sheet to measure wave-height distribution around a ship model advancing in calm water or in periodical incoming waves in a towing tank. The light sheet was emitted transversely from the bottom of the tank, and the water surface was detected using the high contrast of illuminated light between air and water.

Gui et al. (2000) carried out an experiment for a DTMB 5512 model ship in regular head waves, and measured unsteady resistance, heave force, pitch moment and free-surface elevations both in near and far fields. The ini-

tial phase of the data was adjusted using the first FS (Fourier Spectrum) component.

Waves in the bow and stern regions of a ship are difficult both to measure and to compute, and significant disagreement often exists between the two. Stern et al. (1996) carried out detailed re-measurement of the bow wave of the Series 60 $C_B = 0.6$ hull using various techniques, but the disagreement remained, although slightly reduced. The difficulty comes from the facts that often bow waves on the hulls are very thin and that often the stern wave intersects with the hull surface at a very small angle. The difficulty occurs both in EFD and CFD, which therefore should cooperate to solve it.

Wave breaking around a ship’s body causes problems such as increase in resistance and deterioration in sound detection. Iafrati et al. (2000) carried out close observation of the wave breaking phenomenon that occurred behind a 2D submerged hydrofoil, by adding fluorescent substance in water and illuminating the water surface from both above and below. They observed ripples on the forward face of the second and third wave crests, before the breaking region reached the first crest and the breaking fully developed.

Wave breaking on the sea surface is believed to play a significant role in the transport phenomena such as CO_2 between air and sea. Siddiqui et al. (2001) measured momentum and heat transfer across microscale breaking waves, i.e., very short gravity waves occurring at low to moderate wind speeds (4 to 12 m/s), by the simultaneous measurement of the velocity field using PIV, the wave height distribution using laser sheet illumination for PIV, and the heat transfer rate by infrared imagery. Dynamic and 2D measurement of radiation and diffraction waves from a ship model advancing in waves is a technical challenge. Erwandi & Suzuki (2001) developed the Projected Light Distribution method and measured the wave to obtain Kochin functions.

To carry out full-scale wave measurement, Scragg et al. (1998) designed a wave-slope meter to be installed on a support vessel. The refraction of a laser beam emitted upward through the water surface was measured optically. The pitch and roll of the sensor was also measured. They applied the technique to the full-scale trial of the SEA SHADOW, a SWATH ship.

Bubbly and cavitating flows. In bubbly flows, the reflection of light from the bubble surface makes measurement difficult. A way to circumvent the problem is a PIV/LIF technique, in which a camera filter is used to get images of fluorescent light emitted from tracers, whose wave frequency is different from that of the incident light.

Nagaya et al. (2001) applied the technique to measure velocity of the fluid part in bubbly flows. Pereira et al. (1999) applied the defocusing DPIV technique to measure the motion and size of bubbles that passed through a propeller.

Stultz & Reboud (2000) measured void ratio inside unsteady cavitation using a double optical probe. The probe consists of two optical fibers fixed at a small distance from each other in the flow direction. Infrared light is emitted from each tip, and the phase, water or gas, is detected by the change of refraction, and further the flow speed by the time it takes between the two tips. The probe was set in the test section of a cavitation tunnel, and local void ratio and flow speed inside unsteady cavitation behind a bump were measured.

Waniewski et al. (2001) developed an impedance based void fraction meter (IVFM), which consisted of two concentric stainless steel electrodes between which 500 kHz excitation was applied. The impedance across the two electrodes increased with void fraction, and the output was low-pass filtered and demodulated to provide a DC signal proportional to the local void fraction. Using the device they measured

void fraction distribution in the bubble cloud generated by breaking waves.

Forces and moments. Gui et al. (2000) measured unsteady resistance, heave force, and pitch moment acting on a DTMB 5512 model ship in regular head waves. Talotte et al. (1997) developed a six-component dynamometer for sailing yacht testing in a towing tank while keeping heave and pitch free.

Sutcliffe & Millward (1998) developed a new dynamometer for yacht testing, and measurements of motion and resistance in earth and body axes were compared. Doi et al. (1999) developed a new testing device for rowing, and oar size and rowing pattern were investigated. Fujiwara et al. (1998) collected experimental data of wind forces and moments acting on ships of different types such as tankers, cargo carriers, container ships, and passenger ships.

Uncertainty assessment. The field of application of uncertainty assessment steadily increases. The uncertainty analysis for sinkage and trim, wave profiles, and wave elevations in towing tank tests are described in detail in Section 6. Gui et al. (2000), in the measurement of wave pattern around a DTMB 5512 model ship in regular head waves, carried out uncertainty assessment of raw time histories, FS harmonics, and FS-reconstructed time histories. Gui et al. (2001a) carried out uncertainty assessment for their wake measurement using PIV in a towing tank, and found that PIV uncertainties were about 1% lower than those for 5-hole Pitot tubes. Lalli et al. (2000) investigated main error sources in determining wave pattern resistance by the longitudinal cut method. In the experiments using a Series 60 and a hard-chine catamaran models, they found that two sources of uncertainty, i.e. the air pressure disturbance generated by the towing carriage motion and the unsteadiness of the free surface flow, play a significant role, and that they increase with the model speed. They also found that propagation of the experimental errors in wave resistance,

as determined via longitudinal cut, is significantly damped.

In order to improve the accuracy of measurements, sources of bias errors should be detected and removed. Gui et al. (2000) found that there was significant disagreement in the V and W velocity components near the ship hull measured by PIV and those by 5-hole Pitot tubes. They estimated the bias error in the 5-hole Pitot tube results due to large velocity gradient, and found that it has the magnitude comparable to the disagreement.

Chang & Liu (2000) showed, in measuring turbulence in wave-breaking, that the bias error (or pseudo turbulence) due to finite pixel resolution becomes significant if tracer particle size is comparable to pixel resolution and that the error can be reduced by subtracting pseudo turbulence component measured in non-breaking waves. De Graaff & Eaton (2001) discussed LDA bias errors in detail, i.e., fringe bias, velocity bias, and velocity gradient bias. Again, in order to improve the accuracy of measurements, it is instructive to look at data scattering in detail. Talotte et al. (1997) measured drag of two sailing yacht in a towing tank over 10 hours with 15 minutes stop between two runs, and obtained steady drifts of 1%.

3.3. Developments Related to Experimental Facilities

Research papers. Ogura & Tamashima (1996) showed a design procedure for a circulating water channel, and measured flow properties of a channel thus designed and equipped with a rotor-type surface accelerator and a ridge-type steady wave reducer. The flow uniformity within 1% in the test section was obtained at $U = 4.0$ m/s Callan & Marusic (2001), studied the influence of the aspect ratio, AR defined as the width/height, in the rectangular contraction section upstream of the working

section in a wind tunnel. The contraction section was rectangular, with AR=1 at inlet, and AR=1 to 4 at exit, while keeping the contraction ratio unchanged. For a given AR, at the exit of the contraction, the side wall boundary layer was thicker than that on the floor for AR>1, and the 45-deg corner boundary layer decreased with increasing AR.

Questionnaire on new experimental facilities et al. A questionnaire on new experimental facilities, new model manufacture, and new measurement systems was distributed to all ITTC organizations by e-mail. To those to which the e-mail did not reach, the questionnaire was sent by airmail. 43 responded, which were compiled and re-distributed by e-mail to all the organizations for confirmation and further questions. This time, 33 gave replies. The results are summarized as follows.

New experimental facilities: Table 3.1 summarizes towing tanks newly built or renewed in the past few years. There are two large towing tanks newly built in the past few years. In renovation of existing towing tanks, most of them have been aimed at high-speed testing. There was no reply on new circulating water channels or wind tunnels. The information on ocean engineering tanks and cavitation tunnels is not shown here. In today's world of internet, computers on a towing carriage are connected to the LAN on land. Table 3.2 summarizes the replies from ITTC organizations on the connection. About half of the organizations have some connections, and the majority has Ethernet wireless LAN at the speed of several Mbps.

New model manufacture: Table 3.3 summarizes the replies from ITTC organizations on new NC model manufacturing systems. The ones at HSVA and MARIN are the newest and the largest.

Table 3.1 Towing tank facilities newly built or renewed.

Org.	Year	Content
IHL, BPPT, Indonesia	1995	A new towing tank $L \times W \times D = 235.4 \text{ m} \times 11 \text{ m} \times 5.5 \text{ m}$ Max. towing speed = 9 m/s
SSMB, Korea	1996	A new towing tank $L \times W \times D = 400 \text{ m} \times 14 \text{ m} \times 7 \text{ m}$ Max. towing speed = 18 m/s A high-speed carriage (18 m/s), a low-speed carriage (5 m/s), and a sub-carriage for CMT.
Bassin d'Essais des Carenes, France	2001	A new towing tank (B600) $L \times W \times D = 545 \text{ m} \times 15 \text{ m} \times 7 \text{ m}$ Max. towing speed = 12 m/sec Model size: 4 m to 10 m Wave generator: Regular and irregular. 1m crest to crest
Ecole Centrale de Nantes, France	2001	Renewal of a towing tank $L \times W \times D = 148 \text{ m} \times 5 \text{ m} \times 3 \text{ m}$ (initially 70 m \times 5 m \times 3 m) Max. towing speed = 10 m/s (previously 5 m/s)
MARIN, the Netherlands	2001	Renovation of Depressurised Towing Tank Max. towing speed = 8 m/s (previously 4 m/s) Time to depressurise = 4 hrs (previously 8 hrs) Remote-controlled open-frame towing carriage (previously manned)
VBD, Univ. of Duisburg, Germany	2001	A new towing carriage in the shallow water basin Rail length = 150 m Unmanned, remote control Max. towing speed = 15 m/s

Table 3.2 LAN connection between towing tank carriages and land.

Equipped?	12 Yes, 13 No
Cable	10 Ethernet, 1 RS232C, 1 Unknown
Connection	7 Wireless, 3 Optical, 1 Detached while running, 1 Unknown
Speed (bps)	1 (9600), 4 (1 to 2 M), 6 (10 to 11 M), 1 Unknown

Table 3.3 NC milling system for ship models.

Organization	Year	Content
MHI, Japan	1994	Material: wood, wax Max. stroke: $L = 10.4 \text{ m}$, $B = 2.5 \text{ m}$, $D = 1.3 \text{ m}$
SSMB, Korea	1996	Material: wood Max. $L = 10 \text{ m}$, $B = 1.7 \text{ m}$, $D = 0.8 \text{ m}$
Univ. of Ulsan, Korea	1998	Material: wood or foam Maximum model size: $L = 2 \text{ m}$ Geometry data: NURBS
MARIN, the Netherlands	1999	Material: wood or foam Max. $L = 13 \text{ m}$, $B = 3 \text{ m}$, $D = 1.5 \text{ m}$. Geometry data: NURBS Transfer from CAD: IGES
KRISO, Korea	1999	Material: wood Max. $L = 10 \text{ m}$, $B = 2 \text{ m}$, $D = 1 \text{ m}$
HSVA, Germany	2000	Max. $L = 16 \text{ m}$, $B = 4 \text{ m}$, $D = 2 \text{ m}$.

New measurement systems: According to replies to the questionnaire, many organizations renewed or introduced data acquisition and reduction systems. As a new trend, 14 sets of optical, non-contact, 6-DOF ship motion measurement systems developed by Krypton were introduced to ITTC organizations in the past few years.

3.4. Conclusions

There is a steady trend from point measurements to distribution measurements such as PIV and PSP. New developments continue in optical techniques such as PIV, LDV, and non-contact motion measurements. New manufacturing techniques such as MEMS are used to develop new measurement devices such as skin friction sensors. Uncertainty analysis (UA) in experimental fluid dynamics (EFD) has not become a common practice yet, but it has widened its application area to more complicated derived quantities. At the same time, improvements in measurement accuracy have been reported in various papers, by identifying sources of bias errors and data scatter and quantifying such errors by estimating bias and precision limits. In spite of its importance, there have been few reports on new measurement techniques for full-scale testing. New construction and renovation of towing tanks continue. Most of them are aimed at high-speed testing. Wireless LAN is the most common communication tool between the towing carriage and land. New NC manufacturing machines for ship models of length over 13 m have been constructed.

4. TRENDS IN COMPUTATIONAL FLUID DYNAMICS

4.1. Introduction

This chapter summarises the ongoing research effort toward the development of efficient numerical tools in the area of computational hydrodynamic analysis and design of ships, reporting trends in research and experience in industrial applications as emerged from the literature of the last three years. A summary of main results and conclusions coming out from the Gothenburg 2000 Workshop (G2K) on CFD open the section (4.2). After a paragraph on practical application of CFD (4.3), other sections provide information on new

trends and development in viscous flow methods (4.4), with emphasis on those issues on which research activity has focused in the last 3 years. Applications of CFD solvers to new and more complex problems (4.5), and development of CFD-based Design Optimization (4.6) are finally described.

4.2. Results of Gothenburg 2000 Workshop

Organized by Lars Larsson, Fred Stern and Volker Bertram and held in Gothenburg, Sweden, in September 2000, the fourth workshop of the series (Gothenburg 1980 and 1990, Tokyo 1994) had the purpose to update the state of the art in ship viscous calculation and find directions for the further research and developments. Papers and discussions at the workshop, as well as an in-depth analysis of all results to appear in the final Proceedings (Larsson et al., 2002), contribute in forming a clearer picture of recent advances in numerical ship hydrodynamics. In the following, a brief summary of the objectives of the Workshop, the participating groups, results on V&V, predicted quantities such resistance, wake fields and viscous flow at model- and at full-scale, free surface pattern, and most relevant issues raised during the Workshop will be given. The reader is referred to the final Proceedings for a detailed summary, (Larsson et al., 2002).

Objectives of the workshop. The G2K was prepared with the aim of updating the overall picture of the capabilities and the accuracy of the computational prediction of ship flows. The set of benchmark-ships has hence been updated with new modern hull forms: a surface combatant with large sonar dome and transom stern, a container ship with an operating propeller and a modern tanker. An effort has been made to introduce the computational ship hydrodynamic community to the use of Verification and Validation (V&V) procedures. Furthermore, for the first time the capability of current solvers in predicting full-scale flows and propeller-hull interaction has been tested. Information about

tested geometries, flow conditions and results may be obtained at the URL:

<http://www.iihr.uiowa.edu/gothenburg2000>.

Benchmark hull forms. The three hull forms selected for the computations are:

- the VLCC tanker designed by the Korean towing tank KRISO (version 2, named KVLCC2), for which accurate and comprehensive sets of data had been presented both from towing tank measurements (Van et al. 1998a, b) and wind tunnel experiments (Lee et al., 1998);
- the KRISO Container Ship (named KCS) for which experimental data (with and without propeller) are available from KRISO (Van et al., 1998a, b) and the Ship Research Institute of Japan (Kume et al., 2000);
- the David Taylor Model Basin (DTMB) design of a Navy Combatant, Model 5415. Data for 5415 were procured by DTMB (Ratcliffe, 2000) the Italian towing tank INSEAN (Olivieri et al., 2001) and the Iowa Institute of Hydraulic Research (IIHR), USA (Gui et al., 2001a, 2001b, 2001c). Stern et al. (2000) provides an overview of the cooperative effort done by the three institutions.

Main focus of the three cases was respectively on the stern flow prediction for a full ship form, the propeller/hull interaction and wave field of a transom stern hull.

Participants and codes. Twenty groups participated, representing 16 institutes and one commercial CFD company. To help in the classification of the computations, all the participants have filled up a questionnaire with the details of the adopted method. While for a careful description of all the codes the reader is referred to Larsson et al. (2002), the typical profile of the participating solver is the following: the majority of the computation use full RANS code based on primitive variables (pressure and velocities) mostly with one- or two-equation turbulence models. Second order, finite volume

approach, is largely used, and both single or multi-block structured grids are used in the discretization of the equation. Some of the codes are parallel.

Verification results. As a major change with respect to the previous workshops, participating groups were asked to perform uncertainty analysis, either according to the 22nd ITTC suggested procedures or by proposing alternatives, and most groups tried verification by using three or more grids. In all the three cases, the coefficient of variation V for the force coefficients C ($V = \sigma / C_{(\bullet)} \times 100$, being $C_{(\bullet)}$ the generic force coefficient and σ the standard deviation) has found to be typically small for C_T and C_F (5%-8%). Much larger values have been obtained for C_P (20%-30%). A reasonable explanation is that the latter coefficient seems to be particularly grid-dependent, as also pointed out in Hoekstra et al. (2000). As to the grid convergence for C_T , half of the group that tried the analysis showed an order of accuracy near the theoretical order. Finally, the average numerical uncertainty was 2.9%, 2.3%, and 3.6% respectively for KVLCC2, KCS and 5415.

Validation results. C_T results for five codes were validated for KCS and 5415, with levels ranging from 3-15% C_T . The averaged comparison error E (i.e. the difference between the experimental data and the value from the simulation) for C_T is 4.8%, which is larger than the average validation uncertainty, $U_V = 3.6\%$. The average experimental uncertainty is $U_D = 1.6\%$ and average simulation numerical uncertainty is $U_{SN} = 3.2\%$. Efforts to reduce levels of validation will require reduction in both numerical and experimental uncertainties since both are of similar order of magnitude.

Results, discussion and trends. From the standpoint of the prediction of the turbulent flow, the KVLCC2 stern flow was a complex problem to deal with, relevant issues being strong pressure gradients, flow separation and embedded longitudinal vortices. An overview of the results has established a strong correla-

tion between model complexity and agreement of computations with data. A definite trend is the demise of Baldwin-Lomax model, and the passing from zero- to two-equation models (mainly $k-\omega$). Reynolds stress models produced the best prediction of the hook shape in the axial velocity contours at the propeller disk. Good results were obtained also with some of the two-equation models ($k-\varepsilon$, $k-\omega$) even if these models are not suited for strong pressure gradients or rotation. The use of wall function results in too smooth flows, especially when looking at the limiting streamlines, and separation tends to be reduced or even removed. Another novelty highlighted by the Workshop was the rapid diffusion of fixed-grid methods to deal with the free surface problem. Even if some details of the implementation of these techniques are still a matter of discussion (see section 4.4), reported results indicate their maturity and capability. A strong point in their favour is the easy implementation and the capability of handling complex free-surface configuration (steep waves) without special treatments. Moreover, grid generation for fixed-grid solvers proved to be a much easier task with respect to what was believed in general and appears to be a promising solution for computation past ships with large flare or for unsteady computations dealing with ship motions. The use of multiblock-structured grids represented another well-assessed trend in the code developers community, and this approach is still preferred with respect to unstructured grids. Almost all multiblock solvers run on parallel computers.

Predicted resistance. Resistance proved once again to be a very sensitive parameter for V&V, and computed results show a large scatter. Indeed, the analysis of the coefficient of variation of the resistance components C_F and C_P reveals that a large part of the variation is due to the scatter in the prediction of the C_P value. Being C_F and C_P dependent from different physics, their numerical convergences proceed at a different rate.

Predicted wake fields and viscous flow. Computed velocity field contours in the propeller plane compare quite well with the data. Most of the general features of the flow are predicted by a majority of the solvers, including the hook-shape. However, a quantitative look at the velocity field reveals that almost all methods under predict the velocity at the centre plane. With regards to the turbulent kinetic energy, codes using Reynolds stress models produce better results.

Predicted free surface. For KCS and 5415, predicted wave patterns were compared against experimental data. A few codes have shown a surprisingly good agreement with the data, and best predictions were able to capture the whole picture of the wave pattern, including bow and stern waves. Furthermore, the workshop has registered the rapid development of a number of fixed grid solvers, based on either interface tracking or capturing algorithms. However, free surface prediction still seems to be a difficult task for many RANS solvers.

Predicted full-scale flow. Full-scale computations were attempted by six groups, but no experimental data were available for validation. There is a general agreement among the computation: from model to full scale, the general picture of the flow is smoother, especially when looking at the limiting streamlines: the boundary layer becomes thinner, backward flow regions tend to disappear as well as the hooks in the wake contours. An increase in the form factor is also uniquely predicted, contrary to the ITTC assumption of constant k , used in the extrapolation from model to full scale value. However, in the lack of validation, this result should be considered with caution.

Propeller-hull interaction. For the KCS propelled case, only three groups carried out the computation: one with a rotating propeller and two with a body force representation. Since the flow is asymmetric, computations were required for both sides. The cross flow is relatively well predicted by the rotating propeller

approach, and the two body force approaches exhibit qualitatively correct results too. The tendency of the pressure at the stern to be reduced by the action of the propeller is also well captured by all methods. Some problems are encountered in prediction of the wake and a tendency to under-predict the wake peak is registered. Finally, the scatter in C_T is larger than that of the same hull without propeller.

Conclusions and recommendations. The overall picture of the different solver used for the G2K offers an up-to-date scenario of the new trends of CFD in ship hydrodynamics. Many codes have now a free-surface capability and capturing methods are coming-up at a fast pace. Among major changes, improvements in the use of turbulence models, from zero- to two-equation models, especially $k-\omega$, have to be highlighted. Only two groups presented results with Reynolds stress models but with improved robustness. The number of grid points, as well as the CPU time, has greatly increased. The emphasis and the efforts put on verification and validation procedures have been granted by the most extensive and detailed collection of results on the subject ever tried in this field. However, the recommended ITTC procedure was not accepted by all and the need for improvements was stressed (see Section 7). Unfortunately, quantitative validation for point variables was not possible since numerical uncertainty was seldom assessed. Full-scale predictions were also presented, and the predicted form factor has found to be much higher at full scale compared to model scale. As a general recommendation, similar workshops should be conducted regularly, maintaining the web site continuously, and new hull forms should be used as soon as they will become available. Surface streamlines, vorticity and pressure distributions, should be taken into account in the next workshop, as well as the analysis of the Reynolds averaged vorticity transport equation as well as Reynolds stresses should be encouraged. More complex conditions, including propeller-hull interaction, effects of drift angle, and unsteady flow (e.g., the forward speed dif-

fraction problem) may be considered. International towing tank facilities are encouraged to procure appropriate data, including rigorous assessment uncertainty estimates.

4.3. Practical Application of CFD

The previous RC report already discussed the practical application of CFD in ship design. The development since then is reviewed below. The use of the CFD is slowly becoming accepted in the ship design process. Like before, rather little is being published on this subject, at least regarding the everyday use and partly the survey is based on the committee's own perception.

Inviscid-flow calculations. The practical use of panel methods based on linearized or non-linear steady free surface boundary conditions was discussed at length in the 22nd ITTC RC report. There has been limited new development since then. Computational methods based on this approach are extensively and routinely used as a practical design tool at institutes and still are the preferred solvers at shipyards. A prospective on the industrial use of potential solvers has been discussed by Raven (1998). More recently, a study comparing different steady solvers for the prediction of global (wave resistance) and local quantities (pressure and wave profiles) has been reported by Gatchell et al. (2000), who compared potential flow calculations with an Euler-VOF solver and with a RANS-VOF solver. As a conclusion, the authors confirm the usefulness of the potential flow solvers in the practical application but foresee the massive use of RANS codes for the future. Additional work on potential flow and some new developments are carried out by Noblesse (2001) who reports an analytical representation of the wave pattern. A mixed Havelock/Rankine approach for free-surface problems was developed by Scragg (1999) and subsequently extended to include some non-linear effects (Scragg, 2001). A practical method for the far field extension of the

steady wave pattern of a ship by the use of a Fourier-Kochin representation has been presented by Yang et al. (1999). The method can be useful in allowing free surface solvers to reduce the extent of the computational domain, or in the prediction of wash effects (see Section 5). The Fourier-Kochin representation has been also used by Guillerm & Alessandrini (1999) for the far-field representation, in combination with a RANS solver for the solution of the near-field. Zhang & Chwang (1999) propose an Euler-equation solver with free surface, which works similarly to RANS methods for the wave pattern, but at reduced cost. A clear trend is the use of some well-established inviscid flow solvers in optimal shape design codes (see section 4.6) and the development of cooperative projects between shipyards, towing tanks and research institutions (Harries et al., 2001).

Viscous flow computation at model scale.

The trend in using RANS solvers for real ship computation at model scale has become stronger and the better CFD codes are ready to be used for design purposes. So far, most RANS computations for practical ship design were just double-body calculations, in which the effect of the wavy surface on the viscous flow and of the viscous flow on the wavemaking were disregarded, while current status of RANS codes incorporate this interaction and free-surface boundary conditions are solved. Indeed, results presented at the 23rd ONR Symposium (2000) and at the G2K (section 4.2) deal with the viscous free surface problem. The prediction of the total resistance C_T is still a difficult task (see section 4.2) and effort should be performed in reducing the numerical uncertainty. For flow separation prediction, a good numerical accuracy is required and no wall functions should be used, but then the better codes can predict the limiting streamline pattern. Useful applications are e.g. the determination of permissible afterbody fullness, and detailed lines improvement to prevent flow separation. Results of a RANS computation with a good visualisation provide much more detail and more possibilities for inspection than

a model tests and in less time, and are found very helpful for design improvements (e.g., Hoekstra et al., 2001). Also for orientation of appendages such as shaft support struts (Jensen & Mewis, 1999), energy-saving devices and propeller tunnels (Abdel-Maksoud et al., 1998) the detailed results of a RANS computation are very helpful. An improvement of the status has been achieved in wake field predictions too. Owing to recent turbulence modelling enhancement, some methods now appear to be able to predict nominal wake fields at model scale in much better agreement with experimental data than before. Results of the G2K report encouraging wave pattern predictions, see Alessandrini and Gentaz, Beddhu et al., Cura-Hochbaum and Vogt, Di Mascio et al., Rhee & Hino, Wilson et al. Also, propeller-hull interactions have been included in some recent developments. The propeller action and its influence on the viscous flow past the ship is being addressed with more effort and some papers at the G2K reported improved RANS prediction of the propeller-hull interaction (Abdel-Maksoud et al., Chou et al., Tahara and Ando). Some commercial general-purpose CFD solvers have been applied with limited success to model scale ship flow without free surface at the G2K (Abdel-Maksoud et al., Svennberg, Kim & Watson). Commercial software performances have been also compared by Min et al. (2000) on 5 different types of ships: two bulk carriers, a LPG ship, a container ship and a destroyer but reported results for the resistance coefficient are not accurate enough and are considerably different from the experimental data. Likely, the quality of the mesh was still poor with respect to the task of computing flow about a ship and still strongly influences the numerical results. In the attempt of simplifying the task of computing a full RANS/FS solution, Hoekstra et al. (2000) use the non-interactive zonal approach: wave pattern, trim and sinkage are first computed by a free-surface potential flow code and subsequently the viscous flow under that wave surface is predicted, imposing free-slip conditions. This technique disregards viscous effects on the

wavemaking, but produces results of quality comparable to full RANS solvers. Finally, the use of integrated CAD systems / CFD solvers in the design of ships is another key issue in the application of CFD for practical design of ships. Most of the grid generation system now in use (ICEM, GRIDGEN, GENIE++ to name a few) read the CAD data via IGES and convert all the surface patches in NURBS patches. This helps in the check for gaps and/or overlaps. These grid generators are then able to produce a volume grid from these data. In Miyata & Gotoda (2000), the hull surfaces produced by the CAD are both used by the grid generator of the CFD pre-processor and by the numerical shaping process in the workshop.

Viscous full-scale computations. The majority of published RANS solutions are still for model scale. The number of codes that predicts full-scale viscous flows without numerical difficulty still seems to be limited (see section 4.2). However little the experience gained at the G2K is, with only 6 groups attempting the full-scale benchmark, it has the merit of revealing the same trend: (i) when passing from model to full scale the general picture of the predicted flow is smoothed, and (ii) contrary to what established in the ITTC procedure for extrapolation to full scale, a remarkable increase of the form factor is showed when passing from model to full scale. Results from the workshop apart, literature on this matter is very limited: Eça & Hoekstra (2000) presented numerical results for the stern flow around a tanker at model and full scale, showing that for increasing Re the differences in the predictions using all the tested turbulent models (one- and two-equation models) decrease. Starke (2001) shows good agreement of the predicted full-scale wake field for another tanker with the measured wake field. Zondervan & Starke (2002) discuss the consequences of using a predicted full-scale wake field, instead of a measured model scale nominal wake with corrections, for propeller analysis, cavitation prediction and pressure fluctuations. It is clear that availability of a good full-scale wake is impor-

tant for critical cases such as high propeller loading, and use of RANS solvers may make an important contribution here in the near future. Validation of full-scale viscous-flow predictions is, however, important; and such validations are still limited due to the scarcity of useful experimental data.

4.4. Progress in Viscous Flow Calculation Methods

The following subsection reviews recent contributions and trends in viscous flow calculation methods, according with the following structure: use of different grid types, free surface modelling, turbulence modelling and numerical algorithms.

Grid type. During the last decade, a variety of grid generation strategies have been developed for volume grid generation about complex 3-D configurations. As representative example of the degree of complexity that a computational grid has to take into account, a recent review of Agarwal (1999) report sophisticated CFD results about whole-body aircrafts, mostly obtained with unstructured grids. Quite obviously, the choice of the grid type is basically driven by the complexity of the geometry of the problem. Nowadays, in the ship hydrodynamic community, it is not unusual to see computational results of the flow past a fully-attached ship at model scale. The issue of grid generation is believed to be a crucial point in the routine application of CFD for industrial purpose, in connection with the human cost associated with the set-up time and hence a matter of interest for towing tanks, shipyards and navies.

Single and Multi-Block Structured grids. Since the 22nd ITTC RC report, little effort has been put in single-block structured solver. Up to a few years ago, this was the standard choice for RANS solvers but the majority of new developed codes now utilize a multi-block structured grid. The main advantage of the latter is that unattached hull geometries can be discre-

tized more easily, while a single-block approach will fail to produce a mesh with an acceptable skewness. Furthermore, a realistic geometry with shafts, brackets and bilge keels may be addressed only with multi-block structure. Hence, it has not been a surprise to observe that about 60% of the G2K papers report the use of a multi-block structured grid. It must be also underlined that, for many reasons, multi-block solvers can be efficiently parallelised (Cowles & Martinelli, 1998). At the G2K workshop, 85% (6 out of 7) of the multiblock solvers were run on parallel machines. Some new applications were reported in the cases for which propeller-hull interaction was addressed. In Abdel-Maksoud et al. (2000), by using a commercial code, the flow past a container ship (KCS) with the propeller operating is studied for unsteady conditions. The real propeller geometry is considered in the computation and the propeller grid is rotated against the fixed grid of the ship, which contains a cylindrical hole to include the propeller grid block. A total of 285 blocks are used in the computation and 10 blocks for each of the 5 propeller blades have been necessary. Overlapping grids of the CHIMERA type have been used by Rengstrom et al. (2000), based on an algorithm developed by Petersson (1999) that developed a hole-cutting technique for assembling overlapping grid systems. Hybrid grids, composed of non-overlapping structured surface grids joined by an unstructured layer of triangles, are constructed from a subset of the physical boundary points on the faces of the component grids. The holes in the component grids are made by locating grid cells that intersect the hybrid surface grids and applying the ray method to determine whether the grid points in these intersected grid cells are inside or outside the region bounded by the hybrid surface grids. An analogous approach is presented also in Chou et al. (2000), using structured background and foreground grids: to include the propeller block, holes are created in the background grid.

Unstructured grids. These type of grid offers a great flexibility in dealing with compli-

cated geometry, leading to a reduction of the grid generation time and this advantage becomes even more relevant when fully appended ship hulls are considered. However, completely unstructured grids waste the regularity offered by some of the boundaries and some numerical schemes (like multigrid acceleration techniques for example) are not easily transferred to unstructured grids. Up to now not so many unstructured solvers have been developed. Hino, following his work presented in (1998), presented results on the KVLCC2 model obtained with an unstructured RANS solver (Rhee & Hino, 2000). However, the employed grid is substantially of the block-structured type and a single unstructured layer was introduced between two structured blocks, corresponding to the inner and the outer regions. Hyams et al. (2000) use an unstructured multi-block parallel solver to compute the flow around realistic ship's geometries. Among the results, the unsteady double-body flow past the DTMB 5415 fully appended with rotating propellers is presented, and 12.7 millions of grid points are used in the computation. The rotation of the propeller grid is handled by a local regridding approach. Finally, Chen et al. (2000), using a commercial RANS solver on an unstructured grid, investigate the flow past two different ships in shallow water.

Free-surface treatment. As the results reported in the G2K demonstrate, developments in the discrete treatment of free surface problems are taking place at an extremely fast pace in the last few years and a number of new methods have been developed to deal with the description of moving interfaces. However, correct prediction of the ship's wave pattern is still a difficult task for RANS solvers and a lot of work has still to be done. In the attempt of illustrating some of the new developments, the classification proposed in the report of the 22nd RC has been reconsidered, depending on the interface treatment and grid type and a general introduction is given for the different approaches. From this general standpoint, well separated classes may be introduced: (1) *Mov-*

ing grids: the grid is deformed to follow the movement of the free surface and the interface is treated as a boundary of the computational domain; (2) *Fixed grids*: the interface is treated as an internal boundary on an underlying grid; (3) *Gridless methods*: there is no grid at all. A recent review of the subject may be found in Scardovelli & Zaleski (1999).

Moving grid solvers. This approach has been till now the most widely used for modelling the free surface in the computational ship hydrodynamic community. The free surface conditions may be precisely applied and a deformable grid is needed to follow the motion of the interface. Only the flow of the water is modelled. In the naval context, fully non-linear computations have been performed solving Laplace, Euler or Navier-Stokes equations, and the deformation of the free surface can be nicely followed even in incipient breaking conditions but only up to formation of a plunging jet. However, some difficulties have been encountered in following the deformation of the mesh at the free surface and threshold values for the maximum wave slope have to be introduced to prevent the formation of the breaking. In two recent papers by Rhee & Stern (2002) and Muscari & Di Mascio (to appear), 2D models have been developed for spilling breaking waves, which can be implemented with steady RANS codes, avoiding threshold values for the slope. Extension to 3D is ongoing work. Other problems are related to special treatments required when some grid points (or grid blocks) have to be excluded from the computation, as in the case of the flow past ships with pronounced flare or when the transom stern of the ship is in “dry condition.” However, moving grid solvers have been considerably improved by their systematic use in computational ship hydrodynamics and their maturity can be assessed by the number of CFD solvers using this approach. Out of the 13 methods with free surface capabilities in the G2K Workshop, 7 are using this technique.

Fixed grid solvers. The fixed grid approach is particularly attractive in view of unsteady simulations, especially if ship’s motions have to be included. Fixed grid methods are able to treat highly deformed water waves, including breaking and post-breaking phenomena. This latter stage can be analysed provided the flow in both air and water is considered (two-fluid approaches). Hence, in this way, all the phases of the breaking process can be simulated: from the jet formation, to the splash-up and the entrainment of air bubbles in the water. The underlying idea of fixed grid approaches is to not deform the grid while following the free surface, but instead to let the free surface be detected by some general scalar, convected by the flow field, which should remain constant on particle paths. Two different techniques have been developed in this context, namely the *Interface Tracking* and *Interface Capturing*. With *Interface Tracking* methods, the interface is explicitly followed with the help of passive markers which are simply convected by the flow (Tryggvason et al., 2001). On the contrary, with *Interface Capturing* methods, once the velocity field has been computed, an additional advection equation is solved to follow the evolution of a scalar field. Depending on the choice of the scalar quantity to be advected one may have: (i) *Level Set* methods (LS), that use a scalar function representing the signed distance from the interface; (ii) *Volume of Fluid* (VOF) methods, that use the volume fraction function (fraction of liquid fluid contained in a single cell); (iii) a combination of both methods, the *Coupled Level Set Volume of Fluids* (CLSVOF).

Interface Tracking Methods. In this case, tracers or marker particles are used in the algorithm to locate the different phases. Interfacial or surface marker methods use marker particles only on the interfaces. An advantage of surface markers is that their use allows the formation of very thin liquid bridges that do not break (this is a real gain only in some cases). A weak point is that, when surface layer come into contact and then convected underwater (e.g. the

impact of a plunging breaker onto the front face of the wave) additional algorithms must be used to cancel markers that are now included in the bulk flow. Extensively used by Tryggvason group in the past (Tryggvason et al., 2001), recent publications (e.g. Popinet & Zaleski, 1999) propose this method as a robust technique for free surface computation.

Level Set Method. One of the advantage of the LS is the simplicity in the implementation and the accuracy displayed in the computation of the interface curvature. The method define a level set function Φ , initialised as the signed normal distance from the interface, and the free surface is represented by the set of points in which $\Phi=0$. A transition region is then introduced, across which the physical variables, density and viscosity, vary from water to air values. Φ is convected by the flow but only the interface (i.e. the zero level set), being a material surface, is correctly convected and Φ is periodically re-initialised to keep the interface sharp. One of the disadvantages of the LS method is that the discretization of the advection equation may lead to numerical inaccuracy and this may lead to loss/gain of mass. In Sussman et al. (1994) re-initialisation problem was eliminated proposing a new iteration method for maintaining the level set function as the signed distance from the zero level set. This scheme has been recently enhanced to be more accurate and efficient by Sussman et al. (1998). A useful resource is the book by Sethian (1999, 2nd edition) containing an overview of LS and Fast Marching methods and other efficient techniques (the narrow band, i.e. Φ is re-initialised only in the region close to the interface) to speed up the procedure. Many papers using the LS have recently been published in the hydrodynamic context, both in 2D and in 3D. Vogt & Larsson (1999) analyse both the two-fluid and the single-fluid approaches. The latter method was tested to maintain the fixed grid approach while avoiding the artificial distribution of density and viscosity in the transition region, leading to non-physical stress distribution near the interface. In this case a dy-

namical free surface boundary condition (FSBC) was applied. However, results on the order of convergence, on the wave height and on the onset of the breaking show that the two-phase formulation performs better. Iafrati et al. (2000) deal with the computation of the wavy flow past a submerged bodies, with attention to the wave breaking effects and in a subsequent work (Iafrati et al., 2001), reported an analysis about the effects of grid resolution and of width of the transition region on the mass conservation. Sussman & Dommermuth (2000) simulated the flow around the bow of a naval vessel (the DTMB 5415) with a LS technique, and a very recent method that combines both LS and VOF (CLSVOF, see below). Preliminary results for Froude number equal to 0.41 are compared with whisker-probe experimental data, showing a general agreement. The authors estimated that the resolution needed for the simulation of the entire flow past a ship, including resolved breaking effects, is of the order $\Delta x = 0.0005 L_{PP}$ and envisaged the use of adaptive grids (Sussman et al., 1999). Cura-Hochbaum & Schumann (1999) and Cura-Hochbaum & Vogt (2000) use the two-phase LS method for computing the free surface flow past a Series 60 ($Fr=0.316$) and past the KCS ($Fr=0.26$) showing good results for the wave pattern. A one-phase LS method, based on the extrapolation of the flow variables into the air region, has been used by Rhee & Hino (2000) to solve the flow around the KCS. As a remark we note that in these latter computations, coarser grids by one order of magnitude have been used compared to Sussman & Dommermuth (2000), and the quality of the mesh strongly influences the numerical results.

Volume of Fluids. The method uses a scalar field F_{ij} , known as volume of fraction, representing the portion of the area of the (i,j) cell, filled with phase 1 (e.g. water). $0 < F < 1$ in cells cut by the interface, $F = 0$ or $F = 1$ away from it. The 2D interface is a continuous piecewise smooth function: its reconstruction can be obtained in several ways. SLIC (simple line interface calculation) and SOLA are first

order methods. More accurate VOF techniques attempt to fit the interface through PLIC (piecewise linear interface construction). The use of VOF technique is widespread for several reasons: it preserve mass in a natural way, no special provision is necessary to perform re-connection or break-up of the interface, simple extension to 3D, and F_{ij} is updated using only the neighbouring cells. However, most of the recent efforts in the area of free surface problems seem to be devoted to the development to other techniques. The VOF method, in conjunction with a new scheme (HRIC, high-resolution interface tracking) has been used by Azcueta et al. (1999a, 1999b) both in 2D and in 3D. Recent papers on VOF maybe found in the Proceeding of the G2K.

Coupled LS and VOF. Recently developed by Sussman & Puckett (2000), is a coupled level-set volume-of-fluid method (CLSVOF) for two-fluid flows that combines some of the advantages of both to obtain a better mass conservation. The method has been applied to simulate the bow flow around the DTMB 5415 by Sussman & Dommermuth (2000).

Gridless solvers. Gridless methods for free surface problems are mostly based on the SPH. The SPH is a fully Lagrangian technique, initially developed in the context of astrophysical hydrodynamics and recently applied to free surface flows (by the group of Monaghan and co-workers, 1992). The basic idea "...to eliminate the problems posed by fixed or moving grid methods is to suppress the computational grid, in part or completely." The domain is then traversed by a number of particles, with or without physical meaning (Scardovelli & Zaleski, 1999). Each particle is characterised by a smoothing kernel defining the intensity of interaction between particles, depending on their mutual distance. Solvers based on this technique have been employed in a "parabolic" fashion. In other engineering filed applications of this method can be found starting from the early nineties (among the first see Batina, 1993). Recently, a gridless Euler solver has

been applied to breaking bow waves by Tulin & Landrini (2000) and Landrini et al. (2001), in combination with a 2D+t BEM code. The method uses an unsteady simulation to give a steady picture of the bow breaking of a surface combatant, and has proved able to capture the breaking of the steepest waves. To have a more accurate simulation of the successive evolution, also air-particles should however be included in the computation, which is an undergoing effort. Free surface flows, including the effects of the surface tension, have been recently computed by Morris (2000). The problems are the same as for other techniques: when very small details of the free surface are to be followed, calculation becomes inaccurate (Morris, 2000). Convergence of the SPH method has been recently analysed by Di Lisio et al. (1998).

Turbulence modelling. There is a wide variety of turbulence models available for the simulation of high Re flows for practical engineering applications (see, for a general review, Wilcox 1998, 2nd edition). The current trend seems to indicate that algebraic turbulence models are less popular than they used to be some years ago, maybe with the exception of very simple flow configurations (attached flows or boundary layer flows). On the other hand, thanks to the increased computer power and the methodical investigation that has been carried on about the subject, one- and two- equation turbulence models are gaining increasing favour in the naval community, as well as very complex Reynolds stress algebraic or differential models. Comparative examples of simulations made by means of the various turbulence models in high Re naval hydrodynamics can be found in the Proceedings of the G2K. Algebraic models were used only in three cases, one-equation models in four cases; most computation were performed by means of two-equation models (both $k-\varepsilon$ and $k-\omega$ models), and there are two examples in which algebraic and transport models for the Reynolds stresses were used. By inspection of the results of the computations, it seems quite clear that there is not a definitive answer about the kind of model to be

used in the simulations of flows past ship-like geometries. In fact, when comparing the velocity prediction in the propeller plane for the KRISO VLCC2 case, for instance, it appears that the use of very simple algebraic models (the Baldwin-Lomax model was used, e.g., by Chou et al., 2000) yields result of the same quality as the ones obtained with the one-equation model by Spalart and Allmaras used by Rhee & Hino (2000) and with the computations made by the commercial code FLUENT with the use of a very sophisticated Reynolds stress transport model based on the work of Gibson & Launder (1978) and Speziale et al. (1991). The same situation can be observed with regard to the prediction of the cross flow at the propeller plane for the DDG 51 model. In this case, the prediction made by Di Mascio et al. (2000) with the Spalart and Allmaras model, by Wilson et al. (2000) with the two equation $k-\omega$ model and by Beddhu et al. (2000) by the two equation $k-\varepsilon$ model furnish comparable results. On the other hand, the prediction made by Chen et al. (2000) using a commercial code (COMET) in conjunction with a two equation model seems to give a rather poor prediction of the wake. An interesting comparison of the performances of several two-equation models and Reynolds stress models for the computation of the stern flow past the HSVA tanker can be found in Deng & Visonneau (1999). The results seem to indicate that the increased complexity of the models is worth the larger CPU effort. In fact, there seems to be a significant improvement in the prediction on the flow details in the wake, when comparing the Reynolds stress transport models with the simpler algebraic Reynolds stress models or the linear eddy viscosity models. However, still the grid dependence of the solution remains an open issue, so, for the time being, no definitive conclusion on the models performances seems possible.

Methods for the numerical solution. As pointed out by the presentation during the G2K, finite volume discretization of the continuous equations is by far the most used approach in the computational ship hydrodynamic commu-

nity, and collocated variables seems to be the standard choice. According to the tables reported in the Proceedings, the trend is to use second or third order upwinding differences for the convective terms while some good results have been obtained also with ENO schemes. Pressure correction methods are the most used, artificial compressibility approach being also frequently used. As acceleration techniques, multigrid algorithms are quite used now and a growing number of applications to the naval hydrodynamic context in the last 2-3 years, mostly in 3D, has appeared. A recognisable trend in other engineering fields is the use of algebraic multigrid (AMG) which is currently undergoing a resurgence in popularity, due in part to the dramatic increase in the need to solve problems posed on very large, unstructured grids. Some of the recent advances and the current directions of research in AMG technology are reported by Cleary et al. (2000). A recent paper by van Brummelen et al. (2001) proposes an iterative approach to solve the steady free-surface flow problem. The method solves the steady Navier-Stokes equations, iteratively updating the free-surface location, in a way similar to that proposed by Raven (1996) for solving steady free-surface potential flows. Requiring extensive CPU time on currently computing platforms, 3D viscous flow computations are natural candidates for the use of parallel architecture. As a matter of fact, about 1/3 of the groups participating at the G2K were running parallel solvers. Today, the great effort is in achieving high efficiencies on workstation clusters using MPI (Message Passing Interface), which seems a promising approach to solve large CFD problems without large investments in dedicated multiprocessor systems.

4.5. New Applications

Steady drift and steady turning motion. Ships advancing in steady drift or turning manoeuvre have also been recently addressed. The task is quite complicated, both because the problem is no longer symmetric and the grid

should obviously cover port and starboard sides, and because of the complicated flow pattern that takes place. The ship travelling in non-symmetric condition will undergo large flow separations and the vorticity shed into the flow largely interacts with the boundary layer. In the pressure side the boundary layer remains thin while in the suction side it grows thick very rapidly and the accurate description of this flow hence requires very fine grids (of the order of several millions of grid points). However some attempts, to be intended as a preliminary calculation, have been performed by Alessandrini & Delhommeau (1998), Cura-Hochbaum (1998), Di Mascio & Campana (1999a, b), Tahara et al. (1998).

Unsteady flows. This item is one of the most challenging for ship hydrodynamics. The perspective of simulating the unsteady motion of a ship, considering resistance, propulsion, seakeeping and manoeuvring aspects simultaneously is still prevented by the enormous computational effort required, but some papers are coming up on the subject. Wilson et al. (1998) building on the work of Rhee & Stern (2001) developed a parallel multi-block solver for unsteady simulation that includes an incident wave field in the unsteady simulation of a ship, giving results for a Wigley hull, a Series 60 and a naval vessel. All simulation have been performed for the ship advancing in head waves. Gentaz et al. (1999) numerically simulated the viscous flow past a Series 60, advancing with a steady forward speed in forced heave or pitch motion. A moving grid technique is used. Added mass and damping coefficient are computed and results are compared with experimental data and inviscid calculations. Some effects of the viscous terms are shown in the results, but probably the grids used are still too coarse. Takada et al. (1999) using an unsteady RANS reported some preliminary results for the simulation of the motions of a submerged vehicle, including the motion of the control surfaces. The proposed technique, called Motion Simulation System (MSS), is the combination of four different modules: a RANS code, a

grid generator, a module solving the 6 equations of motion for the vehicle and a control system for the control surfaces. The same group (Sato et al., 1999) reported results to the problem of the motion of a surface ship obtained with this approach.

4.6. CFD – Based Optimization

Nowadays, the art of computer simulation has reached some maturity and even for complicated and unsolved problems, engineers have learned to obtain useful information and trends from their rough simulations. From the standpoint of the applications, optimal shape design has already received considerable attention. It has become vast enough to branch several disciplines, fluid dynamics and structures among others. Computational tools that combine CFD and optimization methods have already proved to be useful in the design phase and result in enhanced performances and reduced development costs. While in other engineering fields, optimal shape design has reached this maturity level (e.g., Jameson & Alonso, 1999), in the ship hydrodynamic community, a systematic study of optimal flow control and optimization problems has been only very recently undertaken and the papers cited below report recent research development.

Single criteria optimization. A typical optimal control problem for fluid flow has the familiar structure of all optimisation problems, the main elements being state variables (velocity, pressure, etc.), control or design variables (hull shape, shape of the appendages, etc.), a system of equations that models the flow (the Navier-Stokes system, the Euler equations, the potential flow equations, etc.), a functional that is a mathematical realization of the objective of the control, i.e. what we want the flow to do (e.g., minimize drag, match a given flow, minimize the ship vertical motions, etc.). The goal is then to find a set of control and state variables such that the objective functional is minimized (or maximized, depending on the

context) subject to the constraint equations, i.e., the flow equations, being satisfied.

A general classification of optimisation methods may be derived in terms of derivative-based and derivative-free methods. Genetic Algorithms (GA), belong to the latter category. Derivative-based approaches require the knowledge of the gradient of the objective functional with respect to the control or design parameters. This gradient may be determined from either finite difference method (FDM) or sensitivities equation method (SEM). Alternatively, an adjoint method (AM) can be formulated. In FDM, design variables are perturbed one at time according to a centred difference scheme, and the functional is then computed by feeding the perturbed design variables values to the flow solver, considered as a black box. On contrast, SEM directly exploits the existence of a set of partial differential equations describing the flow dynamics, to predict the sensitivity of the flow field to perturbation of the design variables, allowing for a reduction of the number of flow solution required. For large problems, SEM may still be not efficient enough for a fast evaluation of the gradient of the functional. In this case, an AM formulation can be derived by introducing an adjoint functional and adding a number of penalty functions to the original functional. Examples of the application of SEM and AM approaches to hydrodynamic design are the papers by Huan & Huang (1998) and Valorani et al. (2000). In Huan & Huang, the potential flow model is used to build the sensitivity equations and a shape optimization in performed of a 2D hydrofoil. In Valorani et al., SEM and AM are developed and compared to FDM in the shape optimization of a tanker ship at 16 knots. FDM has been applied by Tahara et al. (1998, 2000), Hino (1998, 1999) by using a RANS code for the flow evaluation. Peri et al. (2001a) also performed the optimization of a tanker ship, using a free-surface panel code and comparing two different optimization algorithm, and performing a complete towing test program to assess the success of the optimization process.

A specific problem in the shape optimization is how to automatically handle the variation of the hull geometry. Instead of trying to find a parametric representation of the shape of the ship, using some shape functions, a perturbation approach is used in all the aforementioned papers.

Multidisciplinary optimization. Ship design, as the majority of engineering problems, is basically a multidisciplinary problem. Indeed, the design of a ship, both civil and military, involves a number of disciplines, each contributing in various stages to its detailed definition, for example resistance, structural strength, propulsion, stability, manoeuvring, seakeeping, signature, and manufacturing. Furthermore, once main performance criteria have been defined, their relative importance may change depending on different operational profiles of the ship. Hence, design requirements should be based also on the specified operational profile supplied by the designer.

Traditionally, the analysis in each discipline is performed separately, connections between each discipline being complex, and a sequential approach is adopted, solving this type of optimization problem by a “step-by-step” approach. Success of this procedure is not guaranteed. Scalarization of the problem, obtained by substituting the different disciplines by their linear combination with some weighting coefficients is an adopted alternative. In this form, problems can be tackled within the Multidisciplinary Design Optimization (MDO) approach, a “systematic approach to the design of complex, coupled engineering systems, where *multidisciplinary* refers to different aspects of a design problem” (Alexandrov et al., 2000). The original multiobjective problem is substituted with a scalar one and gradient-based methods can be applied. With this method it is possible to have satisfactory results, but significant and contemporaneous enhancements in several disciplines are not easy to obtain. Unfortunately, the single disciplines are interacting, and very often both disciplines and missions are in conflict, hence improvements in

improvements in some of them results in a deterioration in some others. In these cases, scalarization may not lead to the optimal design of the complete system and the optimal solution must be searched in the framework of multiobjective problems.

Modern methods in multidisciplinary analysis were introduced in the design optimization of aircraft. Today, the industrial use of MDO has become more and more relevant and applications of the MDO methodology to the design of aircraft, spacecraft, automobiles and engines can easily be found in the literature (Alexandrov & Hussaini, 1997); Knill et al., 1999; Newman et al., 1999). Despite the number of papers and the growing recognition of its importance, much less efforts have been put in the ship design field. In Peri et al. (2001b), combining together a RANSE multiblock solver, a free-surface potential code and a 2D-strip theory solver, a first attempt of the design optimization of a naval combatant within a MDO formulation was presented. The objective functions to be minimized, under some linear and nonlinear constraints, were the total resistance, the height of the free surface wave pattern in the bow region, the axial vorticity at the stern region, and the vertical motions of the ship advancing in waves.

4.7. Conclusions

The Gothenburg 2000 Workshop on Numerical Ship Hydrodynamics has provided an in-depth vision of the actual research in computational ship hydrodynamics. The results have shown that the capability of current ship hydrodynamics CFD codes to analyze complex flows has greatly improved, especially with regards to the prediction of the wave pattern, the treatment of complex geometry and the prediction of the velocity field and the wake, as a result of renewed developments in free surface treatment, geometrical modeling and volume grid generation and, partially, in turbulence modeling. The relevant role of the verification and validation methodology and

validation methodology and procedures in the establishment of the quality of the computations has been highlighted too. In sum, compared with the assessment of the 22nd ITTC Resistance Committee Report, we believe that significant progress have been made and a more comprehensive and fruitful use of RANS codes in practical ship design has been achieved. In addition, even if the combined use of mature CFD solvers and optimal techniques has received little attention till now, soon automatic design procedures will become a powerful tool in the design of new ships and emergence of the multidisciplinary design optimization methodology, already used in other areas of research and engineering, may be envisaged.

5. FAR-FIELD WAVES AND WASH

5.1. Introduction

In recent years there has been increasing attention for the effects of ship waves, or wave wash. Ship waves impinging on shores incidentally have been found to cause bank or bottom erosion, damage or nuisance to moored vessels or small craft, to endanger people bathing or walking along the coast, or to harm natural environments. Such effects often occurred due to operation of fast ferry services, sometimes also due to conventional ships as a result of increasing traffic or the use of larger units or higher propulsion power. For the planning of ferry services and for the design of vessels, waterways and harbours it is important to be able to predict wash effects in an early stage. ITTC member institutes may have an important task in this.

Problems caused by ship wash in practice appear to be often related with sailing at critical or supercritical speeds; with wave amplification due to propagation from deep to shallow water; with moored vessels responding more strongly to longer waves. It is therefore related

not only with wave amplitude and length but also with water depth, bathymetry, waterway width, bank outlines and the precise track of a vessel. Thus it is the combination of characteristics of the vessel and the waterway that determines the occurrence of wash effects, and prediction requires considering all these aspects.

It is useful to distinguish the generation of the ship wave pattern and its further propagation to the far field. The latter may be either a simple spreading of the wave pattern in water of constant depth for a ship on a straight course, or it may involve additional processes due to decreasing water depth, refraction and diffraction, wave focussing etc. If such processes are present, a practical prediction approach is a (one-way) coupling between a model for the ship wave generation and a separate model for the wave evolution in the far field, such as phase-averaged spectral models (Kofoed-Hansen et al., 1999) or nonlinear Boussinesq-type models (Raven, 2000). A unified approach incorporating both generation and propagation has been developed by Jiang (2000). Wave propagation prediction methods will not be further discussed here.

The prediction of the ship wave generation and far-field wave heights in case of uniform water depths, which will be the principal task for the ITTC member institutes in this subject and to which we shall confine ourselves here, may seem a standard problem in ship hydrodynamics but still poses some additional problems. Often a prediction needs to be given of wave amplitudes at large distances from the vessel; several ship lengths up to several miles. Direct measurement of wave elevations in a towing tank at such a distance is usually impossible, and they can just be estimated by ‘extrapolating’ wave elevations measured closer to the model. Moreover, the specific conditions of interest for wash cause some additional problems and uncertainties in model testing.

Prediction by computational techniques is not straightforward either. The most common methods for the purpose predict only a near field, and require some kind of ‘extrapolation’ again; and special care is needed to retain numerical accuracy at larger distances.

The whole subject is evolving rapidly, with better insight in the physics being gained and new ideas for prediction being proposed. We believe it is too early for the RC to propose ‘guidelines for model tests and extrapolation methods to predict far-field waves and wash’ as requested. In this section we discuss the problems and possibilities, based on a description of the relevant physics; and we hope this discussion may be a useful step towards the development of such guidelines.

Since the water depth plays an important role in most wash problems, we discuss separately the subcritical, transcritical and supercritical speed regimes (defined by limits on the Froude number based on water depth of about 0.9 and 1.1). For each, we briefly summarise the important physics; discuss problems in model testing and CFD predictions; and pay attention to predicting far-field waves based on these.

5.2. Subcritical Speeds ($Fr_h < 0.9$)

Physics. In the subcritical speed regime, a ship wave pattern contains wave components propagating in all directions, from 0 to 90 degrees off the ship’s course. Wave length and wave direction are related by the dispersion relation. Wave energy travels with the group velocity which in deep water is one-half the wave phase velocity. Together with interference between the wave components this gives rise to a Kelvin-like wave pattern, contained in a Kelvin wedge with a half top angle of 19 deg 28 min in deep water. Close to the ship a near field is present that contains a local disturbance and a variety of nonlinear effects on wave amplitude, phase and direction.

For the Kelvin wave pattern, the decay of wave amplitudes with the distance is as distance^{-1/2}, except for the components right on the Kelvin wedge for which it is as distance^{-1/3}. These relations hold for the Kelvin pattern of an isolated pressure point and application to ship wave patterns is contested by some (Doctors & Day, 2001).

The quantitative data mentioned above hold for deep water. For a depth Froude number Fr_h above 0.75, the values start changing gradually, the Kelvin wedge widens, decay decreases.

Model testing. To estimate far-field wave amplitudes from model tests, wave amplitudes must be measured closer to the vessel and then extrapolated. This extrapolation is based on linear theory and far-field properties only, so the measurement of wave elevations must be carried out sufficiently far from the model; the minimum distance scales not only with model length but also with Fr squared, and may be hard to realise at higher Froude numbers. The wave data must include the entire wave system and must be unaffected by reflections at the tank wall, unless these are explicitly accounted for in the analysis. In practice it may often be hard to meet these conflicting requirements. Possible solutions may be: towing the model out of the centre of the tank; measuring a longitudinal wave cut right at the tank wall, taking into account the reflection; or using smaller models or wider tanks.

An additional complication in towing tank tests may be the larger tank blockage effects at higher values of Fr_h .

CFD prediction. The most common wave pattern prediction methods are nonlinear free-surface potential flow models, implemented using distributions of singularities on the ship hull and the free surface. Their application to wash prediction is discussed in e.g. (Leer-Andersen et al. 2000; Raven, 2000; Hughes, 2001). If Rankine sources are used, a wave pattern is only predicted in the domain covered

with panels. Practical limitations generally limit the width of this domain to a few ship lengths; and here again, reflections at the outer edge may reduce the usable part even further. The problem of translating the results to a far field is quite similar to that of towing tank data and will be discussed below.

In order to apply the known wave decay or other extrapolation techniques, not only the free-surface domain in the computation needs to extend far enough, but also the panel method must predict the correct decay by itself; otherwise the far field extrapolation would depend on the location where it is matched to the computed results. Numerical damping will often cause the decay to be too fast, but as shown in (Raven, 2000), if care is taken to minimise the damping and a fine panelling is used, an accurate reproduction of analytical decay rates can be achieved.

Methods based on Kelvin singularities have an important advantage for predicting the far field, e.g. (Doctors & Day, 2001); but if they are based on a thin-ship approximation, they are quite limited in e.g. their representation of the flow off a transom stern and incorporating dynamic trim and sinkage, both of which may be of substantial influence for wash generation.

In free-surface RANS methods the effect of numerical wave damping is usually far larger, and far-field predictions of sufficient accuracy seem to be impossible so far. On the other hand, all inviscid methods tend to overestimate the stern wave system (but not too much for slender fast vessels) and free-surface RANS methods in due time should improve that.

Extension to far field. The simplest approach to predict the far-field wave amplitudes (in water of uniform or large depth), based on either tank measurements or computations, is the use of the known analytical decay rates. In principle this needs to be applied separately to waves on the Kelvin wedge and other components, and must be based on wave data outside

the near field. The decay rate applies to the wave envelope, and is not a simple scaling of a wave cut. It provides estimates of maximum wave heights, wave directions and wave periods in the far field.

A more complete picture can be obtained by using the far-field wave spectrum. A ship wave spectrum is a one-parameter spectrum by virtue of the dispersion relation, and can be represented e.g. as amplitude and phase against wave number or wave propagation direction. Once the spectrum is known, the wave elevation anywhere in the far field is easily computed by integrating over the spectrum. The spectrum can be derived from wave data by a variety of techniques, provided these data are taken outside the near field and are sufficiently complete (Eggers et al., 1967). For towing-tank measurements, longitudinal cut data are easiest to collect, although subject to limitations connected with the tank width and cut length. This technique was applied by (Gadd, 1999) and proved useful. For ship wave computations, a similar approach was used by (Raven 2000), using a spectrum derived from a series of computed transverse cuts. A far-field wave pattern well matching the near-field panel code prediction could thus be constructed efficiently.

Alternatively, Gadd (1999) proposes a technique in which the wave generation is modelled using a free-surface pressure distribution at the location of the ship's waterplane; the pressure distribution can be chosen such that measured (or computed) wave data are matched. Subsequently, the same pressure distribution can be used to predict the far field, providing again good results in (Gadd, 1999). By including near-field terms in the formulation of the wave pattern, the need for using wave data measured far from the model may perhaps be relaxed.

For extending computed wave patterns to the far field, alternative approaches exist, e.g. the Kochin function approach (Yang et al., 2000) based on a velocity distribution on an interface at some distance from the vessel; or

the combined Rankine/Kelvin source approach proposed by Janson et al. (2001). At present both have just been implemented for deep-water cases.

5.3. Transcritical Speeds ($0.9 < Fr_h < 1.1$)

Physics. If the propagation speed of a wave increases to \sqrt{gh} , it becomes a pure shallow-water wave. At a depth Froude number $Fr_h = 1.0$, the transverse wave components reach this limit (in a linear approximation). The wave energy is then conserved in these waves and not lost to downstream any more. As the ship continues to supply energy, the transverse waves at critical speed increase strongly in amplitude and in lateral extent, and a completely steady situation may not be reached. If the lateral extent is limited somehow, as is the case in a towing tank, the extra energy is spent in an increase in amplitude. Due to non-linear effects, such transverse waves may accelerate and start moving ahead of the ship, forming a series of solitary waves (Jiang, 1998, Dinham-Peren 2001). For ships in laterally unrestricted water, formation of solitary waves preceding the vessel is still subject to some debate, but appears to be a minor effect anyhow and to be limited to extremely small water depths (Whittaker et al., 2000).

Critical speed thus can lead to a strong increase in resistance, sinkage and trim, and unsteadiness of the flow. However, it is important to realise that it is only the transverse waves that become critical at critical speed; and if a vessel hardly generates any transverse waves, the critical speed may have little effect. This may e.g. be the case when critical speed occurs at a length Fr far above the hull speed (Stumbo et al., 2000).

Channel effects are particularly pronounced in the transcritical speed range, since the sinkage and water level decrease next to the hull (drawdown) virtually increase the blockage, in turn causing again a larger sinkage and water

level decrease. This results in an apparent reduction of the critical speed and a large increase in drawdown.

Decay of wave amplitude with distance is hard to estimate in the transcritical range. While diverging waves may behave like subcritical and display the corresponding decay rate, the transverse wave system in theory may have no decay at all for $Fr_h = 1.0$. However, it will take time before it has built up at large distances; after a limited time spent running at critical speed, the decrease of wave amplitudes with distance can actually be rather fast; but it will become slower with increasing time (Doyle et al., 2001).

Model testing. In cases for which significant transverse waves are generated and critical speed effects are strong, model testing will be very hard and probably inaccurate. It has been found that, the closer the speed to critical and the shallower the water, the larger the variability of the results (Cox, 2000). Towing tank testing at critical speed may be significantly affected by tank width, causing exaggerated sinkage, surge and draw down, solitary wave formation and unsteadiness that may not occur, or occur differently, in reality. Wave amplitudes have been found to increase slowly along the length of the towing tank (Doyle et al., 2001). In short: model testing at critical speed may be only accurate if both the tank width and depth are scaled, or if transverse wavemaking is modest.

CFD predictions. For computations using steady free-surface panel codes, similar restrictions apply: if significant transverse waves are generated, these will be computed rather inaccurately due to their sensitivity to all sorts of disturbances; may be affected by the limited width of the free-surface panel domain, and miss any unsteady effects that occur in reality. Few comparisons of computed and measured waves at critical speed have been published, but an example in (Leer-Andersen et al., 2000) shows poor agreement.

Special computational methods have been developed for the transcritical regime which provide a more complete modelling of the wave phenomena in that regime. Such methods exploit simplifications appropriate for nonlinear shallow water waves, e.g. KP-equations (Chen, 1999) or Boussinesq-type equations (Jiang, 1998, 2000). Unsteady problems can thus be solved, if desired in a large domain, including soliton formation in channels or effects of bottom topography. Good agreement has been obtained.

Extension to far field. Since the transverse waves are nondispersive, a conservative assumption is that there is no decay of wave amplitude with distance. In practice, significant decay may be present, as mentioned above. Diverging wave components are still subcritical and will display the usual decay rates.

Using a wave spectrum seems not a viable route if critical speed effects are large, since it will be hard to make measurements outside the near field, which extends much further out in these conditions.

5.4. Supercritical Speeds ($Fr_h > 1.1$)

Physics. In linear wave theory, the maximum wave propagation speed is \sqrt{gh} ; for large-amplitude waves this is somewhat larger. Once the vessel speed substantially exceeds this critical speed, transverse waves are absent. The fastest wave components have critical speed of $c = \sqrt{gh}$, and therefore must have a direction $\theta = \arccos(1/Fr_h)$ in the far field. These are nondispersive waves, therefore they have very little decay with distance and consist of basically straight, continuous crests and troughs. All ship waves are contained in a sector bounded by these outer wave crests. Simultaneously, more strongly divergent waves are present which are still subcritical, have usual decay rates, but can cause wash effects as well.

It has been found (Whittaker et al., 2000) that the first two crests diverge from each other at a small angle, which appeared to be well explained by linear theory (Whittaker et al., 2001). The angle decreases to zero slowly with increasing distance, causing an apparently very large first wave length at large distances from the vessel's track. Since the first two wave crests are substantial, they can cause very large wave impact on coasts, after increasing in magnitude due to shoaling effects. This is even more so since wave decay is very small, with observed rates as low as distance^{-0.2}, such that these wave components can be quite substantial even miles away.

Model testing. Since the geometry of the outer, critical waves in the wave pattern is determined by the depth Froude number Fr_h , precise scaling of the water depth is important at least if wash due to these waves needs to be predicted. Problems in model testing gradually disappear for increasing supercritical speeds; at low supercritical speeds, the outer waves may reflect at the tank walls and come back to the vessel itself, causing potentially large tank width effects.

CFD predictions. The main problem in panel code computations may be the required width of the panel domain to avoid wave reflections. Not much validation has been published for supercritical wave patterns, but results seem plausible in general. Leer-Andersen et al. (2000) show a favourable agreement. Raven (2000) shows predictions that well represent the general features of a supercritical pattern. Bertram & Bulgarelli (1999) report 18% underestimation of the bow wave system for a supercritical case using a nonlinear panel code.

Gadd (2000) shows fair predictions of the far field for a supercritical vessel, but the precise approach he has used remains somewhat unclear.

Extension to far field. There is no fixed decay rate for the wave pattern; since, the outer

waves theoretically have no decay, being non-dispersive (but in practice have been found to show some decay); while more strongly diverging components are still subcritical. Doyle et al. (2001) show graphs of decay rates for constant supercritical speed against the water depth / ship length ratio, suggesting a trend that shallower water leads to slower decay. Reconstruction of the far field from a ship wave spectrum should work, if due account is taken for the dispersion relation in shallow water; but accurate determination of the spectrum itself from tank measurements will not always be possible. Similarly, for CFD computations the use of a wave spectrum could well work, but this needs to be attempted and validated. In particular it should be checked whether the far field predictions do show the very large first wave periods observed at large distances.

5.5. Conclusions

ITTC member institutes have a task in predicting the ship wave generation for conditions relevant for wash. Main tools are towing tank tests with wave height measurements, and computational techniques, in particular nonlinear free-surface panel methods. Specific complications are the need to predict far field wave amplitudes from near-field data, and shallow-water and critical-speed effects. For subcritical speeds, good possibilities exist to predict the far field wave pattern based on either tank tests or computations, but some additional tools and care for specific properties are required. Reconstruction of the far field from a ship wave spectrum, derived from either measurements or computations, seems to be a quite practical option. For transcritical speeds, if substantial transverse waves are present it seems impossible to guarantee that measurements or computations by usual methods represent the actual situation, as a result of large variability, unsteadiness, effect of the limited tank width etc. For supercritical speeds, a regime most relevant for fast ferry operation in many situa-

tions, possibilities are better again, but more validation is desired.

6. UNCERTAINTY ANALYSIS FOR TOWING TANK TESTS: SINKAGE AND TRIM, WAVE PROFILES, AND WAVE ELEVATIONS

6.1. Introduction

Towing tank testing is undergoing change from routine tests for global variables to detailed measurements for local variables for model development and CFD validation, as design methodology changes from model testing and theory to simulation-based design. Such detailed testing requires that towing tanks utilise advanced modern instrumentation with complete documentation of test conditions, procedures, and uncertainty assessment. The requirements for levels of uncertainties are even more stringent than those required previously since they are a limiting factor in establishing the level of validation and credibility of simulation technology. In Section 3 the progress has been pointed out concerning uncertainty assessment with regard to new developments in measurements techniques.

In this context, the 22nd ITTC adopted an uncertainty assessment methodology and guideline for towing-tank experiments based on the AIAA (1995) standard, which is an update and improvement of the previously adopted and currently used methodology by the ITTC. This AIAA (1995) standard is based on Coleman and Steele (1999), which is an update to the ANSI/ASME (1985) standard, and the most current drafts of international guidelines and standards (ISO, 1993a, b).

For implementing this methodology, several procedures were adopted and included in the QM as 4.9-03-01-01, "Uncertainty Analysis in EFD (Experimental Fluid Dynamics), Uncertainty Assessment Methodology", where the

methodology is reproduced, the QM procedure 4.9-03-01-02 "Uncertainty Analysis in EFD, Guidelines for Resistance Towing Tank Tests", which provided guidelines for towing tank experiments including a philosophy for testing and recommendations for application/integration of uncertainty assessment methodology into the test process and documentation of results as well as recommendations for management. In addition to above, procedures were also adopted, the QM procedure 4.9-03-02-02 "Uncertainty Analysis in EFD, Example for Resistance Test" which provides an example, the uncertainty for the total resistance coefficient C_T for a model scale resistance test.

On this basis and in order to identify possible facility/conceptual biases and scale effects, Stern et al. (2000) presented results from overlapping towing tank tests between three institutes for resistance, sinkage and trim, wave profiles and elevations, and nominal wake using the same model geometry and conditions, including rigorous applications of standard uncertainty assessment procedures. Two of the institutes used 5.7 m models whereas the third institute used a smaller 3 m model. Comparison variables were defined for data-reduction equations, data differences and data-difference uncertainties.

The overlapping work points out unaccounted errors for bias and precision limits and that current uncertainty estimates are often too optimistic. In particular, effects on facility and model geometry seem not well accounted for, although clearly there are others as yet unknown factors. These results seem to indicate that efforts must be done towards improvement of individual institute uncertainty estimates. In these overlapping tests, scale effects were also found for 3 m model which were only evident for resistance and trim measurements at high Froude numbers. Model size and turbulence stimulation need to be reviewed in the light of these results. These problems were pointed out in the previous RC report based on the work

done by Bruzzone et al. (1997) and Garofallidis (1996).

Following the recommendation of the 22nd ITTC, uncertainty assessment for additional model-scale towing tank tests, such as sinkage and trim, wave profiles, and wave elevations have been performed. In this line, the 23rd ITTC RC prepared a series of spreadsheets for calculating the bias and precision limits and total uncertainty using single or multiple test methods of some towing tests that are commented in the section 6.2. Examples have been included in these procedures in order to clarify its use and interpretation.

The sections 6.3, 6.4 and 6.5 present detailed examples of the uncertainty analysis for the sinkage and trim measurements, wave profile on the hull and wave elevation measurement for longitudinal cuts parallel to the ship centre line.

In the previous RC Committee, eight facilities contributed to the example of performing uncertainty assessment for a towing-tank resistance test. In the present case four facilities have contributed to the uncertainty assessment for the sinkage and trim, and wave elevations test the results of which are presented in section 6.6.

6.2. Spreadsheets for EFD Uncertainty Analysis

In order to improve and facilitate the uncertainty analysis, spreadsheets for calculating the bias and precision limits and total uncertainty using single or multiple test methods, have been prepared as QM procedures. The QM procedure 4.9-03-02-03 “Uncertainty Analysis Spreadsheet for Resistance Measurements”, provides the procedure referred to the resistance test. The QM procedure 4.9-03-02-04 “Uncertainty analysis Spreadsheets for Speed Measurements” is referred to the analysis of speed errors. The speed is considered as an in-

dependent procedure because of its importance in several tests. The sinkage and trim analysis is presented as QM procedure 4.9-03-02-05 “Uncertainty Analysis Spreadsheets for Sinkage and Trim Measurements”. The QM procedure 4.9-03-02-06 “Uncertainty Analysis Spreadsheets for Wave Profile Measurements” is dedicated to the analysis of the wave profile on the model hull. The wave elevation analysis can be done using the same spreadsheets as for the wave profile analysis.

6.3. Example for Sinkage and Trim Measurements

In this example, the uncertainty assessment for a model-scale sinkage and trim measurements is performed. The model corresponds to a combatant ship, specifically the DTMB model 5512 of 3 m length (geosym of DTMB model 5415). The uncertainty is estimated at one Fr , 0.28, for the average results of several tests (M) and for a single run (S). The dimensions of the model basin were, 100 m-long and 3.048 m wide and deep.

This example is based in the work from the 23rd ITTC RC and is included in the QM procedure 4.9-03-02-05 “Uncertainty Analysis Spreadsheets for Sinkage and Trim Measurements”.

Test Design. The purpose of the sinkage and trim test is to procure data for the sinkage σ and trim τ coefficients. The data-reduction equations are

$$\sigma = \frac{2}{Fr^2} \frac{\Delta FP + \Delta AP}{2L}, \quad \tau = \frac{2}{Fr^2} \frac{\Delta FP - \Delta AP}{L}$$

where ΔFP and ΔAP are the measured displacement of forward perpendicular (FP) and after perpendicular (AP) and L the ship length.

Measurement system and Procedure. The measurement system consists of two resistive-type linear motion potentiometers, data-transfer box, 5-volt power supply, and carriage PC with

12 bit, 16 channel AD card. The potentiometers are rigidly fixed to the trailer carriage and plumb to the model above the FP and AP . The cores extend to their midpoints and make contact with the model hard points.

An end-to-end calibration is used for the sinkage and trim test before and after data procurement. The potentiometers, data-transfer box, 5-volt power supply, and carriage PC AD card are statically calibrated to determine its voltage-displacement relationship. The potentiometer is placed plum to a PC controlled vertical-axis traversing system, which displaces the cores up and down in specified increments and the output recorded. Starting and ending from zero elevation, the traverse is moved up to 90 mm and down in increments of 10 mm. Data is sampled at 500 Hz for 4 seconds for each displacement and statistically analysed. The two data average values for each displacement increment are averaged, except for the maximum displacement for which there is only one value. The voltage-displacement relationship is linear. A first-order polynomial linear regression curve fit is used to determine the slope/intercept, which are then used to convert voltage to displacement. The repeatability of the calibration between data procurement cycles is monitored.

Data acquisition is done in two steps: (1) voltage from potentiometer is sampled; and (2) AD conversion in carriage PC. Data are sampled at 800 Hz using 4 channels for 10 seconds (i.e., 2000 samples per channel). At-rest data are used for zero-reference value.

Data reduction and/or calibration are done three times: (1) AD card output is statistically analysed; (2) the average value is converted to mm using the voltage-displacement calibration with linear interpolation; and (3) σ and τ are calculated using the equations previously indicated.

Errors and Uncertainties. There are three elemental bias errors for ΔFP and ΔAP . A computer-controlled traverse with a positional uncertainty of 0.0071% is the calibration standard for the potentiometers. Calibration is done over 90 mm in 10 mm increments. The bias error is the product of the traverse uncertainty and the RSS of the traverse increments

$$B_{\Delta FP1, \Delta AP1} = 0.000071 \sqrt{\sum_{i=1}^9 (z_i^2)} = 0.000071 \sqrt{0.0285} = 1.19 \cdot 10^{-5} \text{ m}$$

Misalignment of the potentiometers with respect to the vertical plane is a data-acquisition bias error. The angle is small ($< 0.25^\circ$) and the bias is

$$B_{\Delta FP2} = \Delta FP - \cos(0.25^\circ) \Delta FP = 8.89 \cdot 10^{-8}$$

$$B_{\Delta AP2} = \Delta AP - \cos(0.25^\circ) \Delta AP = 2.08 \cdot 10^{-8}$$

The scatter in the potentiometer calibration data is quantified with the SEE. Four calibrations are completed (two before the sinkage and trim tests begin and two after the test program is completed), and four values of the SEE are computed. An averaged of the four values is used as the data-reduction bias limit $B_{\Delta FP3, \Delta AP3}$.

$$B_{\Delta FP3} = 0.00006025 \text{ m}, \quad B_{\Delta AP3} = 0.000035 \text{ m}$$

The potentiometer calibration standard contributes 3.8 and 10.5% to the bias uncertainty in ΔFP and ΔAP , respectively. The scatter in the potentiometer calibration data contributes 96.2 and 89.5 % to the bias uncertainty in ΔFP and ΔAP , respectively. Contribution of the installation error to the bias uncertainty is negligible. Considering a bias error of 0.003574615 m/s for the speed of the carriage and the sensitivity coefficients for sinkage and trim, the total bias limit are

$$\text{Sinkage} \quad B_\sigma = 0.000375$$

$$\text{Trim} \quad B_\tau = 0.000662$$

Considering a multiple test of 10 measurement, the precision limits are

$$\text{Sinkage} \quad P_{\sigma} = 0.000654$$

$$\text{Trim} \quad P_{\tau} = 0.000866$$

The contribution of the precision limit to the total uncertainty is 75.3% and 63.1% in sinkage σ and trim τ , respectively. The total uncertainty is,

$$(U_{\sigma}) = [(B_{\sigma})^2 + (P_{\sigma})^2]^{1/2} = [0.000375^2 + 0.000654^2]^{1/2} = 0.000754$$

$$(U_{\tau}) = [(B_{\tau})^2 + (P_{\tau})^2]^{1/2} = [0.000662^2 + 0.000866^2]^{1/2} = 0.00109$$

which represents an error of 1.56% for the sinkage and 1.82% for the trim. For a single experiment, the precision limits are,

$$\text{Sinkage} \quad P_{\sigma} = 0.00207$$

$$\text{Trim} \quad P_{\tau} = 0.00274$$

The contribution of the precision limit, in a single run, to the total uncertainty is 96.8 and 94.5% in sinkage σ and trim τ , respectively. The total uncertainty is,

$$(U_{\sigma}) = [(B_{\sigma})^2 + (P_{\sigma})^2]^{1/2} = [0.000375^2 + 0.00207^2]^{1/2} = 0.00210$$

$$(U_{\tau}) = [(B_{\tau})^2 + (P_{\tau})^2]^{1/2} = [0.000662^2 + 0.00274^2]^{1/2} = 0.00281$$

which represents an error of 4.34% for the sinkage and 4.81% for the trim.

6.4. Example for Wave Profile Measurements

In this example the uncertainty for the wave profile is estimated at one Fr , again 0.28, for the average results of several tests (M) and for a single run (S). The model and the facilities are the same as in the previous example. Three runs were considered as multiple measurements.

This example is based also in the work from the 23rd ITTC RC and is included in the QM procedure 4.9-03-02-06 “Uncertainty Analysis Spreadsheets for Wave Profile Measurements”.

Test Design. The purpose of these measurements is to procure data for the wave profile on the hull. The data-reduction equation is

$$\zeta = \frac{z}{L}$$

where z is the measured wave height and L the ship length.

Measurement system and Procedure. The measurements system consists of adhesive markers, painted grid on the hull, flexible ruler, level table, and height gauge. The data acquisition is done in 5 steps: (1) at each x -station, adhesive markers are fixed to the side of the hull with the marker tip at the top of the wave profile; (2) after all x -stations are marked, the model is removed from the tank and a flexible ruler is used to measure the wave profile distance along the girth of the model from the calm waterline; (3) steps (1) and (2) are repeated to obtain different sets of data; (4) the model was inverted and mounted on the level table and the averaged values from step (3) were marked along the girth of the model from the calm waterline; and (5) the height z is normalised by L .

Errors and Uncertainties. Assuming that the bias error in the model length L is negligible, there are four elemental bias errors for ζ . The first is associated with the error in the place-

ment of the draft and vertical scale at each x -station line on the model and is estimated as $B_{\zeta_1} = 1.0$ mm. The second is associated with the error in the placement of the marker on the hull and is estimated as $B_{\zeta_2} = 1.5$ mm. The third is associated with reapplying the marks on the hull when the model is on the level table and is estimated as $B_{\zeta_3} = 1.0$ mm. The fourth and final bias error is associated with reading the wave elevation in the Cartesian coordinate system from the height and is estimated as $B_{\zeta_4} = 0.5$ mm. In this case the total bias error is

$$B_{\zeta} = [0.001^2 + 0.0015^2 + 0.001^2 + 0.0005^2]^{1/2} = 0.00212$$

The bias error due to the uncertainty of the x -station situation was estimated as 2.5 mm.

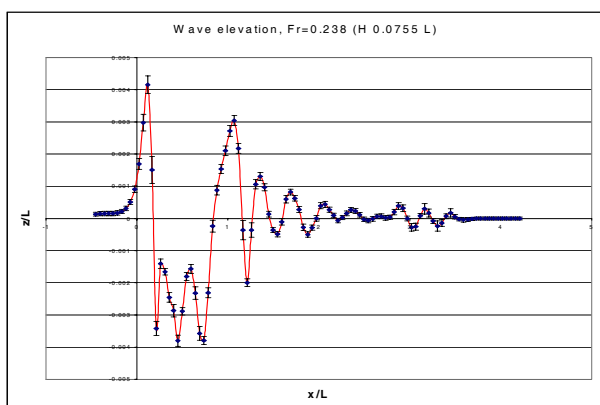


Figure 6.1 Uncertainty on the wave profile.

The precision error depend upon the x -station. 43 x -station were considered from $x = -0.00443$ to $x = 1.0023$. The highest precision error was 0.000725 at $x = 1.0018$ and the lowest was $7.89 \cdot 10^{-5}$ at $x = 0.76$. The total uncertainty in these two points was 0.0013 and 0.0007, which represent an error or 6.03% and 3.16%, respectively. If we consider a single run, the precision error is increased and the highest total uncertainty is 0.00258 at $x = 1.0023$ and the lowest is 0.00176 in several points. These values represent an error of 11.5% and 7.9% respectively. In the Figure 6.1, the uncertainty for the multiple measurements case is presented.

6.5. Example for a Wave Elevation Measurements

In this example, the uncertainty assessment for the farfield wave elevations ζ_w is presented. The model corresponds to a Series-60 ship, with 2.5 m length and the facilities have the dimensions of 100 m long, 3.80 m wide and 2.2 m deep. The uncertainty is estimated at one Fr , 0.238, for the average results of several tests (M) and for a single run (S). 20 runs were done.

This example is based also in the work from the 23rd ITTC RC and follows the QM procedure 4.9-03-02-06 “Uncertainty Analysis Spreadsheets for Wave Profile Measurements”.

Test Design. The purpose of these measurements is to procure data for the wave elevations in a parallel plane to the ship centre line at a certain distance from the hull. The data-reduction equation is

$$\zeta_w = \frac{z}{L}$$

where z is the measured wave height and L the ship length.

Measurement system and Procedure. The measurements system consists of resistive probes and PC data acquisition. A longitudinal-cut method is used to acquire the data. Data-reduction is completed by conversion of longitudinal-cut time histories to a ship coordinate system and then normalising the elevations with model length. The probes are cantilevered from the tank sidewall on a boom. They are statically calibrated to determine their voltage-elevation relationship.

Errors and Uncertainties. Assuming that the bias error in the model length L is negligible, we consider two elemental bias errors for ζ_w . The first is associated with the error in the A/D conversion and the second with the static calibration. The error in vertical orientation of the probe has been considered very small in comparison to the other errors. In this case the total bias error is

$$B_{\zeta_w} = [0.0000242^2 + 0.000107^2]^{1/2} = 0.000108$$

100 x-stations were considered, between $x/L = -0.452$ and $x/L = 4.25$, at a distance of $0.0755L$ from ship centerline. The bias error due to the uncertainty of the x-station situation was estimated as 1 mm.

The precision error depends upon the x-station. The highest precision error was 0.000417 at $x = 0.165$ and the lowest was $3.77 \cdot 10^{-7}$ at several points. The total uncertainty in these two points was 0.000422 and 0.000439, which represent an error of 5.31 and 0.55%, respectively.

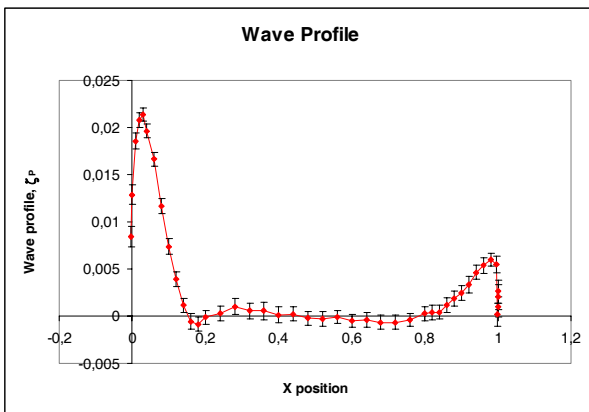


Figure 6.2 Uncertainty on the wave measurements.

If we consider a single run, the precision error is increased and the highest total uncertainty is 0.00187 at $x = 0.166$ and the lowest is 4.4×10^{-5} at several points. These values represent an error of 25.5 and 0.5%, respectively. In Figure 6.2, the uncertainty for the multiple measurements case is presented.

6.6. Comparison Between Facilities

Five facilities, four of them represented by members of the 23rd ITTC RC, contributed to the examples in the previous sections by performing uncertainty assessment for sinkage, trim and wave elevations measurements. Three combatants (CBT), one series 60 model and one KRISO VLCC were used. The bias and the

precision limits were estimated and the total uncertainty was calculated. The values given in this section correspond to a medium speed tested at the respective facilities.

In the Figures 6.3, 6.4 and 6.5 the bias and precision percentage to the total uncertainty are presented for the different measurements. These results present reasonable differences. For the wave elevation, the bias limits are more significant, but for the sinkage and trim the relative magnitude of the bias and precision limits depends on the model used and the facility, which can be due to the previously mentioned unaccounted for error sources.

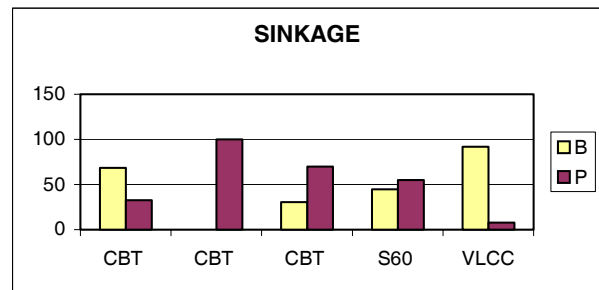


Figure 6.3 Sinkage. Bias and Precision Percentages.

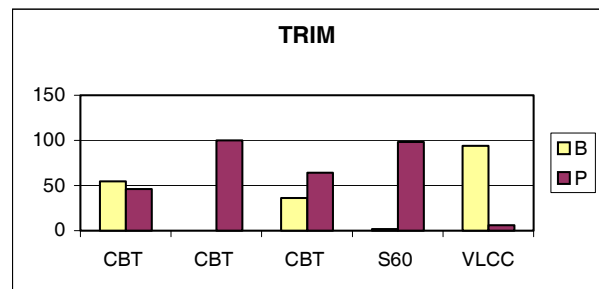


Figure 6.4 Trim. Bias and Precision Percentages.

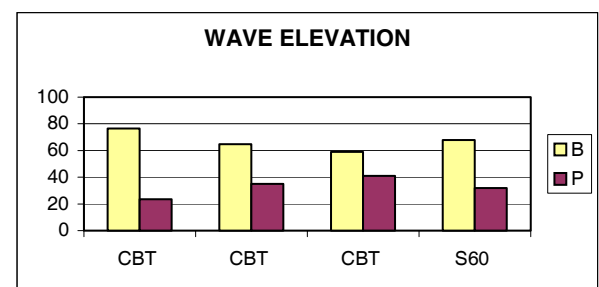


Figure 6.5 Wave elevation. Bias and Precision Percentages.

One facility has not considered bias error in trim and sinkage and in another facility, due to the small value of the trim, the precision error represents almost the total (98%) of the uncertainty.

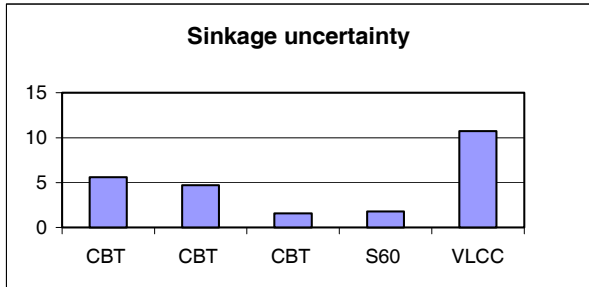


Figure 6.6 Sinkage. Total uncertainty (%).

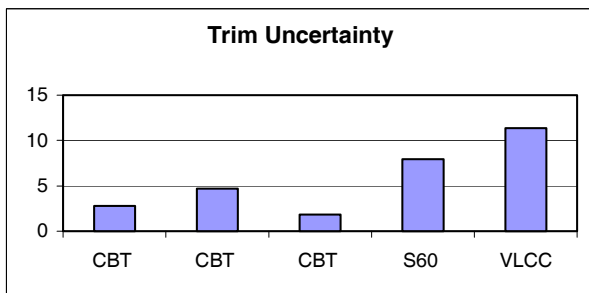


Figure 6.7 Trim Total Uncertainty (%).

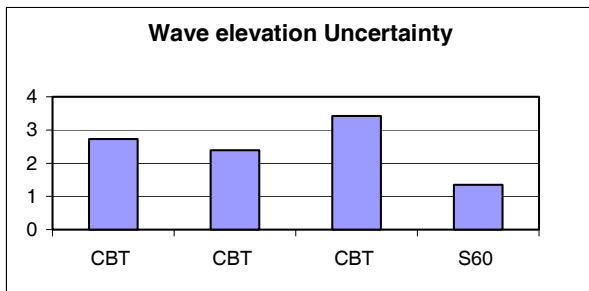


Figure 6.8 Wave elevation. Total Uncertainty (%).

The total uncertainties are presented in the Figures 6.6, 6.7 and 6.8. Similar values for the total uncertainty in the wave elevation were found, but the discrepancies in the sinkage and trim are more significant, there is not a correlation between the facilities and the uncertainty, if one facility has some uncertainty in the sinkage bigger than the average, the uncertainty in the trim is smaller than the average. This is due to the model used; for the combatant model the

values of sinkage and trim are similar for the *Fr* considered; nevertheless, for the Series 60 model the sinkage is almost six times the trim. In the VLCC case, the trim is twice the sinkage.

With the above results the average of the uncertainties of these tests with the corresponding standard deviation are indicated in the following table.

Table 6.1 Average Uncertainties.

Test	Aver. Uncert.	Std. Dev.
Trim	5.7	3.9
Sinkage	4.9	3.7
Wave elevation	2.5	0.9

The highest average uncertainty corresponds to the trim and the lowest to the wave elevation. Nevertheless, all these values are bigger than the corresponding to the total resistance coefficient that were slightly greater than 1% as was stated in the previous RC ITTC Report.

6.7. Conclusions

To improve and to facilitate the uncertainty analysis methodology, spreadsheet procedures for calculating the bias and precision limits and total uncertainties using single or multiple test methods are proposed for adoption by the 23rd ITTC. This methodology follows the guidelines and recommendations adopted by the 22nd ITTC. The overlapping tests work done for various institutes point out unaccounted errors for bias and precision limits and that current uncertainty estimates are often too optimistic. In particular, effects of facility and model geometry are not well accounted for, although clearly there are other as yet unknown factors. These results seem to indicate that efforts must be done towards improvement of individual institute uncertainty estimates. In these overlapping tests, scale effects were also found for 3 m model, which were only evident for resistance and trim measurements at high Froude numbers. Model size, turbulence stimulation,

and use of standard models need to be considered in light of these results.

7. UNCERTAINTY ANALYSIS FOR CFD

Work, discussion, and controversy on verification and validation (V&V) of CFD simulations has continued at a healthy rate over the last five years, which will hopefully converge on standards and guidelines that are sorely needed by the CFD community. The literature includes editorial policies (Freitas, 1993), guidelines (AIAA, 1998; Casey and Wintergerste, 2000), and a wide range of V&V methodology, procedures, and case studies.

Verification approaches are largely based on Richardson extrapolation (Richardson, 1910; 1927) (RE) in which convergence studies are conducted with multiple, systematically refined grids. RE was extended to include estimation of uncertainty using the grid convergence index with factor of safety approach (Roache, 1998). A factor of safety $F_S = 1.25$ is recommended for careful grid studies in which three grids are used and order of accuracy estimated and $F_S = 3$ when only two grids are used and order of accuracy is assumed based on the theoretical value. A least squares approach was proposed by Eça & Hoekstra (1999, 2000) to estimate the error by computing the three unknown parameters from RE when more than three grids are used and there is variability between grid studies.

Single grid approaches to estimating numerical error include: solution of supplemental partial differential equations for numerical error; comparing the base solution with a solution obtained with a higher-order method; and algebraic evaluations of the solution through post-processing (e.g., derivatives, conservation variables, and solution reconstruction). Only the first approach provides quantitative error estimates, while the last two only provide qualitative error indicators (e.g., grid adaptation methods). Although single grid approaches

have the advantage of not requiring generation of multiple grids and solutions, additional resources are required for code development, memory, and execution time associated with solution of the error equation. Also, it can be difficult to determine the source terms of the error equation and solution with a higher-order discretization is required to obtain accurate error estimates.

Studies have used the single grid approach (Shimazaki et al., 1993) and also compared single and multiple grid approaches (Stern et al., 1999; Ilinca et al., 2000; Zhang et al., 2001) again for simple model problems. In contrast to single grid approaches, the multiple grid approach can be used to establish convergence and is relatively inexpensive to implement. Other approaches such as “manufactured solutions” (i.e., selecting an exact solution which is applied to the governing PDE to yield a source term that produces the exact solution) can be used to verify various elements of a CFD code but do not provide quantitative error estimates for a particular application.

Validation approaches include general discussion and guidelines (Oberkampf & Trucano, 2000), solution of sensitivity equations for modeling uncertainty (Pelletier et al., 2001), as well as quantitative metrics based on simulation and experimental uncertainties (Coleman & Stern, 1997). Most case studies focus mainly on verification procedures and are for simple 2D model problems (Mehta, 1998; Chen et al., 2002). More experience is needed for detailed V&V of CFD simulations for 3D industrial flows (e.g., optimization, combustion, acoustics, vehicle dynamics) with complex geometry and physics.

Stern et al., (2001) recently developed a comprehensive approach to V&V methodology and procedures, which differs in many respects from the recent literature. Concepts, definitions, and equations derived for simulation errors and uncertainties provide the overall mathematical framework. Verification proce-

dures for estimating errors and uncertainties include (1) the option of treating the numerical error as deterministic or stochastic, (2) the use of generalized RE for J input parameters, and (3) the concept of correction factors based on analytical benchmarks. Previously developed validation procedures are extended to include the option of deterministic numerical error.

The Stern et al. (2001) V&V approach was adopted on an interim basis by the 22nd International Towing Tank Conference (ITTC, 1999) and recommended and used at the recent Gothenburg 2000 Workshop on CFD in Ship Hydrodynamics (Larsson et al., 2000). Most groups implemented the recommended procedures, but lack of familiarity and use of coarser grids with solutions far from the asymptotic range led to difficulties. Results from grid studies showed a mixture of monotonic convergence with orders of accuracy far from expected values in some cases, oscillatory convergence, and even divergence. In spite of the difficulties, the effort was beneficial in quantitative evaluation of levels of V&V, increasing familiarity with V&V procedures, interpretation of results, and identification of grid requirements and modeling issues for decreasing levels of errors and uncertainties. A recent study (Wilson et al., 2001) provides an example for RANS simulations for a cargo/container ship where issues with regard to practical application of the methodology and procedures, variability for order of accuracy, lack of knowledge of asymptotic range for practical applications, and interpretation of V&V results are discussed. Very recently, Wilson et al. (2002) provide a comparison of correction factor and factor of safety multiple-grid verification procedures, develop procedures and tools for efficient generation of multiple solutions and grids, and detailed documentation of levels of V&V for RANS simulation of a naval surface combatant.

In consideration of the above, the 23rd ITTC RC updated QM Procedures 4.9-04-01-01 “Uncertainty Analysis in CFD, Uncertainty As-

essment Methodology” and 4.9-04-01-02 “Uncertainty Analysis in CFD, Guidelines for RANS Codes”, as Revision 01 QM Procedure 4.9-04-01-01 “Uncertainty Analysis in CFD, Uncertainty Assessment Methodology and Procedures”, which is recommended for interim adoption by the 23rd ITTC. It is also recommended that QM Procedure 4.9-04-02-01 “Uncertainty Analysis in CFD, Examples for Resistance and Flow” be deleted from the QM, since it is already available as Wilson et al. (2001) and should be updated by 24th Resistance Committee as a collective example based on work of as many Resistance Committee (and other ITTC) members as possible following QM Procedure 4.9-04-01-01 “Uncertainty Analysis in CFD, Uncertainty Assessment Methodology and Procedures” for the Gothenburg 2000 Workshop test cases.

Revision 01 QM Procedure 4.9-04-01-01 “Uncertainty Analysis in CFD, Verification and Validation Methodology and Procedures” was updated for clarity of presentation and expanded discussion of verification procedures and implementation based on three years experience, as discussed in Section 7 of 23rd ITTC RC Report. In particular, verification procedures are expanded to include user options of either correction factors or factor of safety approaches for estimating numerical errors and uncertainties and discussion is provided on fundamental and practical issues to aid in implementation of verification procedures. It should be recognized that implementation of verification procedures is not easy and require both experience and interpretation of results, especially for practical applications. However, their importance cannot be overemphasized to ensure fidelity and quality of CFD solutions. Present verification procedures are considered best presently available and further work is also recommended for improved procedures, which once available can be incorporated. Validation procedures were not changed.

7.1. Conclusions

Users of CFD should rigorously implement best available approaches for V&V of CFD simulations, as per QM Procedure 4.9-04-01-01 “Uncertainty Analysis in CFD, Uncertainty Assessment Methodology and Procedures”, which hopefully will increase number of trained users and reduce user variability both of which are considered obstacles for achieving simulation based design. Future attention should turn towards procuring sufficient number of documented V&V solutions for practical applications to aid in establishing confidence in CFD codes and developing procedures for their certification. Managers and CFD engineers should set priority and allocate resources for V&V of CFD simulations.

8. UNCERTAINTY ANALYSIS FOR EXTRAPOLATION METHODS

8.1. Introduction

Speed-power prediction is still the most important function of most towing tanks. Various extrapolation methods are in use, which combine towing-tank model-scale test data, model-ship correlations, and speed trial data for predicting full-scale performance. Both two-dimensional and three-dimensional approaches are used such as Froude, British Towing-Tank Panel, and David Taylor Model Basin and Hughes, Japan Towing-Tank Committee, and 1978 ITTC Performance Prediction methods, respectively. The 1978 ITTC Performance Prediction method proposed by the 15th ITTC Performance Committee was later updated by the 17th and 18th ITTC, is available as ITTC QM Procedure 4.9-03-03-01.2, and is widely used. The basic approach combines resistance, open water propeller, and self-propulsion tests with reliable assumptions on scale effects on propulsion coefficients, as described in detail by Lindgren & Dyne (1979). Later updates, in-

cluding addition of speed trial data, are described in 17th and 18th ITTC Proceedings.

The 22nd ITTC RC recommended standard uncertainty analysis procedures for towing-tank tests, including an example for model-scale resistance test. The 23rd ITTC Specialist Committee on Procedures for Resistance, Propulsion and Propeller Open-Water Tests will provide examples for open water propeller and self-propulsion tests. These same procedures along with the results from the resistance, open water propeller, and self-propulsion test examples can be used for performing uncertainty analysis for extrapolation methods by treating the extrapolation equations as data-reduction equations (DRE) and conducting propagation of error analysis with appropriate estimates for resulting uncertainties to estimate the uncertainty in predicting full-scale performance. The 23rd ITTC RC undertook this task, which is the subject of the present section.

As a preliminary, Section 8.2 discusses recent work on friction lines, which play a central role in extrapolation methods through the model-ship correlation for friction resistance. Section 8.3 presents the DRE and uncertainty analysis for full-scale resistance, including a sample calculation. Section 8.4 presents the DRE and uncertainty analysis for full-scale power prediction; however, a sample calculation is not made since uncertainty estimates for open water propeller and self-propulsion tests are currently in preparation, as previously mentioned. Lastly, Section 8.5 provides conclusions.

8.2. Discussion on Correlation and Friction Lines

Model-ship correlations for frictional resistance play an important role in all extrapolation methods. In 1957, ITTC developed the new model-ship correlation line (hereafter referred to as ITTC line), which is currently used by many extrapolation methods. Recent work by

Osaka et al. (1998) and Grigson (2000) based on direct shear stress measurement and rigorous theoretical analysis, respectively, indicate certain improvements over previous friction and model-ship correlation lines.

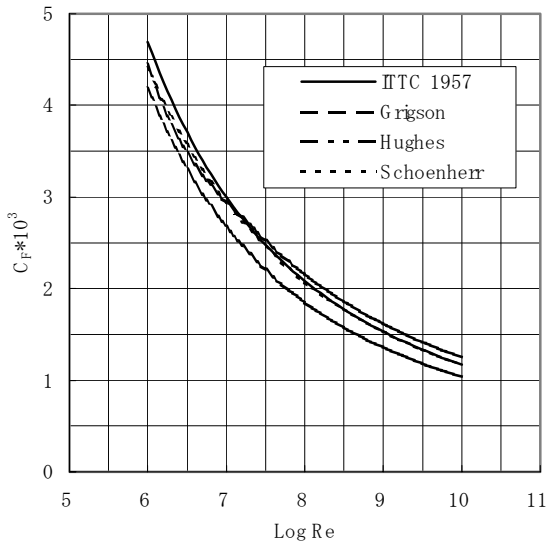


Figure 8.1 Comparison of friction and correlation lines.

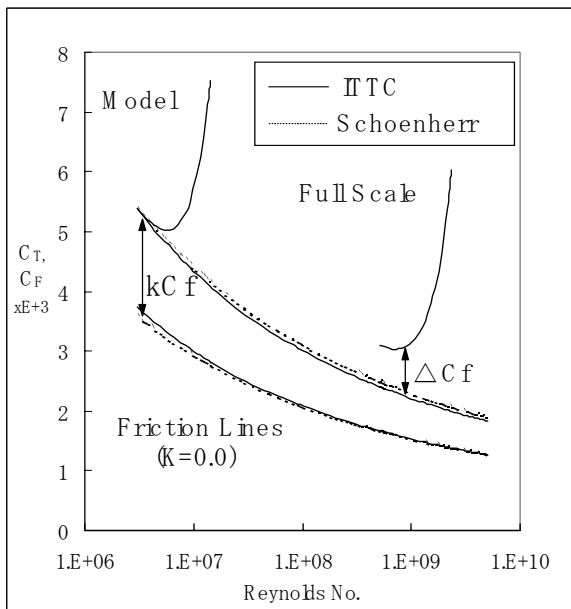


Figure 8.2 ΔC_f vs. correlation lines.

Figure 8.1 shows a comparison of friction and ITTC lines, which displays the well-known

differences between the ITTC and Schoenherr friction lines for low Re .

This tendency results in a relatively larger magnitude of correlation factor (ΔC_f) for the former than the latter, as shown in Figure 8.2.

The Grigson friction line shows similar tendencies as the Schoenherr friction line, i.e., will require relatively smaller magnitude of ΔC_f . Unfortunately, use of new friction lines requires model-ship correlation data and experience; therefore, in spite of improvements they cannot be recommended for adoption. Future work should focus on acquiring such data and experience along with uncertainty analysis.

8.3. Data Reduction Equation and Uncertainty Analysis for Full-Scale Resistance

A review was conducted of the aforementioned two- and three-dimensional extrapolation methods; however, since the 1978 ITTC Performance Prediction Method (hereafter referred to as ITTC method) is widely used, it was selected as appropriate method for conducting uncertainty analysis. This same approach can be followed for the other extrapolation methods to determine the uncertainty in their predictions.

Data-reduction equations. The full-scale total resistance coefficient is given as follows where air resistance and roughness allowance are excluded because at this stage of the prediction they are not measured values and contain no uncertainties.

$$C_{TS} = (1+k)C_{FS} + C_W \tag{1}$$

The wave resistance coefficient has the same value as that of the model ship

$$C_W = C_{TM} - (1+k)C_{FM} \tag{2}$$

such that

$$C_{TS} = (1+k)(C_{FS} - C_{FM}) + C_{TM} \tag{3}$$

Uncertainty analysis for full-scale total resistance. The uncertainty in the full-scale total resistance coefficient can be expressed as follows.

$$C_{TS} = r(k, C_{FS}, C_{FM}, C_{TM})$$

This equation contains values, which depend on each other such as k vs. C_{FM} and C_{FM} vs. C_{FS} . This impropriety will be settled later on.

$$U_{CTS}^2 = \left(\frac{\partial C_{TS}}{\partial k} U_k \right)^2 + \left(\frac{\partial C_{TS}}{\partial C_{FS}} U_{CFS} \right)^2 + \left(\frac{\partial C_{TS}}{\partial C_{FM}} U_{CFM} \right)^2 + \left(\frac{\partial C_{TS}}{\partial C_{TM}} U_{CTM} \right)^2 \quad (4)$$

$$U_{CTS}^2 = [(C_{FS} - C_{FM})U_k]^2 + [(1+k)U_{CFS}]^2 + [(1+k)U_{CFM}]^2 + [U_{CTM}]^2 \quad (5)$$

In the limiting case as L_S approaches L_M , U_{CTS} should be equal to U_{CTM} . From these considerations, both U_{CFM} and U_{CFS} are to be excluded from equation (5). Then we get a following equation.

$$U_{CTS}^2 = [(C_{FS} - C_{FM})U_k]^2 + [U_{CTM}]^2 \quad (6)$$

Uncertainty analysis for form factor.

ITTC recommended Prohaska's method for experimental evaluation of the form factor. In the low speed region (say $0.1 < Fr < 0.2$), the wave resistance component is assumed to be a function of Fr^4 . The straight line plot of C_{TM}/C_{FM} versus Fr^4/C_{FM} will intersect the ordinate ($Fr = 0$) at $(1+k)$, enabling the form factor to be determined.

By using two plots on the straight line, the form factor is given as follows.

$$(1+k) = \frac{C_{TM1} \cdot Fr_2^4 - C_{TM2} \cdot Fr_1^4}{Fr_2^4 \cdot C_{FM1} - Fr_1^4 \cdot C_{FM2}} \quad (7)$$

If we select the $Fr_2 \gg Fr_1$, equation (7) is rewritten as follows.

$$(1+k) = \frac{C_{TM1}}{C_{FM1}} \quad (8)$$

In the low speed region, this equation is expressed in more general form,

$$(1+k) = \frac{C_{TM}}{C_{FM}} \Big|_{Fr:Low} \quad (9)$$

$$U_k^2 = \left(\frac{\partial k}{\partial C_{TM}} \cdot U_{C_{TM}} \right)^2 + \left(\frac{\partial k}{\partial C_{FM}} \cdot U_{C_{FM}} \right)^2$$

$$= \left(\frac{U_{C_{TM}}}{C_{FM}} \right)^2 + \left(\frac{C_{TM}}{C_{FM}} \cdot U_{C_{FM}} \right)^2$$

$$= \frac{1}{C_{FM}^2} \left[(U_{C_{TM}})^2 + \left(\frac{C_{TM}}{C_{FM}} \Big|_{Fr:low} \cdot U_{C_{FM}} \right)^2 \right]$$

$$= \frac{1}{C_{FM}^2} \cdot [(U_{C_{TM}})^2 + (1+k)^2 \cdot (U_{C_{FM}})^2]$$

where U_{CFM} is the uncertainty of friction line, but at this moment, evaluation of the magnitude is impossible. Moreover, in the case of ITTC's correlation line, which was artificially defined, the uncertainty of friction line may be able to be assumed negligible.

$$U_k = \frac{U_{CTM}}{C_{FM}} \Big|_{Fr:Low} \quad (10)$$

Final expression. Uncertainty for full-scale total resistance coefficient is given as follows.

$$U_{CTS}^2 = \left[(C_{FS} - C_{FM}) \cdot \frac{U_{CTM}}{C_{FM}} \Big|_{Fr:Low} \right]^2 + U_{CTM}^2$$

If all values are selected in the low- Fr region, we get followings.

$$U_{CTS}^2 = \left[\left(\frac{C_{FS}}{C_{FM}} - 1 \right) U_{CTM} \right]^2 + U_{CTM}^2 \quad (11)$$

Uncertainty for full-scale resistance coefficient will be in the range as follows.

$$U_{CTM} \Big|_{Fr:Low} \leq U_{CTS} \Big|_{Fr:Low} \leq \sqrt{2} \cdot U_{CTM} \Big|_{Fr:Low} \cdot \quad (12)$$

From these equations, the magnitude of uncertainty of full-scale resistance depends on both C_{FS} and C_{FM} in the region of low Fr , which are function of Re of model ship and full-scale ship, respectively.

8.4. Sample Calculation for Uncertainty of Full-Scale Resistance

Equation (11) is expressed as follows.

$$U_{CTS} = h \cdot U_{CTM}$$

Multiplier h depends on Re of both model and full-scale ship in the region of low Fr . Once the Re are given, the magnitude of h is easily evaluated. For example, the resistance test of model is conducted at water temperature of 15°C and forward speed $Fr = 0.1$. The Re , namely C_{FM} is known for various model ship lengths. The resistance of full-scale ship is usually estimated at sea water temperature of 15°C, so the of full-scale ships at $Fr = 0.1$ are also given for various full-scale ship lengths. Then the magnitude of h can be calculated and tabulated in the following.

Table 8.1 The magnitude of multiplier of uncertainty of full-scale ship against model ship.

L_s L_m	100	150	200	250	300
3	1.25	1.26	1.27	1.27	1.28
4	1.24	1.25	1.26	1.26	1.26
5	1.23	1.24	1.25	1.25	1.26
6	1.22	1.23	1.24	1.24	1.25
7	1.21	1.22	1.23	1.24	1.24

This is the minimum evaluation of uncertainty of extrapolation of resistance. For more exact treatment, the uncertainty of friction line and the error of curve fitting in Prohaska's method are to be taken into consideration.

8.5. Data-Reduction Equations and Uncertainty Analysis for Full-Scale Power Prediction

In the following, DRE and uncertainty analysis for full-scale power prediction is presented; however, a sample calculation is not made since uncertainty estimates for open water propeller and self-propulsion tests are currently in preparation, as previously mentioned.

Data-reduction equation. The relation between EHP (Effective Horse Power) and BHP (Braked Horse Power) is given as follows.

$$\frac{EHP}{BHP} = \frac{EHP}{THP} \cdot \frac{THP}{PHP} \cdot \frac{PHP}{DHP} \cdot \frac{DHP}{BHP}$$

EHP (Effective horse power) is the work done by the resistance with ship speed.

$$EHP = R \cdot V_s$$

THP (Thrust horse power) is the work done by the thrust with advance speed of propeller.

$$THP = T \cdot V_a$$

PHP (Propeller horse power) is the work to generate the thrust (T) in the open water.

$$PHP = 2\pi \cdot n \cdot Q_o$$

(n = number of revolution of propeller).

DHP (Delivered horse power) is the work to generate the T behind the hull.

$$DHP = 2\pi \cdot n \cdot Q_B$$

BHP (Braked horse power) is included the transmission efficiency.

$$\frac{EHP}{THP} = \frac{R \cdot V_s}{T \cdot V_a} = \left(\frac{R}{T} \right) \left/ \left(\frac{V_a}{V_s} \right) \right. = \frac{1-t}{1-w_{TS}} = \eta_H$$

η_H : Hull efficiency, where the thrust deduction fraction ($1-t$) is kept to be constant between model and full-scale ship, the wake fraction of full-scale ship ($1-w_{TS}$) is estimated from model tests.

$$\frac{THP}{PHP} = \frac{T \cdot V_a}{2\pi \cdot n \cdot Q_o} = \eta_{OS}$$

η_{OS} : Full-scale propeller efficiency in the open water, which is estimated from model tests.

$$\frac{PHP}{DHP} = \frac{2\pi \cdot n \cdot Q_o}{2\pi \cdot n \cdot Q_B} = \left(\frac{T \cdot V_a}{2\pi \cdot n \cdot Q_B} \right) \left/ \left(\frac{T \cdot V_a}{2\pi \cdot n \cdot Q_o} \right) \right.$$

$$= \frac{\eta_B}{\eta_{OS}} = \eta_R$$

η_B : Propeller efficiency behind the hull

η_R : Relative rotative efficiency is kept to be constant between model and full-scale ship.

$$\frac{DHP}{BHP} = \eta_T$$

η_T : Transmission efficiency is selected according to the position of main engine.

$$\frac{EHP}{BHP} = \eta_H \cdot \eta_{OS} \cdot \eta_R \cdot \eta_T \quad (13)$$

Then we get the DRE for the power of full-scale ship

$$BHP = \frac{EHP}{\eta_H \cdot \eta_{OS} \cdot \eta_R \cdot \eta_T} \quad (14)$$

Uncertainty Analysis. Uncertainty of BHP is expressed as follows

$$U_{BHP}^2 = \left(\frac{\partial BHP}{\partial EHP} \cdot U_{EHP} \right)^2 + \left(\frac{\partial BHP}{\partial \eta_H} \cdot U_{\eta_H} \right)^2 + \left(\frac{\partial BHP}{\partial \eta_{OS}} \cdot U_{\eta_{OS}} \right)^2 + \left(\frac{\partial BHP}{\partial \eta_R} \cdot U_{\eta_R} \right)^2 + \left(\frac{\partial BHP}{\partial \eta_T} \cdot U_{\eta_T} \right)^2 \quad (15)$$

where transmission efficiency is given value, so $U_{\eta_T} = 0$. For simplicity define the total propulsive efficiency,

$$\begin{aligned} \eta_{PT} &= \eta_H \cdot \eta_{OS} \cdot \eta_R \cdot \eta_T \\ U_{BHP}^2 &= \left(\frac{1}{\eta_{PT}} \cdot U_{EHP} \right)^2 + \left(\frac{EHP}{\eta_{PT}} \cdot \frac{1}{\eta_H} \cdot U_{\eta_H} \right)^2 \\ &+ \left(\frac{EHP}{\eta_{PT}} \cdot \frac{1}{\eta_{OS}} \cdot U_{\eta_{OS}} \right)^2 + \left(\frac{EHP}{\eta_{PT}} \cdot \frac{1}{\eta_R} \cdot U_{\eta_R} \right)^2 \\ &= \left(\frac{EHP}{\eta_{PT}} \right)^2 \left\{ \left(\frac{U_{EHP}}{EHP} \right)^2 + \left(\frac{U_{\eta_H}}{\eta_H} \right)^2 \right. \\ &\quad \left. + \left(\frac{U_{\eta_{OS}}}{\eta_{OS}} \right)^2 + \left(\frac{U_{\eta_R}}{\eta_R} \right)^2 \right\} \quad (16) \end{aligned}$$

$$\begin{aligned} \left(\frac{U_{BHP}}{BHP} \right)^2 &= \left(\frac{U_{EHP}}{EHP} \right)^2 + \left(\frac{U_{\eta_H}}{\eta_H} \right)^2 \\ &+ \left(\frac{U_{\eta_{OS}}}{\eta_{OS}} \right)^2 + \left(\frac{U_{\eta_R}}{\eta_R} \right)^2 \quad (17) \end{aligned}$$

The effective horsepower (EHP) is given as follows.

$$EHP = R \cdot V_s = \frac{1}{2} \rho_s V_s^3 S_s \cdot C_{TS} \quad (18)$$

At the stage of power prediction of full-scale ship from model resistance, those ρ_s , V_s , S_s are defined a priori. The uncertainty of those values should be taken into account at the stage of trial analysis. So, uncertainty of EHP contains only the uncertainty of resistance.

$$U_{EHP} = \frac{1}{2} \rho_s V_s^3 S_s \cdot U_{C_{TS}} \quad (19)$$

Then the uncertainty of EHP is expressed as follows.

$$\frac{U_{EHP}}{EHP} = \frac{U_{C_{TS}}}{C_{TS}} \quad (20)$$

The hull efficiency contains two measured values ($1-t$, $1-w_{TS}$).

$$\begin{aligned} \eta_H &= \frac{1-t}{1-w_{TS}} \\ U_{\eta_H}^2 &= \left(\frac{\partial \eta_H}{\partial t} \cdot U_t \right)^2 + \left(\frac{\partial \eta_H}{\partial w_{TS}} \cdot U_{w_{TS}} \right)^2 \\ &= \left(\frac{U_t}{1-w_{TS}} \right)^2 + \left\{ \frac{1-t}{(1-w_{TS})^2} \cdot U_{w_{TS}} \right\}^2 \end{aligned}$$

Uncertainty expression of hull efficiency is given as follows.

$$\left(\frac{U_{\mu_H}}{\eta_H} \right)^2 = \left(\frac{U_t}{1-t} \right)^2 + \left(\frac{U_{w_{TS}}}{1-w_{TS}} \right)^2 \quad (21)$$

Equation (21) contains two kinds of uncertainties (U_t , $U_{w_{TS}}$).

According to ITTC's extrapolation method for full-scale wake from model wake, w_{TS} is given as the empirical formula.

$$\begin{aligned} w_{TS} &= (t + 0.04) \\ &+ (w_{TM} - t - 0.04) \frac{(1+k)C_{FS} + \Delta C_F}{(1+k)C_{FM}} \end{aligned}$$

For simplicity, we define the following term, which is said as the thickness ratio of boundary layer between model and full-scale ship.

$$r = \frac{(1+k)C_{FS} + \Delta C_F}{(1+k)C_{FM}} \quad (22)$$

The DRE for the wake of full-scale ship is given as follows.

$$\begin{aligned} w_{TS} &= (t + 0.04) + (w_{TM} - t - 0.04) \cdot r \\ &= w_{TM} \cdot r + (t + 0.04)(1 - r) \end{aligned} \quad (23)$$

w_{TM} : wake of model ship,
 t : thrust reduction.

Uncertainty of full-scale wake is given as follows.

$$\begin{aligned} U_{w_{TS}}^2 &= \left(\frac{\partial w_{TS}}{\partial w_{TM}} \cdot U_{w_{TM}} \right)^2 + \left(\frac{\partial w_{TS}}{\partial t} \cdot U_t \right)^2 \\ &\quad + \left(\frac{\partial w_{TS}}{\partial r} \cdot U_r \right)^2 \\ &= (r \cdot U_{w_{TM}})^2 + \{(1 - r) \cdot U_t\}^2 \\ &\quad + \{(w_{TM} - t - 0.04) \cdot U_r\}^2 \end{aligned} \quad (24)$$

From equation (22), an uncertainty expression for “ r ” is given as follows.

$$\begin{aligned} U_r^2 &= \left(\frac{\partial r}{\partial C_{FS}} \cdot U_{C_{FS}} \right)^2 + \left(\frac{\partial r}{\partial C_{FM}} \cdot U_{C_{FM}} \right)^2 \\ &\quad + \left(\frac{\partial r}{\partial k} \cdot U_k \right)^2 + \left(\frac{\partial r}{\partial \Delta C_F} \cdot U_{\Delta C_F} \right)^2 \\ &= \left[(1 + k) \cdot U_{C_{FS}} \right]^2 + \left[\frac{(1 + k) \cdot C_{FS} + \Delta C_F}{(1 + k) C_{FM}^2} \cdot U_{C_{FM}} \right]^2 \\ &\quad + \left[\frac{\Delta C_F}{(1 + k)^2 \cdot C_{FM}} \cdot U_k \right]^2 + \left[\frac{1}{(1 + k) \cdot C_{FM}} \cdot U_{\Delta C_F} \right]^2 \end{aligned} \quad (25)$$

As is discussed in 8.2, it is assumed that $U_{C_{FS}} = 0$, $U_{C_{FM}} = 0$ and $U_{\Delta C_F} = 0$.

$$U_r^2 = \left[\frac{\Delta C_F}{(1 + k)^2 \cdot C_{FM}} \cdot U_k \right]^2 = \left[\frac{\Delta C_F}{(1 + k)^2 \cdot C_{FM}^2} \cdot U_{C_{TM}} \right]^2$$

Then we get uncertainty expression for full-scale wake as follows.

$$\begin{aligned} U_{w_{TS}}^2 &= (r \cdot U_{w_{TM}})^2 + \{(1 - r) \cdot U_t\}^2 \\ &\quad + \left[(w_{TM} - t - 0.04) \cdot \frac{\Delta C_F}{(1 + k)^2 \cdot C_{FM}^2} \cdot U_{C_{TM}} \right]^2 \end{aligned} \quad (26)$$

Equation (26) contains three kinds of uncertainties, $U_{w_{TM}}$, U_t and $U_{C_{TM}}$, which were provided by previous RC. Uncertainty of model ship wake ($U_{w_{TM}}$) will be defined from self-propulsion test and propeller open test. Uncertainty of thrust reduction fraction (U_t) is treated in the next subsection. Equation (23) will have to be validated as the extrapolation method of wake from model ship to full-scale ship because it is an empirical formula.

Uncertainty of (1-t). Uncertainty of thrust reduction fraction is expressed as follows

$$1 - t = \frac{R_S}{T_S} = \frac{R_{Rest} - R_{Self}}{T_M} \quad (27)$$

where R_{Self} is towing force measured during self-propulsion test, and it should be equal to the skin friction correction. R_{Rest} is the resistance measured at resistance test and T_M is the measured thrust:

$$U_t = r(R_{Rest}, R_{Self}, T_M)$$

$$\begin{aligned} U_t^2 &= \left(\frac{\partial t}{\partial R_{Rest}} \cdot U_{R_{Rest}} \right)^2 + \left(\frac{\partial t}{\partial R_{Self}} \cdot U_{R_{Self}} \right)^2 \\ &\quad + \left(\frac{\partial t}{\partial T} \cdot U_T \right)^2 \\ &= \left(\frac{U_{R_{Rest}}}{T_M} \right)^2 + \left(\frac{U_{R_{Self}}}{T_M} \right)^2 + \left(\frac{R_{Rest} - R_{Self}}{T_M^2} \cdot U_T \right)^2 \end{aligned}$$

Usually the same apparatus are used in both resistance and self-propulsion tests.

$$\text{So } U_{R_{Rest}} = U_{R_{Self}} = U_{R_M}$$

$$\begin{aligned} U_t^2 &= 2 \left(\frac{U_{R_M}}{T_M} \right)^2 + \left(\frac{R_{Rest} - R_{Self}}{T_M^2} \cdot U_T \right)^2 \\ U_t^2 &= 2 \left(\frac{U_{R_M}}{T_M} \right)^2 + \left(\frac{1 - t}{T_M} \cdot U_T \right)^2 \end{aligned} \quad (28)$$

U_{R_M} was provided by the previous RC. U_T is uncertainty of measured thrust in the self-propulsion test and to be defined in near future.

Uncertainty of propeller characteristics. According to the ITTC's extrapolation method for full-scale propeller characteristics from model propeller is defined as follows.

$$\eta_{OS} = \frac{T_S \cdot V_a}{2\pi \cdot n \cdot Q_S} = \frac{J}{2\pi} \cdot \frac{K_{TS}}{K_{QS}} = \frac{J}{2\pi} \cdot \frac{K_{TM} - \Delta K_T}{K_{QM} - \Delta K_Q} \quad (29)$$

where no measured values are included in both ΔK_T and ΔK_Q (See Q.M. 4.9-03 03-01.2). ΔK_T and ΔK_Q are correction factors for extrapolation of propeller performance from model to full-scale.

J : advance ratio given as follows:

$$J = r(V_a, n, D_p) = \frac{V_a}{n \cdot D_p}$$

V_a : advance speed of propeller

n : number of revolution of propeller

D_p : diameter of propeller

K_{QM} : torque coefficient of model propeller

$$K_{QM} = r(\rho, n, D_p, Q) = \frac{Q}{\rho \cdot n^2 \cdot D_p^5}$$

K_{TM} : thrust coefficient of model propeller

$$K_{TM} = r(\rho, n, D_p, T) = \frac{T}{\rho \cdot n^2 \cdot D_p^4}$$

$$\begin{aligned} U_{\eta_{OS}}^2 &= \left(\frac{\partial \eta_{OS}}{\partial J} \cdot U_J \right)^2 + \left(\frac{\partial \eta_{OS}}{\partial K_{QM}} \cdot U_{K_{QM}} \right)^2 \\ &\quad + \left(\frac{\partial \eta_{OS}}{\partial K_{TM}} \cdot U_{K_{TM}} \right)^2 \\ &= \left(\frac{1}{2\pi} \cdot \frac{K_{TM} - \Delta K_T}{K_{QM} - \Delta K_Q} \cdot U_J \right)^2 \\ &\quad + \left(\frac{J}{2\pi} \cdot \frac{K_{TM} - \Delta K_T}{(K_{QM} - \Delta K_Q)^2} \cdot U_{K_{QM}} \right)^2 \\ &\quad + \left(\frac{J}{2\pi} \cdot \frac{1}{K_{QM} - \Delta K_Q} \cdot U_{K_{TM}} \right)^2 \\ &= \left(\frac{\eta_{OS}}{J} \cdot U_J \right)^2 + \left(\frac{\eta_{OS}}{K_{QM} - \Delta K_Q} \cdot U_{K_{QM}} \right)^2 \\ &\quad + \left(\frac{\eta_{OS}}{K_{TM} - \Delta K_T} \cdot U_{K_{TM}} \right)^2 \end{aligned}$$

Then,

$$\left(\frac{U_{\eta_{OS}}}{\eta_{OS}} \right)^2 = \left(\frac{U_J}{J} \right)^2 + \left(\frac{U_{K_{QM}}}{K_{QM} - \Delta K_Q} \right)^2 + \left(\frac{U_{K_{TM}}}{K_{TM} - \Delta K_T} \right)^2$$

or

$$\left(\frac{U_{\eta_{OS}}}{\eta_{OS}} \right)^2 = \left(\frac{U_J}{J} \right)^2 + \left(\frac{U_{K_{QM}}}{K_{QS}} \right)^2 + \left(\frac{U_{K_{TM}}}{K_{TS}} \right)^2 \quad (30)$$

or

$$\begin{aligned} \left(\frac{U_{\eta_{OS}}}{\eta_{OS}} \right)^2 &= \left(\frac{U_J}{J} \right)^2 + \left(\frac{U_{K_{QM}}}{K_{QM}} \right)^2 \left(\frac{K_{QM}}{K_{QM} - \Delta K_Q} \right)^2 \\ &\quad + \left(\frac{U_{K_{TM}}}{K_{TM}} \right)^2 \left(\frac{K_{TM}}{K_{TM} - \Delta K_T} \right)^2 \end{aligned} \quad (31)$$

In equation (31), only two terms underlined are different from the uncertainty of model propeller. These two terms indicate the propagation of errors from model to full-scale propeller. Uncertainties such as U_J , $U_{K_{QM}}$ and $U_{K_{TM}}$ of model propeller open test are also to be defined. Equation (29) will have to be validated as the extrapolation method of propeller characteristics from model to full-scale propeller because it is an empirical formula.

8.6. Conclusions

Friction line has a very important role on full-scale performance prediction. The roughness allowance (or correlation factor) ΔC_f is analyzed by using a friction line as a correlation line between model and full-scale ship performance. Through the analysis of propagation of uncertainty in the process of extrapolation, the following are concluded: (1) extrapolation effects on the uncertainty of resistance depends on both the Reynolds number of the model ship and that of the full-scale ship; (2) uncertainty of full-scale resistance depends on the kind of friction line used; and (3) in the process of ex-

trapolation from model to full-scale ship, uncertainty of resistance will increase by 20-30% in low Fr region. The evaluation of the uncertainty of power prediction was not completed, as it requires the uncertainty analysis of the propeller open-water test and self-propulsion tests, which were not yet available from SC. Once completed, full-scale tests are required for validation of the power prediction.

9. RECOMMENDATIONS

9.1. Recommendations to the Conference

- Adopt the Procedure “Uncertainty Analysis Spreadsheet for Resistance Measurements”, 4.9-03-02-03
- Adopt the Procedure “Uncertainty Analysis Spreadsheet for Speed Measurements”, 4.9-03-02-04
- Adopt the Procedure “Uncertainty Analysis Spreadsheet for Sinkage and Trim Measurements Tests”, 4.9-03-02-05
- Adopt the Procedure “Uncertainty Analysis Spreadsheet for Wave Profile Measurements”, 4.9-03-02-06
- Adopt as an Interim Procedure “Uncertainty Analysis in CFD, Uncertainty Assessment Methodology and Procedures”, 4.9-04-01-01

10. REFERENCES

- Abdel-Maksoud, M., Rieck, K., Pierzynski, M., 1998, “Optimierung von schnellen 2-Schrauben Schiffen mit Hilfe von viskosen Unstroemungsberechnungs – verfahren”, STG Jahrbuch.
- Abdel-Maksoud, M., Hellwig K., and Menter F.R., 2000, “Calculation of the turbulent flow around a model and full scale VLCC ship hull”, Proc. of Gothenburg 2000 - A Workshop on Numerical Ship Hydrodynamics, Chalmers Univ. of Technology, Gothenburg, Sweden.
- Abdel-Maksoud, M., and Menter, F., 2002, “Practical numerical simulation of viscous flow around ships”, The Naval Architect, Jan. 2002, pp. 36-40.
- Abdel-Maksoud, M., Menter, F., and Rieck, K., 2000, “Unsteady numerical investigation of the turbulent flow around the container ship model (KCS) with and without propeller”, Proc. of Gothenburg 2000 – A Workshop on Numerical Ship Hydrodynamics, Chalmers Univ. of Technology, Gothenburg, Sweden.
- Agarwal, R., 1999, “Computational fluid dynamics of whole-body aircraft”, Annu. Rev. Fluid Mech., Vol. 31, pp. 125-169.
- AIAA, 1995, “Assessment of Wind Tunnel Data Uncertainty”, AIAA S-071-1995.
- AIAA, 1998, “Guide for the Verification and Validation of Computational Fluid Dynamics Simulations”, AIAA-G-077-1998.
- Alessandrini, B., and Delhommeau, G., 1998, “Viscous free surface flow past a ship in drift and in rotating motion”, 22nd Symp. on Naval Hydro., Washington, DC, USA, pp. 491-507.
- Alessandrini, B., and Gentaz, L., 2000, “A fully coupled theory for viscous free surface flow computation”, Proc. of Gothenburg 2000 – A Workshop on Numerical Ship Hydrodynamics, Chalmers Univ. of Technology, Gothenburg, Sweden.
- Alexandrov, N.M., Lewis, R.M., Gumbert, C.R., Green, L.L., and Newman, P.A., 2000, “Optimization with Variable-Fidelity

- Models Applied to Wing Design”, 38th Aerospace Sciences Meeting & Exhibit, Reno, NE, USA, AIAA Paper 2000-0841.
- Alexandrov, N.M., and Hussaini, M.Y., eds, 1997, “Multidisciplinary Design Optimization”, Proc. of the ICASE/NASA Workshop on MDO, SIAM, Philadelphia, PA, USA.
- Anderson, E.J., Techet, A., McGillis, W.R., Grosenbaugh, M.A., and Triantafyllou, M.S., 1999, “Visualization and analysis of boundary layer flow in live and robotic fish”, 1st Symp. on Turbulence and Shear Flow Phenomena, Santa Barbara, CA, USA, pp. 945-949.
- ANSI/ASME, 1985, “Measurement Uncertainty: Part 1, Instrument and Apparatus”, ANSI/ASME PTC 19.1-1985.
- Azcueta, R., Muzafarija, S., Peric, M., and Yoo, S.D., 1999a, “Computation of flows around hydrofoils under the free surface”, 7th Int. Conf. on Num. Ship Hydro., Nantes, France, pp. 2.7-1,10.
- Azcueta, R., Muzafarija, S., Peric, M., 1999b, “Computation of breaking bow waves for a very full hull ship”, 7th Int. Conf. on Num. Ship Hydro., Nantes, France, pp. 6.2-1,11.
- Bandyopadhyay, P., Castano, J., Thivierge, D. and Nedderman, W., 1998, “Drag Reduction Experiments on a Small Axisymmetric Body in Saltwater Using Electromagnetic Microtiles”, Proc. of the Int. Symp. on Seawater Drag Reduction, Newport, RI, USA, pp. 373-378.
- Batina, J., 1993, “A gridless Euler / Navier Stokes solution algorithm for complex aircraft applications”, AIAA Paper 93-0333.
- Bechert, D.W., Bruse, M., Hage, W., Van Der Hoeven, J.G.T, and Hoppe, G., 1997, “Experiment on drag reducing surfaces and their optimization with an adjustable geometry”, J. Fluid Mech., Vol. 338, pp. 59-8.
- Becker, S., Durst, F., and Lienhart H., 1999, “Laser Doppler Anemometer for In-Flight Velocity Measurements on Airplane Wings”, AIAA Journal, Vol. 37 (6), pp. 680-687.
- Beddhu, M., Jiang, M.Y., Whitfield, D.L., Taylor, L.K., 1999, “Computation of the wetted transom stern flow over model 5415”, 7th Int. Conf. on Num. Ship Hydro., Nantes, France, pp. 2.5-1,13.
- Beddhu, M., Pankajakshan, R., Jiang, M.Y., Taylor, L., Remotigue, M.G., Briley, W.R., Whitfield, D.L., 2000, “Computation and evaluation of CFD results for practical ship hull forms”, Proc. of Gothenburg 2000 - A Workshop on Numerical Ship Hydrodynamics, Chalmers Univ. of Technology, Gothenburg, Sweden.
- Bell, J.H., Schairer, E.T., Hand, L.A., and Mehta, R.D., 2001, “Surface Pressure Measurements Using Luminescent Coatings”, Annu. Rev. Fluid Mech., Vol. 33, pp.155-206.
- Bertram, V., and Bulgarelli, U.P., 1999, “Numerical wash prediction”, Proc. Int. Conf. on High-Performance Marine Vehicles, HIPER’99, Zevenwacht, South-Africa, pp. 4-11.
- Bonmarin, P., 1989, “Geometric properties of deep-water breaking waves”, J. Fluid Mech., Vol. 209, pp. 405-433.
- Brocchini, M., and Peregrine, D.H., 2001a, “The dynamics of strong turbulence at free surfaces. Part 2. Free-surface boundary conditions”, J. Fluid Mech., Vol. 449, pp. 225-254.

- Brocchini, M., and Peregrine, D.H., 2001b, "The dynamics of strong turbulence at free surfaces. Part 1. Description", J. Fluid Mech., Vol. 449, pp. 255-290.
- Bruzzo, D., Cassella, P., Miranda, S., Pensa, C., and Zotti, I., 1997, "The Form Factor by Means of Multiple Geosim Model Test", Proc. Intl. Conf. on Ships and Marine Research, NAV'97, Sorrento, Italy.
- Bugalski, T., 1997, "Modern methods for investigation of hull-propeller interaction phenomena using CFD", Proc. Intl. Conf. On Ships and Marine Research, NAV'97, Sorrento, Italy.
- Bushnell, D. M., 1998, "Drag reduction 'designer fluid mechanics'-aeronautical status and associated hydrodynamic possibilities", Proc. of the Int. Symp. on Seawater Drag Reduction, Newport, RI, USA.
- Buttsworth, D.R., Elston, S.J., and Jones, T.V., 2000, "Skin friction measurements on reflective surfaces using nematic liquids crystal", Experiments in Fluids, Vol. 28 (1), pp. 64-73.
- Callan, J. and Marusic, I., 2001, "Effects of Changing Aspect Ratio Through a Wind-Tunnel Contraction", AIAA Journal, Vol. 39 (9), pp.1800-1803.
- Casey, M., and Wintergeste, T. (eds.), 2000, "ERCOFTAC Special Interest Group on Quality and Trust in Industrial CFD – Best Practice Guidelines", Version 1, published by ERCOFTAC.
- Ceniceros, H.D., Hou, T.Y., 1999, "Dynamic generation of capillary waves", Phys. Fluids, Vol. 11 (5), pp. 1042-1050.
- Chang, K.A., and Liu, P.L.F., 2000, "Pseudo turbulence in PIV breaking-wave measurements", Experiments in Fluids, Vol. 29 (4), pp. 331-338.
- Chang, K.A., and Liu, P.L.F., 1998, "Velocity, acceleration and vorticity under a breaking wave", Phys. of Fluids, Vol. 10 (1), pp. 327.
- Chanson, H., 1996, "Air Bubble Entrainment in Free-Surface Turbulent Shear Flows", Academic Press, San Diego, CA, USA.
- Chen, X.N., Gronarz, A., List, S., and Stuntz, N., 2000, "Flow around ships sailing in shallow water – experimental and numerical results", 23rd Symp. on Naval Hydro., Val de Reuil, France.
- Chen, C.-F.A., Lotz, R.D., and Thompson, B. E., 2002, "Assessment of Numerical Uncertainty Around Shocks and Corners on Blunt Trailing-Edge Supercritical Airfoils", Computers and Fluids, Vol. 3 (1), pp. 25-40.
- Chen, G., Kharif, C., Zaleski, S., and Li, J., 1999, "Two-dimensional Navier-Stokes simulation of breaking waves", Phys. of Fluids, Vol. 11 (1), pp. 121.
- Chen, X.-N., 1999, "Ship wave making over a natural topography", 7th Int. Conf. Numerical Ship Hydrodynamics, Nantes, France.
- Choi, K.S., 1999, "European drag reduction research – Recent developments and current status", Proc. of Symp. on Smart Control of Turbulence, Tokyo, Japan, pp. 21-36.
- Choi, K.S., Clayton, B. R., 1998, "The mechanism of turbulent drag reduction with wall oscillation", Proc. of the Int. Symp. on Seawater Drag Reduction, Newport, RI, USA, pp. 229-235.
- Choi, K.S., Yang, X., Clayton, B.R., Glover, E.J., Altar, M., Semenov, B.N., and Kulik, V.M., 1997, "Turbulent drag reduction us-

- ing compliant surface”, Proc. of Roy. Soc. London A, Vol. 453, pp. 2229-2240.
- Chou, S.K. Chau, S.W., Chen, W.C., and Hsin, J.Y., 2000, “Computation of ship flow around commercial hull forms with free surface propeller effect”, Proc. of Gothenburg 2000 – A Workshop on Numerical Ship Hydrodynamics, Chalmers Univ. of Technology, Gothenburg, Sweden.
- Cleary, A.J., Falgout, R.D., Van Emden, H., Jones, J.E., Manteuffel, T.A., McCormick, S.F., Miranda, G.N., and Ruge, J.W., 2000, “Robustness and Scalability of Algebraic Multigrid”, SIAM J. on Sci. Computing, Vol. 21 (5), pp. 1886-1908.
- Coleman, G.N., Kim, J., and Spalart, P.R., 2000, “A numerical study of strained three-dimensional wall-bounded turbulence”, J. Fluid Mech., Vol. 416, pp. 75- 116.
- Coleman, H.W., and Steele, W.G., 1999, “Experimentation and Uncertainty Analysis for Engineers”, 2nd Edition, Wiley, New York, NY, USA.
- Coleman, H.W., and Stern, F., 1997, “Uncertainty in CFD code validation”, J. Fluids Eng., Vol. 119, pp. 795-803.
- Cooper, A.J., and Carpenter, P.W., 1997a, “The stability of rotating-disc boundary-layer flow over a compliant wall. Part 1. Type I and II instabilities”, J. Fluid Mech., Vol. 350, pp. 231-259.
- Cooper, A.J., and Carpenter, P.W., 1997b, “The stability of rotating-disc boundary-layer flow over a compliant wall. Part 2. Absolute instability”, J. Fluid Mech., Vol. 350, pp. 261-270.
- Cotroni, A., Di Felice, F., Romano, G.P., and Elefante, M., 1999, “Propeller tip vortex analysis by means of PIV”, PIV'99, Santa Barbara, CA, USA , pp. 249-254.
- Cowles, G., and Martinelli, L., 1998, “A viscous multiblock flow solver for free-surface calculations on complex geometries”, 22nd Symp. on Naval Hydro., Washington, DC, USA, pp. 445-462.
- Cox, G., 2000, “Sex, lies and wave wake”, RINA Int. Conf. Hydrodynamics of High-Speed Craft – Wake wash and motion control , London, UK, paper 2.
- Cura-Hochbaum, A., 1998, “Computation of the turbulent flow around a ship model in steady turn and in steady oblique motion”, 22nd Symp. on Naval Hydro., Washington DC, USA, pp. 550-567.
- Cura-Hochbaum, A., and Schumann, C., 1999, “Free surface viscous flow around ship models”, 7th Int. Conf. on Num. Ship Hydro., Nantes, France.
- Cura-Hochbaum, A., and Vogt, M., 2000, “Flow and resistance prediction for a container ship”, Proc. of Gothenburg 2000 – A Workshop on Numerical Ship Hydrodynamics, Chalmers Univ. of Technology, Gothenburg, Sweden.
- Davies, C., and Carpenter, P.W., 1997, “Numerical Simulation of the Evolution of Tollmien-Schlichting Waves over Finite Compliant Panels”, J. Fluid Mech., Vol. 335, pp. 361-392.
- De Graaff, D.B., and Eaton, J.K., 2000, “Reynolds-Number Scaling of the Flat-Plate Turbulent Boundary Layer”, J. Fluid Mech., Vol. 422, pp. 319-346.
- De Graaff, D.B., and Eaton, J.K., 2001, “A high-resolution laser Doppler anemometer: design, qualification, and uncertainty”, Experiments in Fluids, Vol. 30 (3), pp. 295-301.
- Deng, G.B., and Visonneau, M., 1999, “Comparison of explicit algebraic stress models

- and second order turbulence closures for steady flows around ships”, 7th Int Conf. on Num. Ship Hydro, Nantes, France.
- Deng, G.B., and Visonneau, M., 2000, “Comparison of explicit algebraic stress models and second order turbulence closures for steady flows around the KVLCC2 ship at model and full scales”, Proc. of Gothenburg 2000 – A Workshop on Numerical Ship Hydrodynamics, Chalmers Univ. of Technology, Gothenburg, Sweden.
- Desabrais, K.J., and Johari, H., 2000, “Direct Circulation Measurement of a Tip Vortex”, AIAA Journal, Vol. 39 (9), pp. 1800-1803.
- Di Lisio, R., Grenier, E., and Pulvirenti, M., 1998, “The convergence of the SPH method”, Computers Math Applic., Vol. 35,1/2, pp. 95-102.
- Di Mascio, A., and Campana, E.F., 1999a, “The numerical simulation of the yaw flow of a free surface ship”, 7th Int Conf on Num Ship Hydro, Nantes, France.
- Di Mascio, A., and Campana, E.F., 1999b, “Yaw Flow Simulation for the Series 60”, Ship Technology Research, Vol. 46 (4), pp. 223-229.
- Di Mascio, A., Muscari, R., and Broglia, R., 2000, “Computation of the flow past the U.S. navy combatant DTMB 5415 by a Godunov-type scheme”, Proc. of Gothenburg 2000 – A Workshop on Numerical Ship Hydrodynamics, Chalmers Univ. of Technology, Gothenburg, Sweden.
- Dinham-Peren, T., 2001, “Solitary wave generation by vessels in shallow water”, Int. Conf. Hydrodynamics of High-Speed Craft, Shanghai, China.
- Doctors, L.J., and Day, A.H., 2001, “The generation and decay of waves behind high-speed vessels”, 16th Int. Workshop on Water Waves and Floating Bodies, Hiroshima, Japan, pp. 33-36.
- Doi, Y., Ueda, T., Mori, K., and Ninomiya, S., 1999, “Study on Rowing Simulation and Its Application to Evaluate Oar Size and Rowing Pattern”, J. Soc. of Naval Architects of Japan, Vol. 186, pp. 89-96.
- Dommermuth, D., Innis, G., Luth, T., Novikov, E., Schlageter, E., and Talcott, J., 1998, “Numerical simulation of bow waves”, 22nd Symp. on Naval Hydro., Washington, DC, USA, pp. 508-521.
- Dong, R. R., Katz, J., and Huang, T. T., 1997, “On the structure of bow waves on a ship model”, J. Fluid Mech., Vol. 346, 77-116.
- Doyle, R., Whittaker, T.J.T., and Elsaesser, B., 2001, “Wake wash characteristics of high-speed ferries in shallow water”, Ship Technology Research, Vol. 48, pp. 181-196.
- Duncan J.H., Philomin V., Behres M., and Kimmel J., 1994, “The formation of spilling breaking water waves”, Phys. Fluids, Vol. 6 (8), pp. 2558-2560.
- Duncan J.H., Qiao H., Philomin V., and Wenz A., 1999, “Gentle spilling breakers: crest profile evolution”, J. Fluid Mech., Vol. 379, pp. 191-222.
- Duncan J. H., 2001, “Spilling Breakers”, Annu. Rev. Fluid Mech., Vol. 33, pp.519-547
- Eça L, Hoekstra M., 2000, “Numerical prediction of scale effects in ship stern flows with eddy-viscosity turbulence models”, 23rd Symp. on Naval Hydro., Val de Reuil, France.
- Eça, L., and Hoekstra, M., 1999, “On the numerical verification of ship stern flow cal-

- culations”, 1st MARNET Workshop, Barcelona, Spain.
<http://pronet.wsatkins.co.uk/marnet>
- Eça, L., and Hoekstra, M., 2000, “On the Application of Verification Procedures in Computational Fluid Dynamics”, 2nd MARNET Workshop, Copenhagen, Denmark.
<http://pronet.wsatkins.co.uk/marnet>
- Eggers, K.W.H., Sharma, S.D., and Ward, L.W., 1967, “An assessment of some experimental methods for determining the wavemaking characteristics of a ship form”, SNAME Trans., Vol. 67, pp. 112-157.
- Eidelman, A., Branover, H., Golbraikh, E., and Moiseev, S., 1998, “MHD Turbulence Experiments, Drag Reduction and Application to Non-MHD Flow”, Proc. of the Int. Symp. on Seawater Drag Reduction, Newport, RI, USA, pp. 379-384.
- El Moctar, O., 1999, “Numerical investigation of propeller-rudder interaction”, 2nd Numerical Towing Tank Symp., Rome, Italy.
- Erwandi, and Suzuki, T., 2001, “Analysis of the Unsteady Waves around a Ship Model Using Projected Light Distribution Method”, J. Soc. of Naval Architects of Japan, Vol. 190, pp. 263-270.
- Freitas, C. J., 1993, “Editorial Policy Statement on the Control of Numerical Accuracy”, J. Fluids Eng., Vol. 115, pp. 339-340.
- Fujiwara, T., Ueno, M., and Nimura, T., 1998, “Estimation of Wind Forces and Moments acting on Ships”, J. Soc. of Naval Architects of Japan, Vol. 183, pp.77-90
- Fukuda, H., Tokunaga J., Nobunaga T., 2000, “Frictional drag reduction with air lubricant over a super-water-repellent surface”, J. Marine Science and Tech., Vol. 5, pp. 123-130.
- Gadd, G.E., 2000, “High-speed ferry wash prediction”, The Naval Architect, Sept. 2000.
- Gadd, G.E., 1999, “Far field waves made by high speed ferries”, RINA Int. Conf. Hydrodynamics of High-Speed Craft, London, UK.
- Gad-el-Hak, M., 1998, “Compliant coatings, the simpler alternatives”, Proc. of Int. Symp. on Sea water drag reduction, Newport, RI, USA.
- Garofallidis, D.A., 1996, “Experimental and Numerical Investigation of the Flow around a Ship Model at Various Froude Numbers”, Ph.D. Thesis, Dept. of Naval Architecture and Marine Engineers, National Technical University of Athens, Greece.
- Gasljevic, K., Hoyer, K., and Matthys, E.F., 1998, “Drag-reducing additives for recirculating hydronic systems: full scale system engineering analysis and field test”, Proc. of Int. Symp. on Sea water drag reduction, Newport, RI, USA.
- Gatchell, S., Hafermann, D., Jensen, G., Marzi, J., and Vogt, M., 2000, “Wave resistance computations – A comparison of different approaches”, 23rd Symp. on Naval Hydro., Val de Reuil, France.
- Gentaz, L., Guillerm, P.E., Alessandrini, B., and Delhommeau, G., 1999, “Three-dimensional free surface viscous flow around a ship in forced motion”, 7th Int Conf on Num Ship Hydro, Nantes, France.
- Gibson, M.M., and Launder, B.E., 1978, “Ground effects on pressure fluctuations in the atmospheric boundary layer”, J. Fluid Mech., Vol. 86, 491-511.
- Grigson, C.W.B., 2000, “A Planar Friction Algorithm and its Use in Analysing Hull Resistance”, Trans. R. Inst. of Naval Arch., Vol. 142, 76-115.

- Gui, L., Longo, J., Metcalf, B., Shao, J., and Stern, F., 2000, "Forces, Moment and Wave Pattern for Naval Combatant in Regular Head Waves", 23rd Symp. on Naval Hydro., Val de Reuil, France.
- Gui, L., Longo, J., and Stern, F., 2001a, "Towing Tank PIV Measurement System, Data and Uncertainty Assessment for DTMB Model 5512", Experiments in Fluids, Vol. 31, pp. 336-346.
- Gui, L., Longo, L., Metcalf, B., Shao, J., and Stern, F., 2001b, "Forces, Moment, and Wave Pattern for Naval Combatant in Regular Head Waves – Part 2: Measurement Results and Discussions", Experiments in Fluids, Vol. 32, pp. 27-36.
- Guillerm, P.E., and Alessandrini, B., 1999, "3D RANSE-potential coupling using a Fourier-Kochin approach", 7th Int Conf. on Num. Ship Hydro., Nantes, France, pp. 2.6-1,11
- Hamalainen, R., and Heerd, J. V., 1998, "Hydrodynamics development for a large fast monohull passenger ferry", SNAME Transactions, Vol. 106, pp. 413-442.
- Hanratty, T.J., and Campbell, J.A., 1996, "Measurement of Wall Shear Stress", Fluid Mechanics Measurements, 2nd ed., Goldstein, R.J. ed., Taylor & Francis.
- Harries, S., Valdenazzi, F., Abt, C., and Viviani, U., "Investigation on optimization strategies for the hydrodynamic design of fast ferries", FAST 2001, Seattle, WA, USA.
- Hino, T., 1998, "Navier-Stokes computations of ship flows on unstructured grids", 22nd Symp. on Naval Hydro., Washington DC, USA, pp. 463-475.
- Hino, T., 1999, "Shape optimization of practical ship hull forms using Navier-Stokes analysis", 7th Int Conf. on Num. Ship Hydro., Nantes, France.
- Hino, T., Kodama, Y., and Hirata, N., 1998, "Hydrodynamic shape optimization of ship hull forms using CFD", 3rd Osaka Colloquium on Advanced CFD Applications to Ship Flow and Hull Form Design, Osaka, Japan, pp. 533-541.
- Hoekstra, M., de Jager, A., and Valkhof, H.H., 2001, "Viscous-flow calculations used for dredger design", Proc. PRADS'01, Shanghai, China, pp. 437-444.
- Hoekstra, M., Eça, L., Windt, J. and Raven, H., 2000, "Viscous flow calculation for KVLCC2 and KCS models using the PARNASSOS code", Proc. of Gothenburg 2000 – A Workshop on Numerical Ship Hydrodynamics, Chalmers Univ. of Technology, Gothenburg, Sweden.
- Holzappel, F., Lenze, B., and Leuckel, W., 1999, "Quintuple Hot-Wire Measurements of the Turbulence Structure Swirling Flows", J. Fluids Eng., Vol. 121, pp. 517-525.
- Hong, W.L., and Walker, D.T., 2000, "Reynolds averaged equations for free-surface flows with application to high Froude number jet spreading", J. Fluid Mech., Vol. 417, pp. 183-209.
- Hoyt, J., and Sellin, R., 1998, "A New Tracer Technique for Turbulent Flow", 22nd Symp. on Naval Hydro., Washington, DC, USA, pp. 330-340.
- Hoyt, J. W., 1998, "Polymer solution effects on turbulent friction mechanisms", Proc. of Int. Symp. on Sea water drag reduction, Newport, RI, USA.
- Huan, J., and Huang, T.T., 1998, "Sensitivity analysis methods for shape optimization in non-linear free surface flow", 3rd Osaka Colloquium on Advanced CFD Applica-

- tions to Ship Flow and Hull Form Design, Osaka, Japan, pp. 457-483.
- Hughes, M., 2001, “CFD prediction of wake wash in finite water depth”, Proc. Int. Conf. on High-Performance Marine Vehicles, HIPER’01, Hamburg, Germany, pp. 200-211.
- Hyams, D., Sreenivas, K., Sheng, C., Nichols, S., Taylor, L., Briley, W., Marcum, D., and Whitfield, D., 2000, “An unstructured multi-element solution algorithm for complex geometry hydrodynamic simulations”, 23rd Symp. on Naval Hydro., Val de Reuil, France.
- Hyman, D., Pan, T., Reshotko, E., and Mehregany, M., 1999, “Microfabricated Shear Stress Sensors. Part 2: Testing and Calibration”, AIAA Journal, Vol. 37 (1), pp. 73-78.
- Iafrazi, A., Di Mascio, A., and Campana, E.F., 2001, “A level set technique applied to unsteady free surface flows”, Int J. for Num. Methods in Fluids, Vol. 35, pp. 281-297.
- Iafrazi, A., Olivieri, A., Pistani, F., and Campana, E.F., 2000, “Numerical and experimental study of the wave breaking generated by a submerged hydrofoil”, 23rd Symp. on Naval Hydro., Val de Reuil, France.
- Ilinca, C., Zhang, X. D., Trepanier, J.-Y., and Camarero, R., 2000, “A Comparison of Three Error Estimation Techniques for Finite-Volume Solutions of Compressible Flows”, Computer Methods in Applied Mechanics and Engineering, Vol. 189 (4), pp. 1247-1275.
- ISO, 1993a, “Guide to the Expression of Uncertainty in Measurement”, ISO, ISBN 92-67-10188-9.
- ISO, 1993b, “International Vocabulary of Basic and General Terms in Metrology”, ISO, ISBN 92-67-01075-1.
- ITTC, 1999, “Report of the Resistance Committee”, 22nd Int. Towing Tank Conference, Seoul, Korea & Shanghai, China, Vol. 1, pp. 173-246.
- Jameson, A., and Alonso, J.J., 1999, “Future research avenues in computational engineering and design”, ICIAM 99, 4th Int. Cong. on Industrial & Applied Mathematics, Edinburgh, UK, Oxford Univ. Press., pp. 79-95.
- Jang J., Kim, H., and Lee, S-H., 1999, “On the drag reduction of a passenger ship with air cavity”, J. of Ship & Ocean Tech., Vol. 3 (4), pp. 15-22.
- Jang, J., Ahn, I.J., Kim, J., Suh, J.C., Kim, H., Lee, S-H., and Song, M., 2001, “A practical application of air lubrication on a small high speed boat”, Proc. PRADS’01, Shanghai, China, pp. 113-118.
- Janson, C.E., Leer-Andersson, M., and Larsson, L., 2001, “A combined Rankine/Kelvin source method for farfield wash wave calculations”, Proc. Int. Conf. on High-Performance Marine Vehicles HIPER’01, Hamburg, Germany, pp. 236-250.
- Jensen, G., Mewis, F., 1999, “Schiffsformoptimierung unter Verwendung numerischer und experimenteller Techniken in der Praxis”, 100 Jahre STG.
- Jiang, T., 1998, “Investigation of waves generated by ships in shallow water”, 22nd Symp. on Naval Hydro., Washington, DC, USA, pp. 601-612.
- Jiang, T., 2000, “Ship waves in shallow water”, Mercator Univ. Duisburg, Fortschritt – Bericht VDI Reihe 12 Nr. 466.

- Joslin, R.D., 1998, "Aircraft laminar flow control", Annu. Rev. Fluid Mech., Vol. 30, pp. 11-29.
- Kang, K.J., Lee, C.J., and Kim, D.H., 2001, "Hull form development and powering performance characteristics for a 2,500 ton class trimaran", Proc. PRADS'01, Shanghai, China, pp. 151-157.
- Kato, H., Miura, K., Yamaguchi, H., and Miyanaga, M., 1998, "Experimental study on micro bubble ejection method for frictional drag reduction", J. Marine Science and Tech., Vol. 3, pp. 122-129.
- Kato, H., Iwashina, T., Miyanaga, M., and Yamaguchi H., 1999, "Effect of microbubbles on the structure of turbulence in a turbulent boundary layer", J. Marine Science and Tech., Vol. 4, pp. 155-162.
- Kim, S.E., 2000, "Reynolds stress transport modelling of turbulent shear flow past a modern VLCC hull form", Proc. of Gothenburg 2000 – A Workshop on Numerical Ship Hydrodynamics, Chalmers Univ. of Technology, Gothenburg, Sweden.
- Kim, O., Okuno, T., and Sugii, Y., 2001, "Image Measurement of Velocity Distribution Based on Wavelet Transform", J. Kansai Soc. N. A., Vol. 235, pp. 199-205.
- Knill, D.L., Giunta, A., Baker, C.A., Grossman, B., Mason, W.H., Haftka, R.T., and Watson, L.T., 1999, "Response Surface Models Combining Linear and Euler Aerodynamics for Supersonic Transport Design", Journal of Aircraft, Vol. 36 (1), pp. 75-86.
- Kodama, Y., and Kakugawa, A., 1999, "Preliminary Experiments on microbubbles for drag reduction using a long flat plate ship", ONR Workshop on Gas Based Surface Ship Drag Reduction, Newport, RI, USA.
- Kodama, Y., Kakugawa, A., Takahashi, T., and Kawashima, H., 2000, "Experimental study on micro bubbles and their applicability to ships for skin friction reduction", Int. J. of Heat and Fluid Flow, Vol. 21, pp. 582-588.
- Kofoed-Hansen, H., Jensen, T., Kirkegaard, J., and Fuchs, J., 1999, "Prediction of wake wash from high-speed craft in coastal areas", RINA Int. Conf. Hydrodynamics of High-Speed Craft, London, UK, paper No. 5.
- Kofoed-Hansen, H., Jensen, T., Sorensen, R., and Fuchs, J., 2000, "Wake wash risk assessment of high-speed ferry routes - a case study and suggestions for model improvements", RINA Int. Conf. Hydrodynamics of High-Speed Craft - Wake wash and motion control, London, UK, paper No. 3.
- Kulik, V. M., and Semenov, B. N., 1996, "The measurement of dynamic properties of viscoelastic materials for turbulent drag reduction", Emerging Techniques in Drag Reduction, Mechanical Engineering Publ., London, UK, pp. 207-217.
- Lalli, F., Di Felice, F., Esposito, P.G., Moriconi, A., and Piscopia, R., 2000, "Longitudinal Cut Method Revisited: A Survey on Main Error Sources", J. Ship Research, Vol. 44 (2), pp. 120-139.
- Landrini, M., Colagrossi, A., and Tulin, M.P., 2001, "Breaking bow and stern waves: numerical simulations", 16th Int. Workshop on Water Waves and Floating Bodies, Hiroshima, Japan, pp. 89-92.
- Larsson, L., Stern, F., and Bertram, V., 2002, "Summary and Assessment of the Gothenburg 2000 Workshop", Proc. of Gothenburg 2000 – A Workshop on Numerical Ship Hydrodynamics, Chalmers Univ. of Technology, Gothenburg, Sweden.

- Latorre, R., 1997, “Ship hull drag reduction using bottom air injection”, Ocean Engineering, Vol. 24, pp. 161-175.
- Laurens, J.-M., and Grosjean, F., 2002, “Numerical simulation of the propeller-rudder interaction”, Ship Technology Research, Vol. 49, pp. 3-12.
- Lee, I., and Sung, H.J., 1999, “Development of an array of pressure sensors with PVDF film”, Experiments in Fluids, Vol. 26, pp. 27-35.
- Lee, J., Lee, S.J., and Van, S.H., 1998, “Wind Tunnel Test on a Double Deck Shaped Ship Model”, 3rd Int. Conference on Hydrodynamics, Seoul, Korea, pp. 815-820.
- Leer-Andersen, M., Clason, P., Ottoson, P., Andreasson, H., and Svensson, U., 2000, “Wash Waves Problems and Solutions”, SNAME Annual Meeting, Vancouver, BC, Canada, paper No. 1.
- Lin, H.J., and Perlin, M., 2001, “The velocity and vorticity fields beneath gravity-capillary waves exhibiting parasitic ripples”, Wave Motion, Vol. 33 (3), pp. 245-257.
- Lin, J.C., and Rockwell, D., 1995, “Evolution of a quasi-steady breaking wave”, J. Fluid Mech., Vol. 302, pp. 29-44.
- Lindgren, H., and Dyne, G., 1979, “Ship Performance Prediction”, Proc. Int. Symposium on Advances in Marine Technology, Trondheim, Norway.
- Longuet-Higgins, M.S., 1997, “Progress towards understanding how waves break”, 21st Symp. Nav. Hydro., Trondheim, Norway, pp. 7-28.
- Longuet-Higgins, M.S., 1992, “Capillary rollers and bores”, J. Fluid Mech., Vol. 240, 659-679.
- Longuet-Higgins, M.S., 1994, “Shear instability in spilling breakers”, Proc. R. Soc. London Ser. A, Vol. 446, pp. 399-409.
- Mehta, U.B., 1998, “Credible Computational Fluids Dynamics Simulations”, AIAA Journal, Vol. 36, pp. 665-667.
- Meneveau, C., and Katz, J., 2000, “Scale-invariance and turbulence models for large-eddy simulation”, Annu. Rev. Fluid Mech., Vol. 32, pp. 1-32.
- Meng, J. C. S., 1998, “Engineering insight of near wall micro turbulence for drag reduction and deviation of design map for sea water electromagnetic turbulence control”, Proc. of Int. Symp. on Sea water drag reduction, Newport, RI, USA, pp. 359-367.
- Merienne, M.C., and Bouvier, F., 1999, “Vortical flow field investigation using a two-component pressure sensitive paint at low speed”, 18th Int. Congress on Instrumentation in Aerospace Simulation Facilities, ONERA TP 1999-69.
- Merkle, C.L., and Deutsch, S., 1990, “Drag reduction in liquid boundary layers by gas injection”, Viscous Drag Reduction in Boundary Layer, Progr. in Astronautics and Aeronautics, Vol. 124, pp. 351-412.
- Milgram, J.H., 1998, “Fluid mechanics for sailing vessel design”, Annu. Rev. Fluid Mech., Vol. 30, pp. 613-653.
- Min, K.S., Choi, J., Yum, D., Chung, K., Chang, B., Chung, S., and Han, B., 2000, “Study on the prediction of flow characteristics around a ship hull”, 23rd Symp. on Naval Hydro., Val de Reuil, France.

- Miyata, H., and Gotoda, K., 2000, "Hull design by CAD/CFD simulation", 23rd Symp. on Naval Hydro., Val de Reuil, France.
- Morris, J.P., 2000, "Simulating surface tension with smoothed particle hydrodynamics", Int. J. for Num. Methods in Fluids, Vol. 33, pp. 333-353.
- Mui, R.C.Y., and Dommermuth D.G., 1995, "The vortical structure of parasitic capillary waves", J. Fluids Eng., Vol. 117, pp. 355-361.
- Muscari, R., and Di Mascio, A., 2002, "A model for the simulation of steady spilling breaking waves", J. Ship Res., to appear.
- Na, Y., and Moin, P., 1998, "Direct numerical simulation of a separated turbulent boundary layer", J. Fluid Mech., Vol. 370, pp. 175.
- Nagaosa, R., 1999, "Direct numerical simulation of vortex structures and turbulent scalar transfer across a free surface in a fully developed turbulence", Phys. Fluids, Vol. 11, pp. 1581-1591.
- Nagaya, S., Kakugawa, A., Kodama, Y., and Hishida, K., 2001, "PIV/LIF Measurements on 2-D Turbulence Channel Flow with Microbubbles", PIV'01, Gottingen, Germany.
- Newman III, J.C., Taylor III, A.C., Barnwell, R.W., Newman, P.A., and Hou, G.J.-W., 1999, "Overview of sensitivity analysis and shape optimization for complex aerodynamic configurations", Journal of Aircraft, Vol. 36 (1), pp. 87-96.
- Nishio, S., and Okuno, T., 1997, "Development of image measurement system by means of statistical analysis (3rd report: measurement of three-dimensional flow field)", J. of Kansai Soc. N.A., Vol. 228, pp. 59-65.
- Nishio, S., Nakao, S., and Okuno, T., 1998, "Image measurement of the wave height distributions around a ship hull in regular wave", J. Soc. of Naval Architects of Japan, Vol. 184, pp. 93-100.
- Noblesse, F., 2001, "Analytical representation of ship waves", Ship Technology Research, Vol. 48, pp. 23-48.
- Oberkampf, W.L., and Trucano, T.G., 2000, "Validation Methodology in Computational Fluid Dynamics", AIAA Fluids 2000, Paper No. 2549, Denver, CO, USA.
- Ogura, M., and Tamashima, M., 1996, "On a method to design the circulating water channel with the performance for measurements", Trans. West-Japan Soc. Naval Architects, Vol. 92, pp. 59-80.
- Okamoto, Y., and Matsuda, S., 1999, "Interaction between two energy-saving devices", J. of the Kansai Soc. of N.A., Vol. 232, pp. 25-30.
- Olivieri, A., Pistani, F., and Penna, R., 2001, "Towing Tank Experiments of Boundary Layer and Wake, and Free Surface Flow Around a Naval Combatant", 26th American Towing Tank Conference, Glenn Cove, NY, USA.
- Osaka H., Kameda T., and Mochizuki, S., 1998, "Re-examination of the Reynolds – Number – Effect on the Mean Flow Quantities in a Smooth Wall Turbulent Boundary Layer", Int. Journal of Japan Society of Mechanical Engineering, pp. 123-129.
- Ostafichuk, P.M., Calisal, S.M., Field, A.I., and Cherchas, D.B., 2000, "Improvement of submarine control surface effectiveness through wind tunnel testing", 4th Int. Conf. on Hydrodynamics, Vol. 1, pp. 223-228.
- Osterlund, J. M., and Johansson, A. V., 1999, "Measurements in a flat plate turbulent

- boundary layer”, 1st Int. Symp. on Turbulence and Shear Flow Phenomena, Santa Barbara, CA, USA, pp. 297-302.
- Pan, T., Hyman, D., Mehregany, M., Reshotko, E., and Gaeverick S., 1999, “Microfabricated Shear Stress Sensors, Part1: Design and Fabrication”, AIAA Journal, Vol. 37 (1), pp. 66-72.
- Pelletier, D. Turgeon, E., Lacasse, D., and Borggaard, J., 2001, “Adaptivity, Sensitivity, and Uncertainty: Towards Standards in CFD”, 39th AIAA Aerospace Sciences Meeting and Exhibit, Reno, NV, USA, AIAA Paper 2001-0192.
- Pereira, F., Gharib, M., Modarress, D., and Dabiri, D., 1999, “Defocusing DPIV: A 3-Component 3-D DPIV Measurement Technique. Application to Bubbly Flows”, PIV'99, Santa Barbara, CA, USA, pp. 275-280.
- Peri, D., Campana, E.F., and Di Mascio, A., 2001b, “Development of CFD based design optimization architecture”, Computational Fluid and Solid Mechanics, ed. KJ Bathe, Elsevier, Proc. 1st MIT Conf. on Comput. Fluid and Solid Mech., Cambridge, MA, USA, pp. 708-710.
- Peri, D., Rossetti, M., and Campana, E.F., 2001a, “Design Optimization of Ship Hulls via CFD techniques”, J. Ship Research, Vol. 45 (2), pp.140-149.
- Petersson, N.A., 1999, “Hole-Cutting for Three-Dimensional Overlapping Grids”, SIAM J. on Sci. Computing, Vol. 21 (2), pp. 646-665.
- Popinet, S., and Zaleski, S., 1999, “A front tracking algorithm for the accurate representation of the surface tension”, Int. J. for Num. Methods in Fluids, Vol. 30, pp. 775-793.
- Prasad, A.K., 2000, “Stereoscopic particle image velocimetry”, Experiments in Fluids, Vol. 29 (2), pp. 103-116.
- Pu, Y., and Meng, H., 2000, “An advanced off-axis holographic particle image velocimetry (HPIV) system”, Experiments in Fluids, Vol. 29 (2), pp. 184-197.
- Qiao, H., and Duncan, J.H., 2001, “Gentle spilling breakers: crest flow-field evolution”, J. Fluid Mech. Vol. 439, pp. 57-85.
- Ratcliffe, T., 2000, “An Experimental and Computational Study of the Effects of Propulsion on the Free-Surface Flow Astern of Model 5415”, 23rd Symp. on Nav. Hydro., Val de Reuil, France.
- Raven, H.C., 2000, “Numerical wash prediction using a free-surface panel code”, RINA Int. Conf. Hydrodynamics of High-Speed Craft, Wake wash and motion control, London, UK, paper No. 10.
- Raven, H.C., 1998, “Inviscid calculations of ship wave making – capabilities, limitations and prospects”, 22nd Symp. on Naval Hydro., Washington DC, USA, pp. 738-754.
- Raven, H.C., 1996, “A solution method for the nonlinear ship wave resistance problem”, Ph.D. Thesis, Delft Univ. of Technology, The Netherlands.
- Rediniotis, O.K., and Vijayagopal, R., 1999, “Miniature Multihole Pressure Probes and Their Neural-Network-Based Calibration”, AIAA Journal, Vol. 37 (6), pp. 666-674.
- Rengstrom, B., Broberg, L., and Larson, L., 2000, “Ship stern flow calculations on overlapping composite grids”, 23rd Symp. on Naval Hydro., Val de Reuil, France.
- Rhee, S.H., and Hino, T., 2000, “Unstructured grid flow solver for practical ship hulls”, Proc. of Gothenburg 2000 – A Workshop

- on Numerical Ship Hydrodynamics, Chalmers Univ. of Technology, Gothenburg, Sweden.
- Rhee, S.H., and Stern, F., 2001, "Unsteady RANS Method for Surface Ship Boundary Layer and Wake and Wave Field", Int. J. Numerical Methods In Fluids, Vol. 37, pp. 445-478.
- Rhee, S.H., and Stern, F., 2002, "RANS model for spilling breaking waves", J. Fluids Eng., Vol. 124, pp. 1-9.
- Richardson, L., 1910, "The Approximate Solution of Finite Differences of Physical Problems Involving Differential Equations, with an Application to the Stresses in a Masonry Dam", Trans. R. Soc. London, Series A, Vol. 210, pp. 307-357.
- Richardson, L., 1927, "The Deferred Approach to the Limit", Trans. R. Soc. London, Series A, Vol. 226, pp. 299-361.
- Roache, P.J., 1998, "Verification and Validation in Computational Science and Engineering", Hermosa publishers, Albuquerque, NM, USA.
- Roesgen, T., Lang, A., and Gharib, M., 1998, "Fluid surface imaging using microlens arrays", Experiments in Fluids, Vol. 25 (2), pp. 126-132.
- Roth G.I., Mascenik D.T., and Katz J., 1999, "Measurements of the flow structure and turbulence within a ship bow wave", Phys. Fluids, Vol. 11 (11), pp. 3512-3523.
- Rothmann, D.H., and Zaleski, S, 1997, "Lattice-Gas Cellular Automata, Simple Models of Complex Hydrodynamics", Cambridge University Press, UK.
- Sato, Y., Miyata, H., and Sato, T., 1999, "CFD simulation of 3-dimensional motion of a ship in waves: application to an advancing ship in regular heading waves", J. Marine Science and Tech., Vol. 4, pp. 108-116.
- Sato, R., Furukawa, Y., and Naganuma, K., 1998, "Full-scale measurement of boundary layer on sonar dome by laser-doppler velocimeter", UDT Pacific 98, Australia, pp. 6-10.
- Scardovelli, R., and Zaleski, S., 1999, "Direct numerical simulation of free surface and interfacial flow", Annu. Rev. Fluid Mech., Vol. 31, pp. 567-603.
- Schultz, M.P., and Swain, G.W., 1999, "The effect of biofilms on turbulent boundary layers", J. Fluids Eng., Vol. 121, pp. 44-51.
- Scragg, C.A., 1999, "On the use of Free Surface Distributions of Havelock Singularities", 14th Int. Workshop on Water Waves and Floating Bodies, Port Huron, MI, USA.
- Scragg, C.A., 2001, "Extension of the Havelock/Dawson method to include nonlinear free-surface boundary conditions", 16th Int. Workshop on Water Waves and Floating Bodies, Hiroshima, Japan, pp. 145-148.
- Scragg, C.A., Reed, A.M., Wyatt, D.C., and Ratcliffe, T.J., 1998, "Hull Form Development of the Sea Shadow and Applications of the Technology to Monohulls", SNAME Trans., Vol. 106, pp. 413-442.
- Segawa, T., Kawaguchi, Y., Kikushima, Y., Abe, H., Matsunuma, T., and Yoshida, H., 2001, "Control of streak structures in wall turbulence using a piezo-ceramic actuator array", Proc. 2nd Symposium on Smart Control of Turbulence, Tokyo, Japan, pp. 33-42.
- Sethian, J.A., 1999, "Level set methods and fast marching methods", Cambridge Univ Press, 2nd edition, UK.

- Shen, L., Triantafyllou, G.S., and Yue, D.K.P., 2000, “Turbulent diffusion near a free surface”, J. Fluid Mech., Vol. 407, pp. 145-166.
- Shen, L., Yue, D.K.P., 2001, “Large-eddy simulation of free-surface turbulence”, J. Fluid Mech., Vol. 440, pp. 75-116.
- Shimazaki, K., Himeno, Y., and Baba, N., 1993, “An Attempt at Evaluating Numerical Errors in a 2D Navier-Stokes Solver”, FED Vol. 158, Symp. on Quantification of Uncertainty in CFD, ASME Fluids Engineering Division, Summer Meeting, Washington, DC, USA, pp. 19-28.
- Siddiqui, K., Loewen, M.R., Richardson, C., Asher, W.E., and Jessup, A.T., 2001, “Simultaneous particle image velocimetry and infrared imagery of microscale breaking waves”, Phys. Fluids, Vol. 13 (7), pp. 1891-1903.
- Simonsen, C.D., 2000, “Rudder, Propeller and Hull Interaction by Rans”, Ph.D. Thesis, Department of Naval Architecture and Off-shore Engineering, Danish Technical University, Lyngby, Denmark.
- Sirviente, A.I., and Patel, V.C., 2000a, “Wake of a self-propelled body, Part 1: Momentumless wake”, AIAA Journal, Vol. 38 (4), pp. 613-619.
- Sirviente, A.I., and Patel, V.C., 2000b, “Wake of a self-propelled body, Part 2: Momentumless wake with swirl”, AIAA Journal, Vol. 38 (4), pp. 620-627.
- Smirnov, A., Shi, S., and Celik, I., 2001, “Random flow generation technique for large eddy simulations and particle-dynamics modeling”, J. Fluids Eng., Vol. 123, pp. 359-371.
- Speziale, C.G., Sarkar, S., and Gatski, T.B., 1991, “Modeling the pressure-strain correlation of turbulence”, J. Fluid Mech., Vol. 227, pp. 24-272.
- Starke, A.R., 2001, “A validation study of wake-field predictions at model and full scale Reynolds numbers”, 4th Numerical Towing Tank Symposium, Hamburg, Germany.
- Stella, A., Guj, G., Di Felice, F., and Elefante, M., 2000, “Experimental Investigation of Propeller Wake Evolution by Means of LDV and Flow Visualizations”, J. Ship Research, Vol. 44 (3), pp. 155-169.
- Stern, F., Longo, J., Penna, R., Olivieri, A., Ratcliffe, T., and Coleman, H., 2000, “International Collaboration on Benchmark CFD Validation Data for Naval Surface Combatant”, 23rd Symp. on Naval Hydro., Val de Reuil, France.
- Stern, F., Wilson, R.V., Coleman, H., and Paterson, E., 2001, “Comprehensive Approach to Verification and Validation of CFD Simulations – Part 1: Methodology and Procedures”, J. Fluids Eng., Vol. 123, pp. 793-802.
- Stern, F., Longo, J., and Subramani, A.K., 1996, “Detailed Bow-Flow Data and CFD for a Series 60 $C_B=0.6$ Ship Model for Froude Number 0.316”, J. Ship Research, Vol. 40 (3), pp. 193-199.
- Stern, F., Wilson, R.V., Coleman, H., and Paterson, E., 1999, “Verification and Validation of CFD Simulations”, Iowa Institute of Hydraulic Research, The University of Iowa, IIHR Report No. 407.
- Stoev, K., Rame, E., and Garoff, S., 1999, “Effects of inertia on the hydrodynamics near moving contact lines”, Phys. Fluids, Vol. 11 (11), pp. 3209-3215.

- Stultz, B., and Reboud, J.L., 2000, "Measurements within unsteady cavitation", Experiments in Fluids, Vol. 29 (6), pp. 545-552.
- Stumbo, S., Elliott L., and Fox K., "An assessment of wake wash reduction of fast ferries at supercritical Froude numbers and at optimized trim", RINA Int. Conf. Hydrodynamics of High-Speed Craft – Wake wash and motion control, London, 2000, paper No. 4.
- Sturzebecher, D., Anders, S., and Nitsche, W., 2001, "The surface hot wire as a means of measuring mean and fluctuating wall shear stress", Experiments in Fluids, Vol. 31(3), pp. 294-301.
- Sussman, M., and Dommermuth, D., 2000, "The numerical simulation of ship waves using cartesian grid methods", 23rd Symp on Naval Hydro., Val de Reuil, France.
- Sussman, M., and Fatemi, E., 1999, "An efficient, interface-preserving level-set re-distancing algorithm and its application to interfacial incompressible fluid flow", SIAM J. Sci. Comput., Vol. 20 (4), pp. 1165-1191.
- Sussman, M., and Puckett, E.G., 2000, "A coupled Level-Set and Volume-of-Fluid method for computing 3D and axisymmetric incompressible two-phase flows", J. Comp. Phys, Vol. 162, pp. 301-337.
- Sussman, M., Almgren, A., Bull, J., Coltella, P., Howell, L., and Welcome, M., 1999, "An adaptive level set approach for incompressible two-phase flows", J. Comp. Phys, Vol. 148, pp. 81-124.
- Sussman, M., Fatemi, E., Smereka, P., and Osher, S.J., 1998, "An improved level-set method for incompressible two-phase flow", Computers and Fluids, Vol. 27 (5-6), pp. 663-678.
- Sussman, M., Smereka, P., and Osher, S.J., 1994, "A level-set approach for computing solutions to incompressible two-phase flow", J. Comp Phys, Vol. 114, pp. 146-159.
- Sutcliffe, C.J., and Millward, A., 1998, "A Comparison of the Motion and Resistance of a Yacht in Waves in Earth and Body Axes", Trans. R. Inst. of Naval Arch., Vol. 140, pp. 184-209.
- Svennberg, S.U., 2000, "A test on turbulence models for steady flows around ships", Proc. of Gothenburg 2000 – A Workshop on Numerical Ship Hydrodynamics, Chalmers Univ. of Technology, Gothenburg, Sweden.
- Svennberg, S.U., 2001, "On turbulence modelling for bilge vortices", Ph.D. Thesis, Chalmers University of Technology, Gothenburg, Sweden.
- Tahara, Y., Himeno, Y., and Tsukahara, T., 1998, "An application of CFD to tanker hull form optimization problem", 3rd Osaka Colloquium on Advanced CFD Applications to Ship Flow and Hull Form Design, Osaka, Japan, pp. 515-531.
- Tahara, Y., Longo, J., Stern, F., and Himeno, Y., 1998, "Comparison of CFD and EFD for the series 60 $C_B=0.6$ in steady yaw motion", 22nd Symp. on Naval Hydro., Washington DC, USA, pp. 981-999.
- Tahara, Y., Paterson, E.G., Stern, F., and Himeno, Y., 2000, "Flow and wave field optimization of surface combatants using CFD-based optimization methods", 23rd Symp. on Naval Hydro., Val de Reuil, France.
- Tahara, Y., and Ando J., 2001, "Comparison of CFD and EFD for KCS container ship in without/with-propeller conditions", Proc. of Gothenburg 2000 – A Workshop on Nu-

- merical Ship Hydrodynamics, Chalmers Univ. of Technology, Gothenburg, Sweden.
- Takada, N., Miyata, H., and Sato, T., 1999, “CFD simulation of a 3-dimensional motion of a vehicle with movable wings”, 7th Int. Conf. on Num Ship Hydro, Nantes, France, pp. 4.6-1,15.
- Talotte, C., Delhommeau, G., and Kobus, J.M., 1997, “Adaptation of Experimental Methods for Sailing Yachts in Towing Tank Testing – Comparing Experimental and Numerical Results”, Int. Shipbuilding Progress, Vol. 44 (439), pp. 181-207.
- Tanaka, K., Nishimoto, H., Kataoka, K., Nakato, M., and Nakatani, T., 1999, “Wave-locking catamaran; her resistance and wave making phenomena”, West-Japan Soc. of Naval Arch., Vol. 98, pp. 59-66.
- Techet, A.H., Luthi, B., Anderson, E.J., McGillis, W.R., Grosenbaugh, M.A., and Triantafyllou, M.S., 1999, “Flow visualization of swimming robotic fish in the near boundary region”, PIV'99, Santa Barbara, CA, USA, pp. 57-61.
- Thibault, J.P., Botton, V., and Rossi, L., 1998, “Electromagnetic Effects on Low Speed Coherent Structures Embedded in a Wall Layer”, Proc. of the Int. Symp. on Seawater Drag Reduction, Newport, RI, USA, pp. 389-394.
- Triantafyllou, M.S., Triantafyllou, G.S., and Yue, D.K.P., 2000, “Hydrodynamics of fish like swimming”, Annu. Rev. Fluid Mech., Vol. 32, pp. 33-54.
- Tryggvason G., Bunner B., Esmaeli A., Juric D., Al-Rawahi N., Tauber W., Han J., Nas S., and Jan Y.J., 2001, “A front-tracking method for the computation of multiphase flow”, J. Comp Phys., Vol. 169, pp. 708-759.
- Tsukada, Y., Hinatsu, M., and Hasegawa, J., 1997, “Measurement of Unsteady Ship Wakes in Waves”, J. Kansai Soc. of Naval Arch., Vol. 228, pp. 15-20.
- Tulin, M.P., 1996, “Breaking of ocean waves and downshifting”, in Waves and Nonlinear Processes in Hydrodynamics, ed. J. Grue, B. Gjevik, J.E. Weber, Dordrecht, The Netherlands, Kluwer, pp. 177-190.
- Tulin, M.P., Waseda, T., 1999, “Laboratory observations of wave group evolution, including breaking effects”, J. Fluid Mech., Vol. 378, pp. 197-232.
- Tulin, M.P., and Landrini, M., 2000, “Breaking waves in the ocean and around ships”, 23rd Symp. on Naval Hydro., Val de Reuil, France.
- Valorani, M., Peri, D., and Campana, E.F., 2000, “Efficient strategies to design optimal ship hulls”, 8th Multidisciplinary analysis and optimization AIAA Conf., Long Beach, CA, USA.
- van Brummelen, E.H., Raven, H.C., and Koren B., 2001, “Efficient numerical solution of steady free-surface Navier-Stokes flow”, J. Comp. Phys., Vol. 174, pp. 120-137.
- Van, S.H., Kim, W.J., Kim, D.H., Yim, G.T., Lee, C.J., and Eom, J.Y., 1998a, “Flow Measurement Around a 300K VLCC Model”, SNAK Annual Spring Meeting, Ulsan, Korea.
- Van, S.H., Kim, W.J., Yim, G.T., Kim, D.H., and Lee, C.J., 1998b, “Experimental Investigation of the Flow Characteristics Around Practical Hull Forms”, 3rd Osaka Colloquium on Advanced CFD Applications to Ship Flow and Hull Form Design, Osaka, Japan, pp. 215-228.
- Vogt, M., and Larsson, L., 1999, “Level set methods for predicting viscous free surface

- flows”, 7th Int. Conf. on Num. Ship Hydro., Nantes, France, pp. 2.4-1,19.
- Waniewski, T.A., Brennen, C.E., and Raichlen, F., 2001, “Measurements of Air Entrainment by Bow Waves”, J. Fluids Eng., Vol. 123, pp. 57-63.
- Watson S., 2000, “Validation of CFD software for the model hull of a US Navy combatant”, Proc. of Gothenburg 2000 – A Workshop on Numerical Ship Hydrodynamics, Chalmers Univ. of Technology, Gothenburg, Sweden.
- Wenger, C.W., and Devenport, W.J., 1999, “Seven-Hole Pressure Probe Calibration Method Utilizing Look-Up Error Tables”, AIAA Journal, Vol. 37 (6), pp. 675-679.
- Whittaker, T.J.T., Bell, A., Shaw, M., and Patterson, K., 1999, “An investigation of fast ferry wash in confined waters”, RINA Conf. Hydrodynamics of High-Speed Craft, London, UK.
- Whittaker, T.J.T., Doyle, R., and Elsaesser, B., 2000, “A study of the leading long period waves in fast-ferry wash”, RINA Int. Conf. ‘Hydrodynamics of High-Speed Craft – Wake wash and motion control’, London, UK, paper No. 7.
- Whittaker, T.J.T., Doyle, R., and Elsaesser, B., 2001, “An experimental investigation of the physical characteristics of fast ferry wash”, Proc. Int. Conf. on High-Performance Marine Vehicles, HIPER’01, Hamburg, Germany, pp. 480-491.
- Wilcox, D.C., 1998, “Turbulence modelling for CFD”, DCW industries, ISBN 0-9636051-5-1, La Cañada, CA, USA, 2nd edition.
- Wilson, R., Paterson, E., and Stern, F., 1998, “Unsteady RANS CFD method for naval combatants in waves”, 22nd Symp. on Naval Hydro., Washington DC, USA, pp. 532-549.
- Wilson, R., Paterson, E., and Stern, F., 2000, “Verification and validation for RANS simulation of a naval combatant”, Proc. of Gothenburg 2000 – A Workshop on Numerical Ship Hydrodynamics, Chalmers Univ. of Technology, Gothenburg, Sweden.
- Wilson, R., and Stern, F., 2002, “Verification and Validation for RANS Simulation of a Naval Surface Combatant”, Standards for CFD in the Aerospace Industry, AIAA Aerospace Sciences Meeting, Reno, NV, USA.
- Wilson, R., Stern, F., Coleman, H., and Paterson, E., 2001, “Comprehensive Approach to Verification and Validation of CFD Simulations – Part 2: Application for RANS Simulation of A Cargo/Container Ship”, J. Fluids Eng., Vol. 123, pp. 803-818.
- Yang, C., Loehner, R., and Noblesse, F., 2000, “Farfield extension of nearfield steady ship waves”, Ship Technology Research, Vol. 47, pp. 22-34.
- Yang, C., Lohner, R., Hendrix, D., and Noblesse, F., 1999, “Fourier-Kochin extension of fully non linear nearfield ship waves”, 7th Int. Conf. on Num. Ship Hydro., Nantes, France, pp. 1.2-1,14.
- Yoon, H.S., Van, S.H., Kang, K.J., Lee, C.J., Kim, K.J., and Lee, J.K., 1999, “A study on the influence of rudder and propeller position on the self-propulsion factors”, Proc. 4th Japan-Korea Joint Workshop on Marine Hydrodynamics, Fukuoka, Japan, pp. 171-176.
- Yoshida, Y., Takahashi, Y., Kato, H., and Guin, M.M., 1998, “Distribution of void fraction in bubbly flow through a horizontal channel: bubbly boundary layer flow”, 2nd

- Report, J. Marine Science and Technology, Vol. 3 (1), pp. 30-36.
- Zhang, C., Shen, L., and Yue, D.K.P., 1999, “The mechanism of vortex connection at a free surface”, J. Fluid Mech., Vol. 384, pp. 207-242.
- Zhang, D., and Chwang, A.T., 1999, “On nonlinear ship waves and wave resistance calculations”, J. Marine Science and Technology, Vol. 4, pp. 7-15.
- Zhang, X. D., Pelletier, D., Trepanier, J.-Y., and Camarero, R., 2001, “Numerical Assessment of Error Estimators for Euler Equations”, AIAA Journal, Vol. 39 (9), pp. 1706-1715.
- Zhou, J., Meinhart, C. D., Balachandar S., and Adrian, R. J., 1997, “Formation of coherent hairpin packets in wall turbulence”, Advances in Fluid Mechanics, Vol. 15, Computational Mechanics Publications, Southampton, UK.
- Zhu, Y., and Antonia, R.A., 1999, “Performance of a three-component vorticity probe in a turbulent far-wake”, Experiments in Fluids, Vol. 27, pp. 21-30.
- Zondervan G.J., and Starke, B., 2002, “Advances in full-scale wake field predictions and the implications for the propeller design”, 10th Conf. of the Int. Marit. Ass. of the Mediterranean (IMAM 2002), Crete, Greece.

The Resistance Committee

Committee Chair: Prof. Fred Stern (IIHR-University of Iowa)

Session Chair: Dr. Hans Broberg (SSPA)

I. DISCUSSIONS

I.1. Discussion on the Report of the 23rd ITTC Resistance Committee: Uncertainty Analysis for Extrapolation Methods

By: Jan Holtrop, MARIN, The Netherlands

In Chapter 8 of its report the Resistance Committee presents an Uncertainty Analysis for Extrapolation Methods. This difficult subject deserves special attention as improvement of the elementary components (friction formulation, form corrections and other scale effects) should eventually render power predictions with less uncertainty, whilst the largest sources of the uncertainty should be identified. Moreover, the uncertainty of experimental form factors continues to worry those working in this field for several decades. Therefore, it is a pity that so little of the ongoing concern about an accurate determination of the form factor from the experiments, which form a part of the extrapolation process, is reflected by this chapter. A comparison with Chapter 5.4 of the present report of the Propulsion Committee, shows that none of the frequently encountered problems leading to lack of confidence in the procedures have been mentioned in the uncertainty analysis of the form factor procedure. The Resistance Committee implicitly supposes that the assumptions underlying Prohaska's plotting procedure are perfectly true. In reality, the presence of bulbous bow waves, immersed tran-

soms and unintentional flow separation seriously hamper an accurate determination of $1+k$ at the correct level in many cases. Some wording could have been devoted to these quite common exceptions of the ideal situation.

Another point of concern is the model-ship correlation allowance coefficient, C_A (not ΔC_F as it concerns correlation and not an allowance for hull roughness). The impact of the model-ship correlation allowance coefficient is fully expressed in Chapter 8.2, even to such an extent that its variation as a function of the flat plate friction formulation is considered to give such an uncertainty that it would prevent changing from one flat-plate friction line to a more accurate at present. However, in the actual uncertainty analysis in Chapter 8.3 the coupling with the correlation allowance has fully disappeared and variations in the results of the extrapolation are now related solely to the variations in the flat plate friction. Even when acknowledging the coupling between C_A and the flat-plate friction formulation, it appears extremely difficult to prove statistically that a certain flat-plate friction formulation is to be preferred over another [See e.g. the discussion of Grigson (RINA, 1995)]. The conclusion, see the first line of Chapter 8.6, should take the role of C_A fully into consideration.

A final comment concerns the uniform approach to the problem as followed by the committee, irrespective of the type of ship and the Froude regime. It will be clear that the uncertainty of the extrapolation will be completely different for a slender ship running at a Froude

number of 0.5, from that of e.g. a dredger, prone to flow separation, running at a Froude number of about 0.17. Some distinction in classes could have clarified the relative importance of the components in various situations.

I.2. Discussion on the Report of the 23rd ITTC Resistance Committee: Uncertainty Analysis for CFD

By: M. Hoekstra, MARIN, The Netherlands, L. Eça, Instituto Superior Técnico, Lisbon, Portugal, H.C. Raven, MARIN, The Netherlands

The Resistance Committee (RC) of the 23rd ITTC recommends the adoption by this Conference of a revised interim procedure for Uncertainty Assessment in CFD. Section 7 of the RC report states that CFD users should rigorously implement this Procedure, “which hopefully will increase number of trained users and reduce user variability”.

However, in the application of the previous interim procedure (proposed by the 22nd RC) many problems have appeared (such as at the Gothenburg Workshop 2000). These problems are insufficiently addressed or even ignored by the update now proposed, and rigorous application of the Procedure will hardly be possible. Dependent on how one handles the various advices given, the Procedure may turn out to be confusing, potentially erroneous, or inadequate.

Suppose that verification is to be carried out for the computation of viscous flow around a ship. Following the suggested procedure a grid refinement study is conducted, using three grids, geometrically similar as well as possible, the finest having e.g. 2-3 million nodes as is usual today. The procedure then analyses the results based on Richardson Extrapolation, using a single-term series expansion of the numerical error. This requires that the first term in the series expansion is dominant, in other words that the solutions on the three grids must be in the asymptotic range. Are we sure to sat-

isfy that requirement? No, on the contrary, we can be pretty sure to be outside the asymptotic range even on the finest grid; but a single 3-grid study as recommended in the Procedure gives no reliable indication of this.

Unless divergence is found, the Procedure then provides an ‘observed order’ of convergence. If by coincidence this appears to have a reasonable value, the “correction factor” proposed will be near 1.0. The Procedure then advises to estimate error and uncertainty “with correction factor”,

- if C_k is “close to 1.0”; but there is no indication of what that means.
- but only if C_k is not too close to 1.0, since otherwise the uncertainty would be unreasonably small;
- and only if one has confidence in the results. However, “Since the variability of the order of accuracy cannot be determined from solutions on 3 grids, confidence is difficult to establish in this case”.

Following this advice, estimating error and uncertainty using the correction factor approach should never be done for a 3-grid study for a ship flow case. The complicated and extensive description of the “Correction factor approach” thus seems to find little application to cases of interest to the ITTC.

In such cases the Procedure refers to a Factor of Safety approach which is actually another method proposed by Patrick Roache and maybe better known as the GCI (Grid Convergence Index) procedure. This method is, however, poorly presented in the Procedure proposed, and is extended in a way not supported by its originator.

Quite appropriately, Section 4.6 of the Procedure advises: “For complex flows with relatively coarse grids, solutions may be far from asymptotic range (...). Order of accuracy and

therefore correction factors and factors of safety may display large variability indicating the need for finer grids. Clearly, more than 3 grids are required to estimate errors and uncertainties for such cases.” However, any indication of how to estimate error and uncertainty with more than three grids is lacking.

In addition, we feel that there is insufficient proof or demonstration of the validity of the Procedure. Expressions for 95% uncertainty intervals are stated without any proof or motivation; while several published examples of the failure of these expressions cast serious doubt on their validity.

For the progress of our profession it is very important that Verification and Validation gets serious attention, and that verification approaches are proposed and tested. However, we believe that immature procedures presented without enough discussion and reservation should not be adopted as a Quality Manual Procedure by the ITTC. Instead, in order that progress is being made, we propose:

“Give the 24th ITTC RC the task of stimulating the ITTC member organisations to apply and report grid refinement studies and gathering the outcome; of verifying the various Verification Procedures proposed in the literature; and of working towards a robust and reliable procedure for estimating CFD uncertainty and error, for future adoption.”

I.3. Discussion on the Report of the 23rd ITTC Resistance Committee: Comparison of EFD to CFD results

By: G. Grigoropoulos, T. Loukakis, NTUA, Greece

In a paper entitled “Resistance and Seakeeping Characteristics of a Systematic Series in the Pre-planing Condition (Part I)”, to be

presented in the forthcoming Annual Meeting of SNAME (Sept. 25-28, 2002) the experimental resistance characteristics of a new systematic Series of double-chine hull forms, developed at NTUA, are compared to numerical predictions. The Series are suitable for operation at pre-planing speeds and consists of five models with $L/B = 4.00, 4.75, 5.50, 6.25$ and 7.00 , each tested at six displacements, including very light ones. The loading conditions tested correspond to volume of displacement coefficients, $C_{DL} = \nabla/(0.1L_{WL})^3$ of $1.00, 1.61, 2.23, 3.00, 3.61$ and 4.23 .

Modern large fast ferries with 40 knots service speed and lengths around 100 m are designed at $C_{DL} \approx 1.7$, whereas smaller fast ships are designed at higher C_{DL} values. Repeating them for the parent hull form at a different facility has validated the experimental results.

A by-product of the test program has been the comparison of the EFD to the CFD results obtained using two well known and commercially available computer codes (SHIPFLOW and SWAN). Thus, the residual resistance coefficients C_R obtained experimentally have been compared to the wave resistance coefficients C_W obtained numerically. The comparison of EFD and CFD for the parent hull form ($L/B = 5.50$) is shown in Figures I.3.1 and I.3.2. From these figures and for the $Fr = 0.50$ to 0.90 one can deduce that:

- At the heavier values of C_{DL} the numerically obtained C_W values are close and, as expected, somewhat lower than the C_R values
- As C_{DL} decreases, the agreement becomes progressively worse and at the very light value of C_{DL} ($C_{DL} = 1.00$) is very bad indeed with the numerical codes predicting about 40% of the experimental results.

It seems that as the planing surface approaches the free surface, the physics of the

flow change, a phenomenon that the potential flow numerical codes, which validate one another, do not seem to take into account.

I.4. Discussion on the Report of the 23rd ITTC Resistance Committee: Reconsideration of the correlation of roughness and drag characteristics of surfaces coated with antifoulings

By: M. Candries, M. Atlar, University of Newcastle-upon-Tyne, United Kingdom

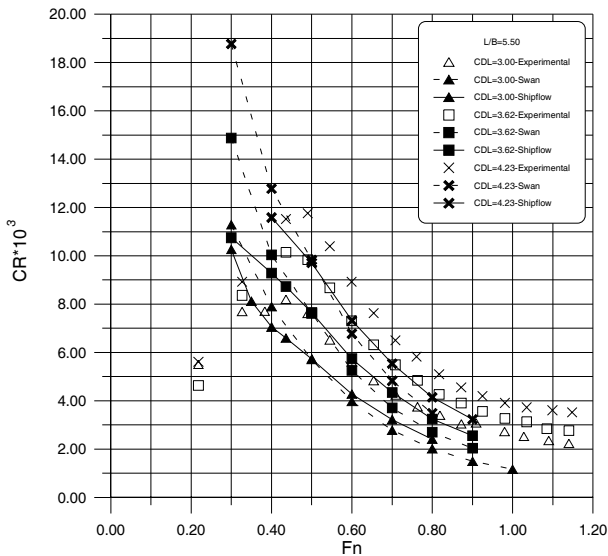


Figure I.3.1 Comparing experimental and analytical results (heavier displacements).

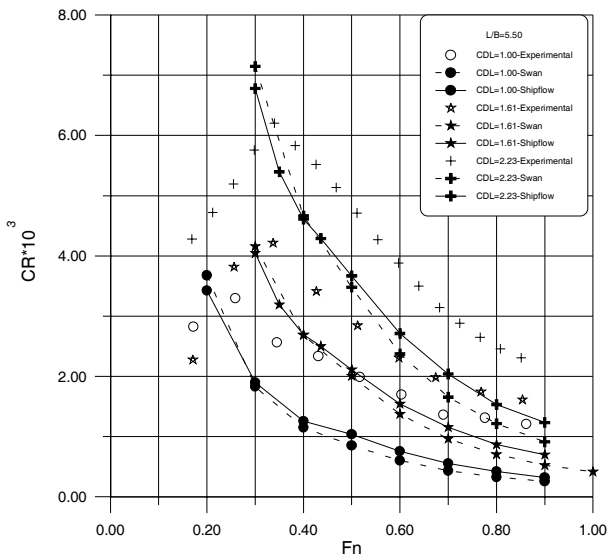


Figure I.3.2 Comparing experimental and analytical results (lighter displacements).

This topic was last considered extensively by the Committee in 1990 (ITTC, 1990a, 1990b). The recommendations of the Powering Performance Committee were to include only a single roughness parameter to account for the effect of roughness on the correlation allowance for a moderately rough ship hull. Various experiments had shown that a single height parameter was sufficient since moderately rough ship hulls differ little in texture (Townsin, 1990; Townsin & Dey, 1990).

For the last 15 to 20 years, Tributyl-Tin Self-Polishing Co-Polymers (TAT-SPC), which can keep a ship free of fouling for 5 years by means of a steady release of the TBT toxin, have dominated the antifoulings market. However, due to environmental side-effects related with TBT, the International Maritime Organisation (IMO) has decided in October 2001 to prohibit the application of TBT-SPCs from 2003 and hence completely phase out their use by 2008. There are currently two alternatives on the market that can also offer 5 years of satisfactory antifouling performance. The first alternative, Tin-free SPC, operate by the same chemical principle but, instead of TBT, gradually leach copper-based toxins that are complemented by booster biocides. The second alternative, Foul(ing) Release coatings, act as a physical rather than a chemical defence against fouling. These coatings are silicone elastomers which have entirely different surface characteristics, notably their surface energy, so that firm attachment of fouling organisms is avoided and the release of the fouling organisms occurs at sufficiently high service speeds (> 15 knots).

This contribution summarises the findings of a research project carried out at the University of Newcastle-upon-Tyne to systematically compare the drag, boundary-layer and roughness characteristics of a Foul Release system and a Tin-free SPC system (Candries, 2001) and recommends the ITTC to reconsider the procedure adopted to correlate between roughness and drag.

Towing tank experiments have been carried out with two friction Planes of different size. Three series of measurements were carried out for

each plane, uncoated, coated with Foul Release and coated with Tin-free SPC. It was found that the Foul Release system exhibits less drag than the Tin-free SPC system. The difference in frictional resistance varied between 2% and 23%, depending on the quality of application (Candries, 2001, Candries et al., 2001). Rotor experiments were also carried out to measure the difference in torque between coated and uncoated cylinders. The measurements indicated an average 3.6% difference in local frictional resistance coefficient between the Foul Release and Tin-free SPC (Candries et al., 2002a).

Table I.4.1 Overview of the drag characteristics of Foul Release and Tin-free SPC.

Towing tank experiments	ΔC_F (compared to reference, %)	ΔU^+ (on average)	Average Roughness (μm)
2.55 m long plate	$2.0 \cdot 10^6 < Re < 4.2 \cdot 10^6$		
Sprayed Foul Release	3.9	0.20	44
Sprayed SPC	23.4	2.17	75
6.3 m long plate	$2.0 \cdot 10^7 < Re < 4.0 \cdot 10^7$		
Sprayed Foul Release	3.9	0.21	62
Sprayed SPC	23.4	0.62	39
Rotor experiments	ΔC_F (compared to reference, %)	ΔU^+ (on average)	Average Roughness (μm)
Cylinder	$1.0 \cdot 10^6 < Re < 2.1 \cdot 10^6$		
Sprayed Foul Release	4.3	1.00	108
Rollered Foul Release	5.7	1.31	218
Sprayed SPC	8.0	1.80	54
Water tunnel experiments	ΔC_F (compared to reference, %)	ΔU^+ (on average)	Average Roughness (μm)
1m long vertical plate (Emerson Cavitation Tunnel)	$8.5 \cdot 10^3 < Re_\delta < 3.4 \cdot 10^4$		
Sprayed Foul Release	10.9	1.25	51
Rollered Foul Release	13.1	1.54	60
Sprayed SPC	16	1.80	69
1m long vertical plate (CEHIPAR Cavitation Tunnel)	$1.6 \cdot 10^4 < Re_\delta < 4.6 \cdot 10^4$		
Sprayed Foul Release	14.6	1.68	50
Sprayed SPC	22.9	2.71	30

The friction of a surface in fluid flow is caused by the viscous effects and turbulence production in the boundary layer close to the surface. A study of the boundary-layer characteristics of the coatings was therefore carried out in two different water tunnels using Laser Doppler Velocimetry (LDV). The coatings were applied on 1 m long test sections that were fitted in a 2.1 m long flat plate set-up. An outer-layer wall similarity method and the Reynolds stress method were used to determine the friction velocity and both methods showed good agreement with each other. The experiments indicated that the friction velocity for the Foul Release surfaces is significantly lower than for Tin-free SPC surfaces. This implies that at the same streamwise Reynolds number the ratio of the inner layer to the

outer layer is smaller for Foul Release surfaces. The inner layer is that part of the boundary layer where major turbulence production (and hence drag generation) occurs. The roughness functions of the different surfaces, determined from the measured velocity profiles as illustrated in Figure I.4.1, indicated that on average the Foul Release surfaces exhibit less drag than Tin-free SPC surfaces, which is in agreement with the findings from the towing tank and rotor experiments, as shown in Table I.4.1.

No significant differences between the different coatings were found in the turbulence intensities, although this may have been obscured by the experimental precision uncertainties.

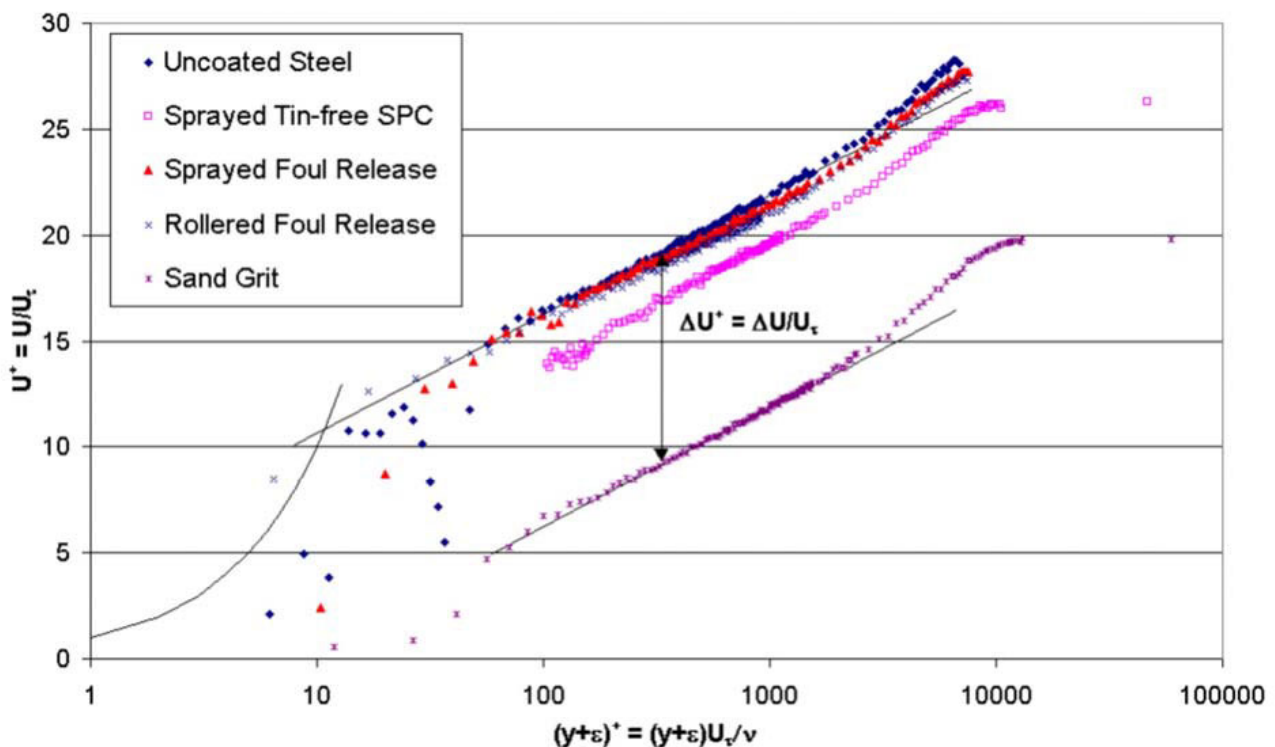


Figure I.4.1 Boundary-layer velocity profiles in inner co-ordinates (i.e. the distance from the surface, $y+\epsilon$, and the streamwise velocity component U have been scaled by the viscous length scale ν/U_τ and the friction velocity U_τ respectively) at a free-stream velocity $U_e = 5$ m/s and at a streamwise location $x = 1.607$ m from the leading edge. A rolled and a sprayed Foul Release surface were tested to investigate the effect of application method. A surface covered with sand grit was tested in order to have a very rough comparison. The velocity loss or roughness function ΔU^+ indicates the difference in frictional resistance between a rough and a smooth surface. (Experimental precision uncertainty over the log-law region: U^+ : $\pm 1.72\%$ for the uncoated steel surface, $\pm 1.94\%$ for the rough surfaces; ΔU^+ : $\pm 14.74\%$).

Roughness measurements were carried out on the tested surfaces using a BMT Hull Roughness Analyser. This stylus instrument measured the extreme roughness amplitude over a 50 mm cut-off length at a sampling interval of 1.25 mm, Rt50. For a Foul Release surface, the average of this roughness parameter will not correlate with the measured drag. One of the towing tank experiments and the rotor experiments, for example, indicated that the average roughness was higher for the Foul Release surface than for the Tin-free SPC, whereas the measured drag was lower (cfr. Table I.4.1).

A detailed roughness analysis of sample plates, coated alongside the tested surfaces and representative of their surface characteristics, was carried out with an optical measurement system fitted with a 3 mW laser. The methodology which was developed to acquire the roughness parameters from six profiles of each sample, applies a moving average ‘boxcar method’ to filter the data. The upper bandwidth limit or cut-off length was set at 2.5 and 5 mm, the sampling interval at 50 μm .

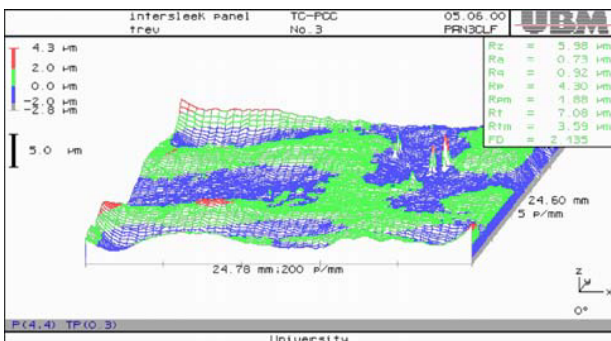


Figure I.4.2 Typical roughness measurement of a Foul Release surface.

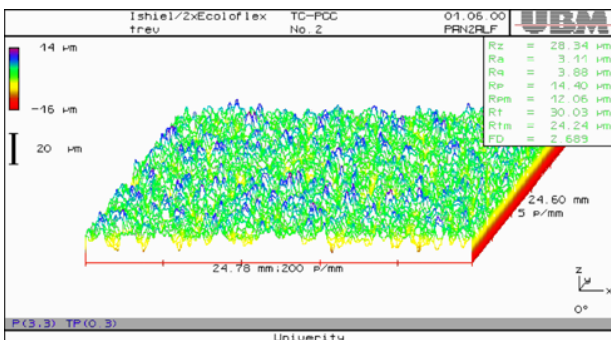


Figure I.4.3 Typical roughness measurement of a Tin-free SPC surface.

Figure I.4.2 and Figure I.4.3 show two typical measurements of a Foul Release and Tin-free SPC surface respectively. The detailed roughness analysis revealed that when the profiles are filtered, the amplitude parameters of the Foul Release surfaces are mostly but not always lower than those of the SPC surfaces. The main difference between the Foul Release and the Tin-free SPC systems lies in the characteristics. Whereas the Tin-free SPC surface displays a typical ‘closed texture’, the Foul Release surface exhibits a wavy, ‘open’ texture. This is particularly evident from parameters such as the mean absolute slope Δa and the Fractal Dimension FD . The spectra of the coated surfaces seem to follow a power law which is dependent on the Fractal Dimension and an implication of self-affine behaviour. A surface with an ‘open texture’ will have a lower Fractal Dimension than a surface with a closed texture (Candries, 2001). There is relatively little data available in literature on the influence of texture of irregular surfaces on drag, but Grigson (1982) shows that open textures have a beneficial effect on drag.

It is thought that the rheology of the paint (which is significantly different for Foul Release systems than for Tin-free SPC systems as is clear from a parameter such as the viscosity) has a direct effect on its texture, whereas amplitudes depend significantly on the application quality. Correlation of the texture parameters with the amplitude parameters, however, shows that the two are inter-related so that bad application can be expected to have a knock-on effect on the texture parameters.

The roughness characteristics of both Tin-free and Foul Release surfaces correlate qualitatively with the drag differences given in Table I.4.1 when a texture parameter is included in the roughness characterisation. A semi-empirical approach was applied to correlate the roughness characteristics with the drag measurements of the surfaces tested here along with the surfaces included by Townsin & Dey (1990). The approach involved the selection of

a characteristic roughness measure h which gives the best correlation assuming that the roughness function of the surfaces follows the Colebrook-White law. The characteristic measure which was found to give the best correlation for the present surfaces is $h = Ra \cdot \Delta a / 2$ for an effective cut-off length, whereby Ra is the average amplitude (which strongly correlates with Rt). The effective cut-off length increases with the degree of roughness and varied in the analysis between 2.5 mm for the Foul Release surfaces and 50 mm for a sand grit surface covered with paint (Candries, 2001).

The procedure presently adopted by the MC uses the formula suggested by Townsin et al. (1984) to predict the added resistance of new ships from roughness measurements:

$$10^3 \cdot \Delta C_F = 44[(h/L)^{1/3} - 10 \cdot Re^{-1/3}] + 0.125$$

where h is the Average Hull Roughness measured by the BMT Hull Roughness Analyser. Townsin & Dey (1990) showed that the roughness function $\Delta U/U_\tau$ correlates well with $Rt50$ for new, moderately rough surfaces ($Rt50 < 225 \mu\text{m}$) and that $Rt50$ was therefore adequate for quality control as well as for measuring the approximate power penalties due to roughness. Townsin and Dey argued that the reason why a single roughness parameter $Rt50$, could well predict the added resistance of a wide range of new ship surfaces, is that their texture is fairly similar, allowing for differences in method of application, paint rheology and the application environment. New ships have several coats of paint, the number and composition of which do not vary greatly.

The advent of Foul Release coatings, however, does not longer support his argument and in future a texture parameter will have to be included in the roughness characterisation if the added drag is to be predicted. This in turn requires the modification of the commercial version of the Hull Roughness Analyser. Roughness profiles are to be stored digitally. In order to calculate the spectral parameters and Fractal Dimension accurately by the acquisition of a

sufficient number of data, a smaller sampling interval is also recommended.

In order to validate any prediction method, the acquisition of full-scale data is ultimately required and to the Authors' knowledge this has not yet been done for hulls coated with Foul Release coatings. Foul Release surfaces, however, quickly acquire a slime film, which unlike other fouling organisms does not release when the vessel is underway. The added drag of a slime film compared to a newly applied coating is likely to be significant, but limited (i.e. restricted to a few percent) (Candries et al., 2002b).

This research project is ongoing and water tunnel experiments are planned at the University of Newcastle-upon-Tyne to study the drag, boundary-layer and roughness characteristics of Foul Release surfaces which have been immersed in seawater for one year.

References

- ITTC, 1990a, "Report of the Resistance and Flow Committee", Proceedings of the 19th International Towing Tank Conference, Madrid, Spain, 16-22 September 1990, Vol. 1, pp. 62-64.
- ITTC, 1990b, "Report of the Powering Performance Committee", Proceedings of the 19th International Towing Tank Conference, Madrid, Spain, 16-22 September 1990, Vol. 1, pp. 262-265.
- Townsin, R.L., 1990, "The MC correlation allowance: the evidence re-examined and supplemented", Marine Roughness and Drag Workshop, RINA, London, UK, Paper 9.
- Townsin, R.L., and Dey, S.K., 1990, "The correlation of roughness drag with surface characteristics", Marine Roughness and Drag Workshop, RINA, London, UK, Paper 8.

Candries, M., 2001, “Drag, boundary-layer and roughness characteristics of marine surfaces coated with antifouling”, PhD Thesis, Department of Marine Technology, University of Newcastle-upon-Tyne, UK.

http://www.geocities.com/maxim_candries

Candries, M., Atlar, M., Guerrero, A., and Anderson, C.D., 2001, “Lower frictional resistance characteristics of Foul Release systems”, Proceedings of the Eight International Symposium on the Practical Design of Ships and Other Floating Structures (PRADS 2001), Elsevier, Amsterdam, The Netherlands, Vol. 1, pp. 517-523.

Candries, M., Atlar, M., Mesbahl, E., and Pazouki, K., 2002a, “The measurement of drag characteristics of Tin-free, Self-Polishing Co-polymers and Foul(ing) Release coatings using a rotor apparatus”, Proceedings of the 11th International Congress on Marine Corrosion and Fouling, San Diego, 21-26 July 2002.

Grigson, C.W.B., 1982, “The drag coefficients of a range of ship surfaces”, 11. Trans. RINA, Vol. 124, pp. 183-198.

Townsin, R.L., Medhurst, J.S., Hamlin, N.A., and Sedat, B.S., 1984, “Progress in calculating the resistance of ships with homogeneous or distributed roughness”, N.E.C.I.E.S. Centenary Conference on Marine Propulsion, Paper 6.

Candries, M., Atlar, M., and Anderson, C.D., 2002b, “Estimating the impact of new-generation antifouling on ship performance: the presence of slime”, Submitted to the Journal of Marine Engineering and Technology.

I.5. Discussion on the Report of the 23rd ITTC Resistance Committee: Average bias uncertainty

By: Ahmed Derradji-Aouat, NRC, IMD, Canada

There is 0.6% average bias uncertainty (as per your survey, for fundamental resistance test). However, when you analyzed the data, you arrive to the conclusion facility bias uncertainty is about 2%, rather than 0.6% (originally reported).

1. Do you think that the difference between the 0.6% bias and 2% bias is largely influenced by human factor – crew dependent uncertainty?
2. If you use the proposed “standard model”, what assurances do you have that all uncertainties form all tanks converge to the same number (the 0.6%, 2%, or other)?

I.6. Discussion on the Report of the 23rd ITTC Resistance Committee: Uncertainty Analysis for sinkage and trim measurements

By: Marc Vantorre, Ghent University, Belgium, Flanders Hydraulics Research, Antwerp, Belgium

I would like to ask a question to the Resistance Committee about chapter 6, “Uncertainty analysis for towing tank test: sinkage and trim, wave profiles, and wave elevations”. The example given for sinkage and trim measurements takes account of calibration uncertainty, misalignment of the potentiometers, and scatter in the potentiometer calibration.

However the report does not mention other sources of errors which may affect the sinkage and trim measurements. Some are related to the reference levels: the horizontality of the carriage rails, and even the horizontality of the water plane, which should be at rest initially, but

which may be disturbed by former tests or by long waves caused by acceleration of the model. Other causes might be friction in the vertical guiding system and deviations of the model speed.

In my opinion, the uncertainty analysis should be extended to incorporate other error sources such as those I mentioned. I would like to know how the Resistance Committee shares this opinion.

I.7. Discussion on the Report of the 23rd ITTC Resistance Committee: Roughness and the ITTC correlation allowance – A new problem

By: Robert L. Townsin, United Kingdom

Although extrapolation problems may not be a central issue at ITTC 2002, it may be appropriate to draw attention to a recent anti-fouling coating development, which affects our understanding of hull roughness.

As Members may recall, at the 19th ITTC in Madrid, the (then) Powering Performance Committee put forward a standard for the model-to-ship correlation allowance. A part of that allowance takes account of the roughness of the hull outer bottom coating.

It is generally understood that the added drag of roughness on a surface, has to correlate, not only with roughness ‘height’ but also with ‘texture’. For example, over a wide range of typical hull paint surface roughness, the roughness function, $\Delta u/u_\tau$ as determined from some 30 published tests in various laboratories, correlated reasonably with $\log(hu/\nu)$ when $h^2 = \alpha m_0 m_2$, where m_n are spectral moments of the roughness profile, and α is the bandwidth parameter (Townsin & Dey, 1990).

Whilst colleagues familiar with spectral representation of the seaway might have little difficulty with the above, it was a relief to find that those

surfaces where the peak-to-trough roughness height, $Rt(50)$, was less than $230 \mu\text{m}$, $\Delta u/u_\tau$ correlated well enough when $h = Rt(50)$. This simplicity arose because the texture of anti-fouling paint roughness, at the time, correlated with its height. It will be noted that the values of $Rt(50) < 230 \mu\text{m}$ cover the new ship and moderately rough range. The way was now open to correlate the roughness added resistance coefficient, ΔC_F , with the average hull roughness, AHR , as measured by the BMT Hull Roughness Analyser, which records $Rt(50)$. The resulting hull roughness to added drag formulation is:

$$1000C_F = 44 [(AHR/L)^{1/3} - 10(Re)^{-1/3}] + 0.125$$

The recent development referred to earlier, is the production of low surface energy anti-fouling coatings, which are biocide free. In the industry, these are variously called non-stick or foul-release coatings. When in the dry, the coatings feel like rubber to the finger, whereas, underwater they are fish-slippery. Fouling species cannot readily attach and are washed off under fluid shear, although slime tends to remain.

Two problems arise when considering the roughness of these coatings and the consequent added drag. The first problem is that they have a different relationship between peak-to-valley height and texture when compared with conventional ablative anti-fouling, (which, nowadays, are copper-laden with booster biocides). The curing of these new coatings results in relatively more spectral energy in the longer wavelengths, suggesting lower drag for the same roughness height when compared with conventional coatings. What little research has been undertaken into the roughness-to-drag relationship for these surfaces, tends to confirm this view (Candries et al., 2002). It follows that the formulation quoted above may not be adequate in respect to these coatings.

The second problem concerns the measurement of the roughness of low surface energy coatings. The current instrument, the Hull Roughness Analyser, has a stylus which jud-

ders when moved over these surfaces when dry, whereas, when the surface is wet, the drive wheel slips. In the laboratory, judicious wetting in the region of the stylus path, can produce a reliable result, but whole-ship surveys in dry dock or underwater, would not be reliable. It should not be difficult to modify the measuring instrument and this is in hand. Another valuable development would be to record the roughness digitally (Chuah et al., 1990).

Clearly, some extensive research is required to see if the peak-to-valley roughness height of these new surfaces can still be correlated with their added drag. Meanwhile, in the short term, comparisons can be made between the added drag of conventional ablative coatings and these new surfaces, for the same roughness height (Candries et al., 2002). Such comparisons should give an indication of the required (small) reduction in ΔC_F in the above formula when foul-release coatings are being considered.

Finally, the persistence of slime on these new foul-release coatings, reminds us that we know little about the added drag of a slime film. We do know that slime develops shortly after undocking and that it can have a significant effect upon resistance; for example, the Lucy Ashton trials, 50 years ago, measured a 5% increase in frictional resistance due to slime alone, after only 40 days from out-docking, and similar augments due to slime have been measured since.

References

- Townsin, R.L., and Dey, S.K., 1990, “The correlation of roughness drag with surface characteristics”, Marine Roughness and Drag Workshop, RINA, London, UK, Paper 8.
- Candries, M., Atlar, M., Mesbahl, E., and Pazouki, K., 2002, “The measurement of drag characteristics of Tin-free, Self-Polishing Co-polymers and Foul(ing) Release coatings using a rotor apparatus”, Proceedings of the 11th International Congress on Marine Corrosion and Fouling, San Diego, California, USA, 21-26 July 2002.
- Chuah, K.B., Dey, S.K., Thomas, T.R., and Townsin R.L., 1990, “A digital hull roughness analyser”, Marine Roughness and Drag Workshop, RINA, London, UK.

II. COMMITTEE REPLIES

II.1. Reply of the 23rd ITTC Resistance Committee to Jan Holtrop

RC appreciates discussor comments concerning Chapter 8 “Uncertainty Analysis for Extrapolation Methods”. Focus of RC effort was in performing the overall uncertainty analysis beginning with data reduction equations and conducting propagation of error analysis with appropriate estimates for resulting uncertainties to estimate uncertainty in full-scale performance. In our opinion a difficult task at the heart of towing tank work. We agree more attention should be given to many detailed aspects, including form factor, model-ship correlation allowance, and differences for ship types and operations. Hopefully, further work will also include such aspects.

II.2. Reply of the 23rd ITTC Resistance Committee to M. Hoekstra, L. Eça, H.C. Raven

RC appreciates discussor comments concerning Chapter 7 “Uncertainty Analysis for CFD”. RC recognizes discussor contributions to present subject, as referenced in our report. RC also recognizes many difficulties in current interim procedure for Uncertainty Assessment in CFD, but nonetheless consider procedures best presently available and recommend their use until improvements available. Hopefully, further work will also include some of the issues you mention.

II.3. Reply of the 23rd ITTC Resistance Committee to G. Grigoropoulos, T. Loukakis

No reply, as material not directly relevant 23rd RC report.

II.4. Reply of the 23rd ITTC Resistance Committee to M. Candries, M. Atlar

No reply, as material not directly relevant 23rd RC report.

II.5. Reply of the 23rd ITTC Resistance Committee to Ahmed Derradji-Aouat

RC appreciates discussor comments concerning Chapter 6 “Uncertainty Analysis for Towing Tank Tests: Sinkage and Trim, Wave Profiles, and Wave Elevations”. Facility biases take into account differences between facilities of detailed towing tank geometry, working fluid and flow quality, measurement systems, models, conditions and procedures, test engineers, etc. Use of standard measurement sys-

tems and/or models helps isolates other differences.

II.6. Reply of the 23rd ITTC Resistance Committee to Marc Vantorre

RC appreciates discussor comments concerning Chapter 6 “Uncertainty Analysis for Towing Tank Tests: Sinkage and Trim, Wave Profiles, and Wave Elevations”. RC agrees that error sources due to reference levels, friction in the vertical guiding system, and deviations of model speed may be important for sinkage and trim tests. Most facilities considered the former small compared to other bias errors considered. The latter is explicitly included through the sinkage and trim data reduction equations.

II.7. Reply of the 23rd ITTC Resistance Committee to Robert L. Townsin

No reply, as material not directly relevant 23rd RC report.